FAN BLADE DAMAGE DETECTION USING ON-LINE VIBRATION MONITORING

by

Wynand Gerhardus Smit

Submitted in partial fulfilment of the requirements for the MEng degree in the Faculty of Engineering, the Built Environment and Information Technology, University of Pretoria

January 2001

FAN BLADE DAMAGE DETECTION USING ON-LINE VIBRATION MONITORING

by

Wynand Gerhardus Smit
Supervisor: Prof. P.S. Heyns

Department of Mechanical and Aeronautical Engineering
Degree: MEng

Summary

The high cost of unscheduled maintenance on critical machinery has led to the need for on-line monitoring of equipment condition. This study investigated on-line vibration monitoring of fan blades to detect and classify the damage levels of the blades. Due to the loads acting on a fan blade, and the resulting distribution of stress, the maximum stress will nearly always be found at the root of the blade. For this reason the location of damage due to fatigue will also be in this region for normal operating conditions. The condition of the blade can then be determined if the level of damage can be detected. An experimental fan blade damage simulator was designed and built to develop a damage detection technique that will eventually be implemented on an industrial fan.

Prior to the construction of the damage simulator a feasibility study was done to determine the sensitivity of the natural frequencies of the fan blade to damage, by making use of a finite element model. Results obtained from the finite element model showed that certain natural frequencies were substantially more sensitive to damage at the root of a blade. Both piezoelectric lightweight accelerometers and piezoelectric dynamic strain gauges were used as vibration sensors during measurements taken on the blade damage simulator. These sensors were mounted on the blade to give the best possible data regarding the damage level of the blade. A slip ring unit was used to connect the sensors to signal processing equipment and a desktop computer.

The autoregressive moving average, with exogenous signal algorithm was used to fit a polynomial through the power spectral density plots obtained from time domain data. Statistical methods were used to determine the number of measurements and measurement time necessary to detect the natural frequencies with sufficient accurcy to observe small percentage shifts. Results obtained showed very good correlation with that predicted by making use of the finite element model. Damage levels of as low as 10% could be detected by measuring the frequency shift of most modes.

Some descrepencies with predicted shifts were found on certain modes. An extended finite element model was developed to confirm the hypothesis that global mode shapes were responsible for this behaviour. Time domain damage indicators such as Root Mean Square values, Kurtosis, Crest Factors and standard deviation were also evaluated as damage level indicators. Only strain gauge measurements gave usable results as damage level indicators under some operating conditions.

The various damage level indicators, particularly frequency shifts, should make very good features for pattern recognition algorithms such as neural networks or self organising maps. Damage levels can definitely be detected on individual fan blades using one sensor per blade only and possibly less if global mode shapes are used in conjuction with the pattern recognition algorithms.

Keywords: On-line monitoring, Damage detection, Frequency shift, Fan blades, Vibration, Damage level indicator, Local mode, Global mode, Stochastic input.

OPSPORING VAN WAAIERLEMSKADE DEUR GEBRUIK TE MAAK VAN AANLYN VIBRASIEMONITERING

deur

Wynand Gerhardus Smit
Studieleier: Prof. P.S. Heyns

Departement Meganiese en Lugvaartkundige Ingenieurswese
Graad: MIng

Opsomming

Ongeskeduleerde onderhoud van kritieke toerusting kan tot groot finansiële verliese lei. Dit kan verminder word deur aanlyn monitering van hierdie toerusting. Hierdie studie ondersoek die gebruik van aanlyn vibrasiemetings op waaierlemme om skade aan die lemme te bepaal en te klassifiseer. Die maksimum spanning in 'n waaierlem sal meestal by die wortel van die lem voorkom, weens die lastoestande en gevolglike spannings wat op 'n lem inwerk. Die posisie van die skade as gevolg van vermoeidheid is om hierdie rede bekend vir 'n struktuur soos 'n waaier en slegs die vlakke van skade hoef bepaal te word. 'n Eksperimentele waaierlem skade simulator is ontwerp en gebou om 'n tegniek vir die opsporing van skade te ontwikkel wat in die toekoms op 'n industriële waaier geïmplementeer sal word.

'n Eindige Element Model is voor die ontwerp en bou van die simulator gebruik om die sensitiwiteit wat die natuurlike frekwensies van die waaierlem het vir skade te bepaal. Volgens resultate wat van die eindige elementanalise verkry is, is sekere natuurlike frekwensies beduidend meer sensitief vir skade by die wortel van die lem as ander. Daar is van sowel pieso-elektriese versnellingsmeters as pieso-elektriese dinamiese rekstrokies gebruik gemaak tydens vibrasiemetings op die skade-simulator. Hierdie sensors is op die waaierlemme gemonteer om die beste moontlike inligting rakende skade aan die lemme te gee. 'n Sleepring eenheid is gebruik om die sensors te koppel aan 'n seinverwerker en persoonlike rekenaar.

'n O*uto-regressiewe bewegende gemiddelde met eksterne sein* algoritme is gebruik om 'n polinoom deur die drywingspektraaldigtheid (PSD) grafieke wat verkry is van tyddomein data, te pas. Statistiese metodes is gebruik om die aantal- en lengte van metings wat benodig is vir die akkurate bepaling van natuurlike frekwensie-verskuiwings te bepaal. Voorspelde natuurlike frekwensies wat verkry is deur gebruik te maak van die eindige elementmodel het 'n baie goeie korrelasie getoon met eksperimentele resultate. Skadevlakke van so laag as 10% kan opgespoor word deur die natuurlike frekwensieverskuiwings van die meeste modusse te monitor.

Die natuurlike frekwensie van sommige van die modusse het wel afgewyk van die voorspelde natuurlike frekwensieverskuiwings. 'n Uitgebreide eindige elementmodel is toe ontwikkel om die hipotese dat globale modusse verantwoordelik was vir die afwykings, te bevestig. Tyddomein skade-indikators soos die Wortel Gemiddelde Waarde, Kurtose, Kruinfaktore en standaardafwykings is ook as moontlike skadevlak indikators getoets. Slegs die metings wat deur die rekstrokies geneem is kon onder sekere in-bedryf omstandighede.bruikbare resultate vir skadevlak-indikasie gee.

Die verskillende skadevlak indikators, veral die frekwensieverskuiwings, behoort baie goeie kenmerke te maak vir patroon-herkenningsalgoritmes soos neurale netwerke en *selfskikkaarte (Self Organising Maps).* Skadevlakke kan sonder twyfel bepaal word deur van een sensor per lem gebruik te maak. Minder sensors mag nodig wees indien globale modusvorme gebruik word in samewerking met patroonherkennings-algoritmes.

Trefwoorde: Aanlyn monitering, Skade-opsporing, Frekwensieverskuiwing, Waaier-lemme, Vibrasie, Skadevlak indikator, Lokale modus, Globale modus, Stogastiese Insette.

ACKNOWLEDGEMENTS

I would like to thank:

- Prof. PS Heyns for his guidance and encouragement
- Staff of the heavy machinery laboratory for their help manufacturing the experimental fan blade damage simulator
- I gratefully acknowledge ESCOM TESP support for making this research possible.
- Parents for their support

TABLE OF CONTENTS

CHAPTER 1
INTRODUCTION AND LITERATURE SURVEY 11

1.1 Introduction 11

1.2 Non-destructive testing of structures 12

1.3 Damage detection using vibration monitoring 13
1.3.1 Natural frequencies 14
1.3.2 Damping 15
1.3.3 Energy transfer 15
1.3.4 Model updating 16
1.3.5 Modal shape changes 17
1.3.6 Modal parameter changes 19
1.3.7 High frequency techniques 21
1.3.8 Case studies 21

1.4 Output only extraction of modal parameters 24
1.4.1 Time domain techniques 24
1.4.2 Frequency domain techniques 25

1.5 Feasibility of using vibration monitoring on rotating fan 26
1.5.1 Sensors 26
1.5.2 Telemetry 30

1.6 Scope of work 31

CHAPTER 2
MODEL IDENTIFICATION STRATEGIES 35

2.1 Time domain and frequency domain identification 35

2.2 Finite element model 39
2.2.1 Mesh refinement 39
2.2.2 Modelling of experimental fan blade damage simulator 43
2.2.3 Damage modelling using FEM 45
2.2.4 Results for curved blade 48

2.3 Conclusion 51

CHAPTER 3
EXPERIMENTAL TEST STRUCTURE 52

3.1 Design issues. 52

3.2 Concepts and selection 52
3.2.1 Blade attachment 52
3.2.2 Drive design 55
3.2.3 Final design 58

3.3 Manufactured fan blade damage simulator 61

3.4 Conclusion 64

CHAPTER 4
FAN BLADE DAMAGE DETECTION 65

4.1 Introduction 65

4.2 Experimental conditions 66
4.2.1. Placement of sensors 66
4.2.2 Typical results obtained 68

4.3 Experimental results 72
4.3.1 Processing of raw data. 72
4.3.2 Determination of required order for ARMAX curve fits 73
4.3.3 Determination of measurement number and length 76

4.4 Damage detection measurements. 81
4.4.1 Experimental fan blade damage simulator 81
4.4.2 Result of curve fits 82
4.4.3 Time domain damage indicators. 88

4.5 Conclusion 91

CHAPTER 5
THE EFFECT OF GLOBAL AND LOCAL MODES 92

5.1 Introduction 92

5.2 The need for extended FEM modelling in systems 92

5.3 Effects of eight blades. 99

5.4. Conclusion 100

CHAPTER 6
CONCLUSIONS AND RECOMMENDATIONS 101

6.1 Introduction 101

6.2 Conclusions 101
6.2.1 Use of FEM for feasibility study 101
6.2.2 Frequency changes as damage indicator on fan blades 102
6.2.3 Practical implementation of on-line technique 103

6.3 Recommendations 103
6.3.1 Further development of FEM 103
6.3.2 Sensors and telemetry 103
6.3.3 Further development of detection technique 104

6.4 Epilogue 104

REFERENCES 105

APPENDIX A - SENSORS 106

APPENDIX B - WORK DRAWING OF MAJUBA FAN BLADE 112

APPENDIX C - INVESTIGATION OF ARMAX MODELLING TECHNIQUE 113

APPENDIX D - TYPICAL EXPERIMENTAL RESULTS 119

NOMENCLATURE

Uppercase

A	Cross sectional area of uniform beam
A_f	Constant value for analytical calculation of natural frequencies
E	Modulus of elasticity
F_{Blade}	Force acting on blade due to change of momentum
I	Moment of inertia
L	Length of uniform beam
M_{air}	Mass flow of air
M_{shaft}	Moment around shaft due to aerodynamic forces acting on blade
N	Number of elements in $x(k)$
P	Pressure
P_{Blade}	Power absorbed by blade rotating at ω
T	Temperature, Time interval
X_{rms}	*rms* value of $x(t)$
X_{max}	Maximum value of $x(t)$

Lowercase

$a_1, a_2, \ldots, a_n$	AR coefficients
$b_1, b_2, \ldots, b_n$	MA coefficients
$c_1, c_2, \ldots, c_n$	ARMA coefficients
d	Distance from rotational centre
$e(t)$	Sequence of white noise
f_n	Sequence of natural frequencies
n	Number of coefficients in AR, MA, ARMA model, Equal to N-1
na	Number of AR coefficients
nb	Number of MA coefficients
nc	Number of ARMA coefficients
p	Order of AR model
q	Order of MA model
r	Distance from rotational centre
rms	Root Mean Square value
s	Variance
t	Time index
t_n	Normal distribution curve
v	Velocity of blade at distance r from rotational centre
$x(k)$	Random variables
$x(t)$	Function values
$\bar{x}$	Mean of $x(k)$

Greek symbols

α	Empirically calculated value for normal distribution curves
θ	Parameter vector
ρ	Density
σ_x	Standard deviation of x
μ_x	Average value of x
ω	Circular frequency
η	Efficiency factor

Abbreviations

ADSM	Absolute Difference of Strain Mode shapes
AR	AutoRegressive
ARMA	AutoRegressive Moving Average
ARMAV	AutoRegressive Moving Average Vector
ARMAX	AutoRegressive Moving Average with eXogenous variables
ARX	AutoRegressive with eXogenous inputs
CF	Crest Factor
CPU	Central Processing Unit
COMAC	Coordinate MAC
DLAC	Damage Location Assurance Criterion
DOF	Degree Of Freedom
ECOMAC	Enhanced COMAC
EFBDS	Experimental Fan Blade Damage Simulator
ETR	Energy Transfer Ratio
FD	Forced Draft
FEA	Finite Element Analysis
FEM	Finite Element Model
FRF	Frequency Response Function
ID	Induced Draft
IMAC	Inverse MAC
MA	Moving Average
MAC	Modal Assurance Criteria
Mbps	MegaBytes Per Second
MEMS	MicroElectroMechanical Systems
ML	Maximum Likelihood
PMAC	Partial MAC
SOM	Self Organising Maps
TF	Transfer Function

CHAPTER 1

INTRODUCTION AND LITERATURE SURVEY

The monitoring of critical equipment in industry has become more and more important in recent years. This has become necessary since it is not always economically viable to conduct maintenance checks on these equipment at regular intervals before it is required. When critical equipment such as Forced Draft (FD) and Induced Draft (ID) fans at power plants are shut down for maintenance, the whole thermodynamic cycle has to be stopped since these fans provide air to the boilers. It is therefore of cardinal importance to monitor the condition of these high value equipment, not only because of high cost, but also due to the critical nature of the equipment in the process path. A whole power plant, representing a huge capital investment, cannot be allowed to stand idle while a fan, which has failed without warning, is repaired.

The aim of this dissertation was to develop a vibration monitoring technique that will be able to detect damage in fan blades at an early stage, so that maintenance can be properly planned and scheduled. Such damage could be caused by any or all of the following:

- Fatigue.
- Corrosion.
- Imbalance due to the accumulation of residue.

It was not unreasonable to expect that vibration-monitoring techniques developed for the detection of damage in structures such as bridges and trusses may be tailored for this application by making some modifications. Typically, the output from a damage detection technique could have a series of status indicators for maintenance planning. For example:

- Green indicator: No maintenance necessary.
- Yellow indicator: Plan for a maintenance shutdown.
- Red indicator: Blade may fail at any time, immediate shutdown.

It became clear at an early stage that a general-purpose damage detection technique would probably not work for a specific application such as this. Another aspect that was very important is practical implementation. A method requiring expensive equipment such as a laser vibrometer would not at all be suited to industry based applications. The rest of this chapter is devoted to a literature study and defining the scope of this research.

1.1 Introduction to literature study

Before starting on the details of the development of this method, a comprehensive literature study was undertaken. The main focus of the literature study was on structural damage detection techniques that have been used on various structures. It was found that little work has been done in the area of rotating structures (such as fan blades). A brief look was taken at general non-destructive damage detection techniques. A wide range of vibration based damage detection methods developed over the years were investigated next. Optimal location of sensors, telemetry, system identification methods and finite element usage was also studied.

1.2 Non-destructive damage detection

The high cost of maintenance and the need to know when machinery will require maintenance in order to cut down on production loss due to unscheduled stops, has led to the development of various non-destructive damage detection methods. Only a handful of these procedures can be applied when on-line condition monitoring is required.

While techniques such as ultrasonic scanning, x-rays, conductivity and penetrating dies work very well, none of these can easily be implemented on a spinning fan blade. The high cost of the scanning methods also makes it impossible to instrument individual blades and fans. It would for example not be financially viable to install x-ray equipment on every fan for the detection of damage during brief periods when the fan is stationary.

A further disadvantage of methods such as x-rays, ultrasonic scanning etc. is the fact that defects may be overlooked due to shielding by the structure itself. Most of these methods also require highly skilled and trained operators with years of experience.

In the end it became clear that a more promising method of damage detection for an application such as a spinning fan blade was vibration monitoring. The main reasons for this decision are presented in the next section.

1.3 Damage detection using vibration monitoring

Vibration monitoring of structures and machines has received considerable interest in the last few decades. Doebling *et al.* (1996) have presented an extensive survey of this field. The main reasons for the interest in these methods are:

- The ability of such methods to do global monitoring of a structure with a few sensors, as opposed to scanning the whole structure with complex equipment.
- The equipment required for vibration monitoring are generally orders of magnitude cheaper than the equipment required for contemporary scanning methods.
- Online monitoring of equipment and structures is possible in most cases.

There are off course, difficulties when using vibration monitoring methods to detect damage. The most important are:

- It is difficult to find a characteristic to measure, that change sufficiently with increasing levels of damage.
- There are always some errors in the measured data due to sensor inaccuracies, filtering of data and random noise.
- Errors in system identification and modelling.

It became clear quite early in the literature study that different researchers have encountered various difficulties. The most promising results were, not surprisingly, usually obtained when simplistic methods were applied on basic structures. A paper by Friswell and Penny, (1997) considered the state of the art in damage detection and location using vibration data. They noted that algorithms should be tailored to a specific application, as it is unlikely that a single best method will ever emerge. The authors also noted that health assessment of structures by making use of ambient excitation was even more difficult.

The rest of this section gives an overview of the most relevant literature found on vibration based damage detection and modelling techniques and includes four case studies that focused on damage detection in rotating bladed structures.

1.3.1 Frequency changes

Exhaustive research has been done regarding the use of natural frequency shifts to detect damage. The observation that changes in structural properties caused changes in natural frequencies was the stimulus for using modal methods for damage identification and health monitoring. As mentioned earlier it was not possible to include all the work done on damage identification. Only the most relevant and recent work on natural frequency shifts is therefore reviewed here.

It soon became apparent that frequency shifts have significant practical limitations for certain types of structures. These include bridges, offshore oil platforms and other large civil structures. The low sensitivity of frequency shifts to damage requires either very precise measurements, or high levels of damage. For example, in offshore platforms, damage-induced frequency shifts are difficult to distinguish from shifts resulting from an increase of mass due to marine growth. Most of these structures are also designed with a high degree of redundant load paths and safety factors. This sometimes mean that excitation of the system become very difficult and cracks or other damage need to reach relatively high levels, before a damage identification can be done. A further complication is that frequency shifts usually only point to the existence of damage and not the specific location. If different frequencies are used, particularly those frequencies associated with higher mode shapes, it is possible to locate local damage specific to the mode shape.

The accumulation of residue on fan blades can cause a substantial imbalance if part of this residue fly of the blades under centrifugal acceleration. In most cases, it can be expected that this accumulation will not reach the levels found on offshore platforms, largely because of the centrifugal acceleration imposed on the residue. Due to the fact that a fan blade is a relatively simple cantilever system and the crack location is almost always at the position of maximum stress (the root), frequency shift could very well turn out to be a viable method.

Silva and Gomes (1994) covered the use of the inverse problem to determine the location and degree of damage in a simple cantilever system. The inverse problem consists of calculating the damage parameters such as crack length and/or location, from the frequency shifts. This was done by making use of a simple cantilever system with a crack of known depth and location. The theoretical models were devel-

oped by assuming that a cracked beam could be modelled by two shorter beams connected through a torsion spring that simulates the stiffness of the original beam at the section where the cracks exists. Silva and Gomes did a whole range of experiments and investigated modelling techniques along this vein. They found that it was possible to determine the depth of the crack very accurately and the location with a fair degree of accuracy if more than one frequency were used. They developed a computer program that used discrete intervals along the beam and tested various combinations of crack depth and locations until a match closest to the measured frequencies was found. They noted that this was a very time consuming process but obtained fairly good results.

Springer and Reznicek (1994) examined the effect of damage on the dynamics of a vibrating structure. To do this, a beam element that had an L-section and contained a crack was developed. By modelling the crack as a set of four linear springs, stress intensity values were computed. Strain gauge measurements were taken to determine the stiffness values for these springs. The resulting finite element could then be used in Finite Element Analysis (FEA) or structural dynamic modification routines. Examples of crack elements can be found in commercial packages such as MSC Marc. If the necessary physical tests to determine stress concentration values were done at some stage, these elements can be very useful.

1.3.2 Damping

Although damping is usually the most problematic modal parameter to determine accurately, some work using only this parameter as damage indicator has been done. Williams and Salawu (1997) decided to use this indicator because situations do exist in which damping may be the only indicator of distress. Damping properties are very difficult to model analytically and vibration tests are usually necessary to obtain realistic values. Generally speaking the damping of a system will increase with increasing damage. These authors concluded that Auto Regressive Moving Average (ARMA) models provided the most accurate results. For damping to be used as a damage indicator the accuracy of data acquisitioning needed to be high and the testing very well controlled.

1.3.3 Energy Transfer methods

Liang *et al.* (1997) proposed the use of the energy transfer ratio for the classification of damage. They developed the Energy Transfer Ratio (ETR) as a new modal pa-

rameter for studying the dynamics of the test structure. The main reason for using this newly defined parameter was the lack of accurate and repeatable measurements for other parameters. This made the detection of small amounts of damage very difficult. Since the mass, damping and stiffness matrices were usually unknown for a real structure, these modal parameters had to be estimated. This was done by analysing vibrational responses of the structure in the time domain. Interestingly enough, this method did not require the authors to select specific modes sensitive to damage. They found that the ETR was significantly more sensitive to damage than natural frequency and damping ratio changes. Furthermore ETR could also be used to determine the location of the damage by using different modes.

1.3.4 Model-updating techniques

Many researchers have tried to use model-updating techniques to detect damage and the location thereof. Most of the literature found on this method failed to produce good results with even relatively simple structures. The biggest problem with all model-updating algorithms was the small amount of data available, compared to the large number of possible damage locations.

Fritzen *et al.* (1996) developed a model based damage detection method that compared vibration data to a mathematical model of the undamaged structure with local description for the damage. The authors note that it was very important to compile an accurate mathematical model of the structure that was analysed and proposed the updating of the model with vibration data from the undamaged structure. The reason for this was that the residuals generated from the model for the undamaged case and the measurements from the damaged case contain not only information about the damage itself, but were also polluted by modelling errors. They studied the detection of multiple cracks in a T-frame and a three dimensional beam structure. These authors also noted that the model was inclined to spread damage around the location of the actual crack.

Friswell and Penny, (1996) considered the use of Finite Element Model (FEM) updating to detect and locate damage in structures. The authors discussed problems associated with detecting and locating damage using model updating algorithms in some detail. They note that the incompleteness of data, coupled with measurement noise made the location of damage very difficult. The biggest problem, according to the authors, was the large number of possible damage sites, compared to the amount of data available.

Other work that used FEM and model updating in conjunction to detect damage in a space frame structure, also noted the effect of insensitive modes that makes locating the damage very difficult (Pereira *et al.* 1994). The authors used updating techniques based on Frequency Response Functions (FRFs) to monitor measured data and identify the damaged area of the structure. When the updating procedure reached a good correlation between the analytical and experimental data, the model parameters of the damaged structure were compared with those of the undamaged one to find the deteriorated area. This work confirmed that the model updating methods usually struggled to locate damage, largely because of the modes that were insensitive to damage.

One of the major problems with modal analysis has always been the number of sensors required to accurately identify the modal parameters. For a fan with 20 blades, using even one sensor per blade already constitutes a large investment in sensors and a huge amount of data to be processed. Cobb and Liebst (1996) investigated the use of minimal sensors to locate structural damage. The method used, employed mathematical optimisation to minimise the deviations between measured and analytical modal frequencies and partial mode shapes. Damage was identified by determining the change that needed to be made to a FEM, to match the measured data on the damaged structure. Because the method required the decomposition of a large matrix it was computationally very expensive if sparse matrix techniques was not used. The method was demonstrated on an experimental structure and correctly determined the location and extent of structural damage. Eight accelerometers were used on a structure consisting of 64 truss-like connections.

1.3.5 Modal shape changes

Another parameter used for the detection of changes in the characteristics of a system is mode shape changes. The Modal Assurance Criterion (MAC) has been used for some time in various forms as a damage detection criterion. Joon-Ho *et al.* (*S.a.*) used Partial MAC (PMAC) and Coordinate MAC (COMAC) to detect single and multiple faults in a FEM plate model. Ko *et al.* (1994) also presented a method that combined MAC and COMAC to detect damage in steel frames. The sensitivities of the analytically derived mode shapes to particular damage conditions were computed to determine which Degrees of Freedom (DOFs) were most relevant. To determine which mode pairs were to be used, the authors analysed the MAC between measured modes from the undamaged structures and the measured modes from the damaged structure. The results they obtained indicated that particular mode pairs

could indicate damage, when all mode shape pairs were used, the damage was masked by modes that were not sensitive to the damage.

Williams *et al.* (1997) introduced a new assurance criterion using the frequency changes in a number of modes to identify the location of the damage. They used a number of numerical and experimental case studies to illustrate the tolerance of the method to error levels in measurements. They established that standard error values when determining natural frequencies from FRFs were typically less than 0.1% and were all below 0.15%. Williams *et al.* also suggested that the percentage change in frequency shifts should be used rather than the absolute change. The Damage Location Assurance Criterion (DLAC) they used can be defined at a location *j* using a correlation approach similar to the MAC (Allemang *et al.* 1982) value used for comparing modal vectors. Similar to the MAC, DLAC values fell in the range 0 to 1, with 0 indicating no correlation and 1 indicating an exact match between the patterns of frequency changes. The location *j* giving the highest DLAC value determines the predicted damage site. They conclude by suggesting that problems still remain for low damage levels.

Cawley and Adams (1979) were some of the first authors to match measured changes in the natural frequencies with those from a theoretical model of the system. Penny *et al.* (1993) and Williams *et al.* (1995) produced improvements to the technique used by Cawley and Adams. These authors noted that the predicted faults in the structures were usually spread over a much wider area of the structure than was actually the case.

Several criteria for the detection of cracks were compared to each other by Yoo *et al.* (1992). The Inverse Modal Assurance Criteria (IMAC) using inverse strain mode shapes was found to be more sensitive to local changes than the MAC. The COMAC and Enhanced Modal Assurance Criteria (ECOMAC) were studied in order to identify crack location. ECOMAC was found to be less effective than COMAC. Furthermore the Absolute Difference of Strain Mode Shapes (ADSM), a method that identify crack location by strain mode shapes was developed further. It was found that COMAC, ECOMAC and ADSM based strain mode shapes were not applicable for all modes. The modified ADSM method using absolute values only, was found to be the most promising for the accurate identification of crack location.

Another comparison of different modal shape change methods was done by Salawu and Williams (1994). The curvature mode shape method, mode shape relative difference method, MAC and COMAC methods were studied. According to the authors only the curvature mode shape method was able to give an indication of multiple

damage locations. The MAC and COMAC methods were however found to be more tolerant to the use of different mode shapes. The curvature mode shape methods and mode shape relative difference method depended heavily on the choice of damage sensitive modes.

A method using only the mode shape data of a structure was developed by Ratcliffe (1997). A very simple structure was tested and classified by means of a one- dimensional finite element. The author found that applying a finite difference operator to the mode shape could identify damage of 10%. Furthermore it was found that lower mode shape provided better results (detection of 0.5% damage). The higher frequencies were only of use to determine the location of the damage. A slot cut into a steel beam was also successfully located. Since the Laplacian function used, represents the curvature of the mode shape, the author suggests that modal data obtained using strain gauges may be used directly in place of the Laplacian. This was not verified experimentally.

1.3.6 Modal parameter changes

In an attempt to create more robust and reliable damage detection techniques, more and more authors look at more than one modal parameter to classify damage and improve the accuracy of damage detection.

Most of these papers deal with damage detection on large civil structures or simple laboratory based experiments. Peeters *et al.* (1996) developed an experimental program to establish the relationship between damage and changes of the dynamic system characteristics. They used a laboratory based model to simulate a bridge structure. To identify the dynamic system characteristics, they made use of system identification techniques such as polynomial models and state space models. An accurate mathematical model of the system could be compiled because they made use of an electromagnetic shaker to excite the system (input forces therefore known) and a large number of measurement points were used. They found that the modal curvature was the best indicator of location and amount of damage. Natural frequencies also classified the damage accurately, but not the location. Damping also increased with increasing amounts of damage but was found to be difficult to classify.

Mastroddi (2000) recently studied the use of a general procedure based directly on the measurement of FRFs of a structure to identify a numerical model or directly localise and quantify possible damage and failure in terms of mass, stiffness, and damping variations. The author used both a continuum analytical system and two

experimental structures to test the procedure. The structures consisted of a cantilever aluminium plate and a cantilever half-wing constructed from composites. The author found that the procedure had the capability to give significant results in the presence of errors or uncertainties in the measurements.

Klein *et al.* (1994) monitored the change in modal parameters with fatigue of a structure. The authors monitored both the changes in vibration and acoustic variables that occurred with the presence of a fatigue crack. Shifts in natural frequencies, damping and other parameters were documented. The experimental test structure consisted of a simple cantilever beam. Again it was found that some modes were influenced more by damage than others. The authors found that the normalised acoustic intensity spectra also showed large changes for increasing damage for certain modes but noted that that additional tests will have to be performed to confirm these findings.

Sohn and Farrar (2000) made use of the Auto-Regressive (AR) and Auto-Regressive with eXogenous inputs (ARX) techniques to pinpoint the sources of non-linear damage by solely analysing the vibration signatures from a structure. They used the residual error, which is the difference between the actual measurement and the prediction from the previously estimated AR-ARX combined model, as the damage-sensitive feature. The premise that if there were damage in the structure, the prediction model previously defined using the undamaged time history data would not be able to reproduce the newly obtained time series data measured under a damaged state of the structure, was used. They obtained good results on a very simple test structure and noted that further work would be necessary to validate this method. The model used consisted of masses connected with springs in a series system. Damage was induced by introducing bumpers between the masses.

Local frequency changes and modal frequencies were used in a two-stage damage detection method developed by Shi *et al.* (1997). The measured mode shapes were used to obtain the location of the damage, while the modal frequencies was used to determine the magnitude of the damage. The location of the damage was found by making use of the local frequency change ratio, based on the mode shapes. The structure consisted of a two dimensional truss. The authors also noted that the effect of noise and incomplete mode shapes needed to be addressed further.

Santos and Zimmerman (1996) explored the use of the residual modal force vector and component mode synthesis as a structural damage diagnostics tool. Measured modal test data was used along with a correlated analytical substructured finite element model. Depending on the number of modes that was used in each

substructure, the method was able to detect the exact location of the damage, or the substructure that contains the damage.

1.3.7 High frequency methods

Friswell and Penny (1997) recommended that high frequency techniques for damage detection should be investigated further. They reviewed a number of case studies and came to the conclusion that some problems do not seem to be suited to conventional vibration based damage detection. The higher resolution provided by higher frequencies may provide more accurate location and classification of damage. The disadvantage of these higher frequencies in global structural damage localisation is the large number of reflections and transmissions from components that are difficult to model at the higher frequencies and the high number of fixed actuators and sensors required.

Most high frequency damage detection techniques use frequencies so high that microphones usually provide better information. Sound is the result of physical objects vibrating in a medium such as air and somewhere between conventional low frequency vibration detection methods (accelerometers etc.) and ultrasonic methods it should be possible to get better resolution and greater global detection. Colonnello and Morassi, (1998) investigated the use of spectral data to solve the inverse problem. The authors found that the uniqueness results come from the fact that the highest part of the spectrum of a cracked rod separates into branches which correspond to the asymptotic spectrum of the pieces of the bar adjacent to the damaged cross section.

1.3.8 Case studies

Four case studies that applied vibration based damage detection techniques to bladed structures, were investigated.

Case study 1 : Crack in scrubber fan.

One of the most interesting papers found in the literature study, investigated the detection of cracks in a scrubber fan (Wolff *et al.* 1989). The authors used both FEM and experimental measurements to test the effects of induced cracks on a scrubber fan blade. A modal analysis was performed on the scrubber. In order to do a modal

analysis it was necessary to measure the force input and a "stinger" was used in conjunction with a piezo electric force transducer. They used a zero to 3200Hz "pink" noise signal from a dynamic signal analyser.

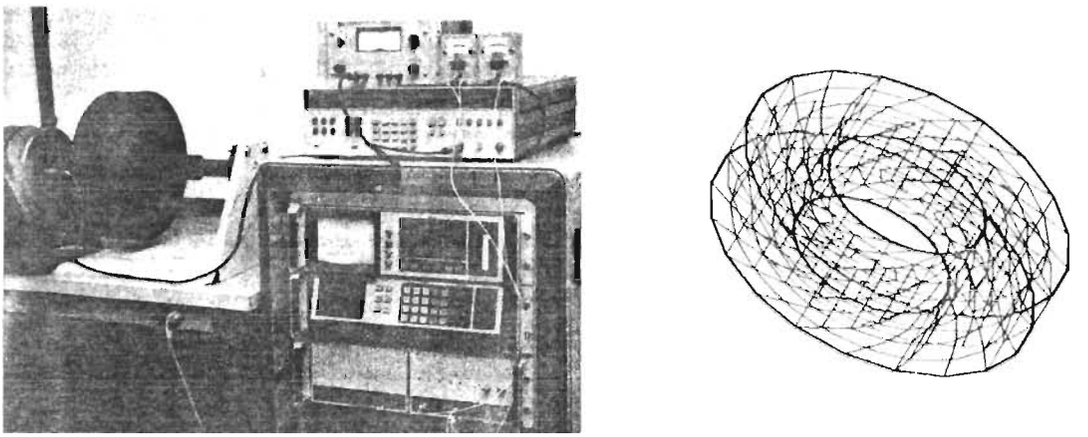

Figure 1.2: The FEM and experimental test rig used by Wolff et al. (1989)

By measuring the output from the force transducer and an accelerometer, a frequency response function can be computed. This allows modal parameters such as frequencies, damping values and mode shapes to be identified. They compared these results with results obtained after inducing cracks (using a fine hack saw) of 1.5 inches and 3 inches. Cawley and Ray (1988), found that this gave a good approximation to an actual crack.

A finite element model of the scrubber fan was constructed. The finite element model was calibrated to give similar results to the experimental model. The cracks introduced on the model consisted of untying various nodes and were therefore dependent on the mesh size. Cracks of 1.84 inches and 2.76 inches were modelled. From the results obtained, it was quite clear that some modes were a lot more sensitive to the damage than others. Furthermore the frequency shifts were very small. The experimental results failed to give an exact indication of damage for 1.5 inches and fared only slightly better with the 3 inch crack.

It was quite clear that although most of the mode shapes were found in the experimental modal analysis and frequency shifts did occur, as a damage indicator, this technique still requires some work. The authors note that the most apparent difference was found in frequency response functions due to separation and splitting of resonant peaks.

Case study 2 : Damage detection in wind turbine blade section

Another paper dealing with damage detection in blades used exotic, state of the art sensors and actuators and showed the possible future of online monitoring. Sundaresan *et al.* (1999) used a scanning vibrometer and piezoceramic actuators for detecting damage on a section of a wind turbine blade. As discussed in paragraph 1.5.1, the laser vibrometer is the ultimate diagnostics tool for vibration measurement. It is a non-contacting sensor that can measure vibration at a large number of points over a wide frequency range. Sundaresan *et al.* used three different methods for detecting damage. These methods used changes in transmissibility, frequency response functions and operational deflection shapes. Damage was simulated by a steel plate clamped to the blade and was detected by all three techniques.

The authors assumed that the wind turbine could be stopped for this application. Since the blade is easily accessible in this case, one vibrometer could be used to test various wind turbines. The Frequency Response Functions (FRF) could be constructed by making use of the periodic excitation equation and the piezoelectric ceramic patches to excite the blade. They found that reasonably good results could be obtained with all the techniques. The authors also noted that operational deflection shapes gave the most repeatable and accurate results.

Case study 3 : Damage detection in helicopter rotor blades.

Corbelli *et al.* (2000) focussed on the development of a method to detect damage in composite helicopter rotor blades in operative conditions. The authors used a FEM to obtain FRF data. The behaviour of the blades in hovering condition could then be described and numerical results were presented to validate the capability of the formulation presented to detect, localise and possibly quantify local variations of system parameters. Previous work of Mastroddi *et al.* (1996), Balis *et al.* (1997), Balis and Mastroddi (1997), Mastroddi and Balis (1998), Agneni *et al.* (2000) and Mastroddi (2000) described the numerical and experimental tests on truss, beam and fixed wing models. As typically happens in all inverse problems, results were strongly effected by noise or uncertainty in the measured FRF data.

Very complex structural and aerodynamic models were compiled by the authors to describe the behaviour of the rotor blade under hovering conditions. In particular, the velocity field induced by the wake vorticity on each blade had a great impact on aerodynamic loading distribution. The aeroelastic system was identified in terms of spatial matrices. FRF data obtained from the helicopter itself was in agreement with the FRF data obtained from the FEM. Unfortunately the authors were not clear on how the FRF data was obtained from the helicopter. The results obtained on damage detection presented in terms of stiffness variation matrices showed a good ca-

pability of damage detection, location and quantification. It was also apparent that the identified damage levels became lower and moved from the root of the blade to the tip for a fixed level of damage if global damage only was evaluated.

Case study 4: Health monitoring of Helicopter Rotor Systems

A project by McDonald Douglas (now Boeing), one of the largest aircraft manufacturing companies in the world, is currently under way to detect damage in composite helicopter rotors. The method make use one piezoceramic actuator and four piezoceramic sensors to determine FRFs and Transfer Functions (TFs) of the blade. The comparison of the measured TFs with TFs taken prior to damage was found to provide excellent results.

It was found that the size of damage that can be detected was heavily depended on the repeatability of the algorithm and the spacing of sensors. The biggest advantage of the method proposed by Schulz *et al.* (1997), was the fact that it was not necessary to compile a model of the structure.

The TFs approach was found to have three main advantages

- For a single force input the force was cancelled by the ratio of responses and thus did not need to be measured.
- The ratio of the peaks and valleys of a transmittance function was very sensitive to structural changes and could identify small amount of damage.
- Changes in the structural response due to global environmental effects were partially cancelled because transmittance functions are the ratio of two response quantities.

1.4 Output only extraction of modal parameters

From the various vibration-based monitoring techniques studied in the previous section of this chapter it became clear that most methods required input and output data for an accurate model. While it was not impossible to obtain input data for a structure such as an operating fan, it would be far more practical to make use of output only data (such as data obtained from accelerometers). This section gives a brief description of the literature found on output only extraction of modal parameters.

1.4.1 Time domain methods

Comparatively little attention has been given to practical damage identification of structures in industry. The single biggest problem with these structures was usually the lack of information on the excitation of the structure. Kriel and Heyns (1998) investigated the feasibility of detecting damage to piping structures in the chemical and petrochemical industries by making use of on-line monitoring of dynamic properties. The authors used both frequency domain (Basic Frequency Domain (BFD)) and time domain (AutoRegressive Moving Average Vector (ARMAV)) methods to estimate modal parameters. The BFD approach by Felber and Ventura (1996) was followed using software developed by Felber and Ventura. The ARMAV approach was implemented by making use of the MATLAB Structural Time Domain Identification Toolbox as implemented by Andersen *et al.* (1997). The authors found that the flow in the piping system provided enough bandwidth to excite the interesting modes. Both the models provided accurate enough determination of natural frequencies to detect damage. The ARMAV method was noted as being very expensive computationally. Mode shapes also seemed to be a viable parameter for damage detection.

Conventional modal testing requires artificial excitation of the test structure under well-controlled conditions. Heyns (1995) presented a technique that utilised time series analysis of the measured response, while assuming the perturbation of the structure through initial displacement, impulse or random excitation. Very good results was obtained when an initial displacement or impulse was applied on the theoretical model used and the responses computed. All modal parameters were found with a high degree of accuracy. For the case of random excitation, especially when some random white noise was introduced, the situation changed drastically however. Although the natural frequencies were still found with a fair degree of accuracy, the damping factors and mode shapes were not. In conclusion the author note that good results could be obtained for random excitation if suitable multi-channel tests were used and the order of the model used was increased.

1.4.2 Frequency domain methods

Hermans and Van der Auweraer (1998) also realised that while modal parameters are traditionally extracted from FRF measurements performed under laboratory conditions, in-operation tests frequently make it impossible to obtain input forces. The frequency domain Maximum Likelihood (ML) identification technique was investigated in this paper. Attention was paid to the modifications that has to be applied to

the ML estimator in order to be applicable to output-only data and the derivation of the noise information required for the ML estimator. It was found that the ML estimator could be used to extract the modal parameters from output only data. Instead of using FRFs the ML estimator was fed by power- and cross-spectral density functions. The spectral densities were estimated by making use of the periodogram and the correlogram methods. Special attention was paid to leakage effects that created bias error. In the end the correlogram method was preferred because of better estimates for damping. Contrary to the stochastic subspace method, the ML estimator also provided uncertainties on the modal parameters, which might be of great interest in case of structural monitoring or damage detection applications.

Another frequency domain analysis using ambient vibration data was performed by Felber and Ventura (1996). Data from the Queensborough Bridge was used to do a frequency domain analysis. The authors found that thirteen natural frequencies could be identified between 0 and 10 Hz. Since more than one time signal were available and taken on different locations of the bridge simultaneously, the authors could also reconstruct some of the mode shapes by using TFs and a reference signal. This could only be done because the test had been carefully planned with these types of signal manipulations in mind. The results obtained compared well to results found with time domain techniques.

1.5 Feasibility of using vibration monitoring on a fan

Although the various signal processing, modelling and identification techniques studied up until now were very important, all would be in vain if accurate, repeatable measurements could not be obtained at a reasonable cost. This section describes some of the sensors that have been used, or may be used in future, along with some aspects regarding placement of sensors.

1.5.1 Sensors

A wide variety of sensors exist to measure the dynamic behaviour of systems. These sensors measure variables such as displacement, velocity or acceleration of the structure and converts this information into an electrical (usually analogue) signal that can be processed using various signal transducers. Since the method for damage detection developed has to be implemented on the an actual fan in industry at some stage, it was important to establish the feasibility and cost of using sensors.

The rest of this section describes various types of sensors and the viability of using them for this application.

A. Vibrometer

Laser Doppler vibrometry is a non-contacting optical technique that relies on the Doppler shift of laser light to measure the velocity of structures. The output consists of voltage signals proportional to the structure velocity. These signals are related to the frequency shift of the reflected light and are therefore accurately calibrated, providing accurate, quantitative measurements.

The application of laser Doppler vibrometry to high speed rotating structures has been hampered by technical limitations. Lomenzo *et al.* (1999) introduced a self-tracking laser vibrometry system which overcame these limitations. This method was first proposed by Maddux (1997). The method proposed made use of a series of mirrors, one of which was attached to the rotating structure's centre of rotation. This mechanical connection to the structure gave better results than other more exotic method making use of short measurement intervals.

A schematic of the typical configuration that will be necessary to monitor the vibration of a rotating blade can be seen in Figure 1.4. The measurement point on the bladed disk could the be adjusted by either tilting the vertex mirror or moving the fold mirror closer or further away from the disk.

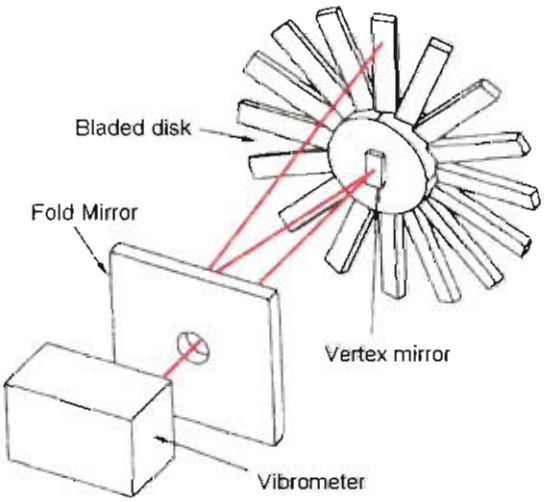

Figure 1.4: The self-tracking system for blade vibration measurements .

Recently a scanning laser vibrometer has been developed. While the entry level laser vibrometers can be acquired for $4500, the scanning vibrometer can cost as much as $80 000. The scanning laser vibrometer has the ability to direct the laser beam through an arc or cone depending on model.

B. Accelerometers

These sensors are the most widely used transducers for vibration measurement in industry. There are two primary types of accelerometers:

- *Piezoelectric:* These make use of a piezoelectric crystal and a seismic mass to measure the acceleration of the sensor and thus the structure. This type usually has a relatively wide frequency range (0.1-10000Hz) and low sensitivity (100mV/g). Because the charge created by the crystals dissipates quickly, lower frequencies can not be measured as accurately as higher frequencies.
- *Capacitive:* These are usually larger (although micro machining techniques are changing that) sensors and can measure very low frequencies (≈0Hz). The sensitivity of these accelerometers is usually higher as well (1-10V/g).

Figure 1.5 shows the trends for accelerometers regarding price, size, frequency response, range, reliability and level of integral electronics. The most exiting development is the advent of MEMS (MicroElectroMechanical Systems) technology (see Figure 1.6).

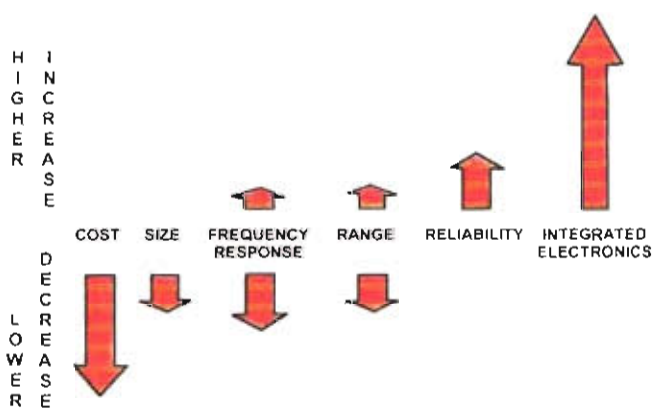

Figure 1.5: Trends regarding accelerometers

Using the same technology as that used by microchips, a very small accelerometer can be constructed and packaged on a circuit board. Furthermore, integrated circuits can be built into the accelerometer, turning it into a "smart sensor". These sensors

measure environmental changes around them (such as pressure, acceleration etc.) and use the integrated circuit to amplify, condition, calibrate and process the raw signal from the transducers. Examples of these sensors include the accelerometers used to deploy air bags in cars.

These sensors typically cost less than $10 and makes a decision regarding the deployment of the air bag before sending a signal to the triggering. An example of MEMS capacitive accelerometer can be seen in Figure 1.6.

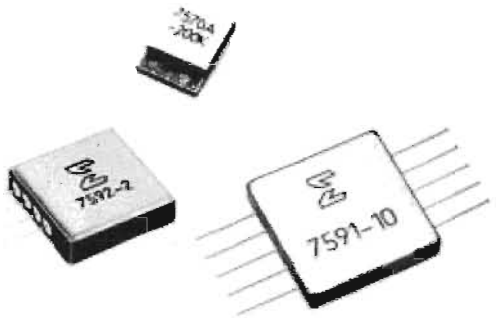

Figure 1.6: Examples of MEMS capacitive accelerometers

The most important aspect of these developments is the fact that while the performance of these devices are getting better and better, the cost is going down dramatically as mass production for MEMS accelerometers come into play. While micro accelerometers such as the one used on the fan blade damage simulator cost around R5000, it is not unreasonable to expect cheaper MEMS accelerometers to be available within the next few years.

The micro accelerometer used for some of the measurements can be seen in Appendix A. The specifications and physical dimensions of the sensor are also provided to give some indications of what is readily available even now.

C. Strain gauges

These devices had been around for some time. Modern strain gauges are inherently sensitive to strain.

The unit output is directly proportional to the unit dimensional change (strain). These generally work by measuring the increase of electrical resistance with increasing strain. The bonded-wire-type strain gauge is the most generally used. Another type work by using the decreasing area of the metal from which the strain gauge is

manufactured as electrical resistance. Figure 1.7 shows the most commonly found type schematically.

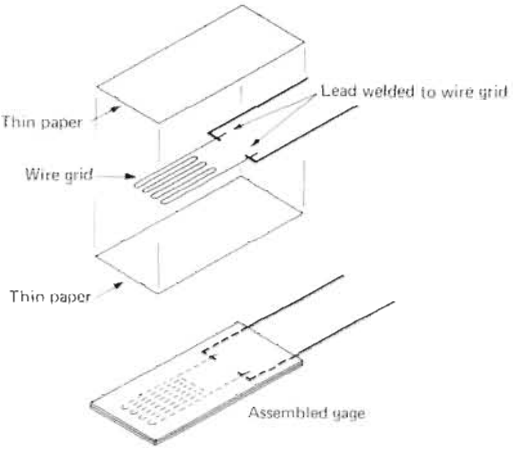

Figure 1.7: Schematic of typical strain gauge (Beckwith (1993))

Recently, the piezoelectric strain gauge has been developed. This sensor can only measure dynamically and is therefore optimised for the dynamic measurement of system response. The strain is measured by using the properties of the piezoelectric crystal. When this crystal deforms it results in a voltage difference across the crystal that can be measured. The big advantage of this sensor is that no balancing circuitry, amplifiers and other peripherals were necessary. The piezoelectric strain gauge used specifications and physical dimensions can be seen in Appendix A.

D. Other sensors

Other sensors that may have been used include various types of displacement and velocity sensors. The vibration of blades has been studied by proximity sensors in the past. The difficulties involved with placement of these sensors make them less than ideal for this particular application however.

1.5.2 Telemetry

One of the biggest problems regarding the monitoring of the dynamic behaviour of fan blades is the transfer of data from the measurement sensor (that will probably be mounted on a blade) to the signal transducer or user interface. The ultimate goal would be to develop an integrated sensor that measures the dynamic behaviour of the blade, process this information, make a decision regarding the conditions of the blade and then send a warning signal to the user if the blade requires maintenance. This scenario is probably still a few years into the future. A more realistic approach

would be to either transmit the signal from the sensor directly to a signal transducer, or to store this data and transfer it in bursts whenever the fan is shut down due to lower power demand from the national electricity grid.

Wireless transfer of data has become more and more available as time has gone by. Local area networks between personal computers have already taken the step to a wireless environment by making use of radio wave connections similar to cellular phones. At the moment, only very specialised and expensive wireless-transfer techniques exist for the precision sensor signal that an accelerometer gives as output. A device that use infra red non-visible light can be imported from America at around $10 000 . A good example of how the prices on sensors and telemetry is going down is that a similar device, using radio waves can now be acquired for $4500.

New wireless transfer standards such as Bluetooth being developed by companies such as Nokia, Intel, Ericson, Microsoft, Motorola, 3COM and various others will play a huge role in future communication between various devices. Bluetooth is a high-speed, low power, microwave wireless link technology which enables devices such as phones, laptops and other portable equipment to communicate with each other. Briefly, Bluetooth technology:

- uses radio waves in the 2.4 GHz band, meaning that line of sight is not required.
- supports multipoint communication
- works in small confined area (10 to 15 meters apart)
- is able to support speeds of 1-2 Mbps
- the chipsets are relatively inexpensive ($10 per chip)
- over 1800 members in industry support this technology

This technology is already used in various mobile phones and laptops and is also being developed for applications such as wireless sensors. Nokia recently displayed a Bluetooth headset that allows users wireless communications with their mobile phones over distances up to 10 meters.

For the purposes of this thesis, it was decided to use a locally developed slip ring unit that can be seen if Figure 1.8.

This unit specifications and physical dimensions can be seen in Chapter 3. It performed very well throughout the experimental tests. The units' location in the signal path can also be seen in Chapter 3.

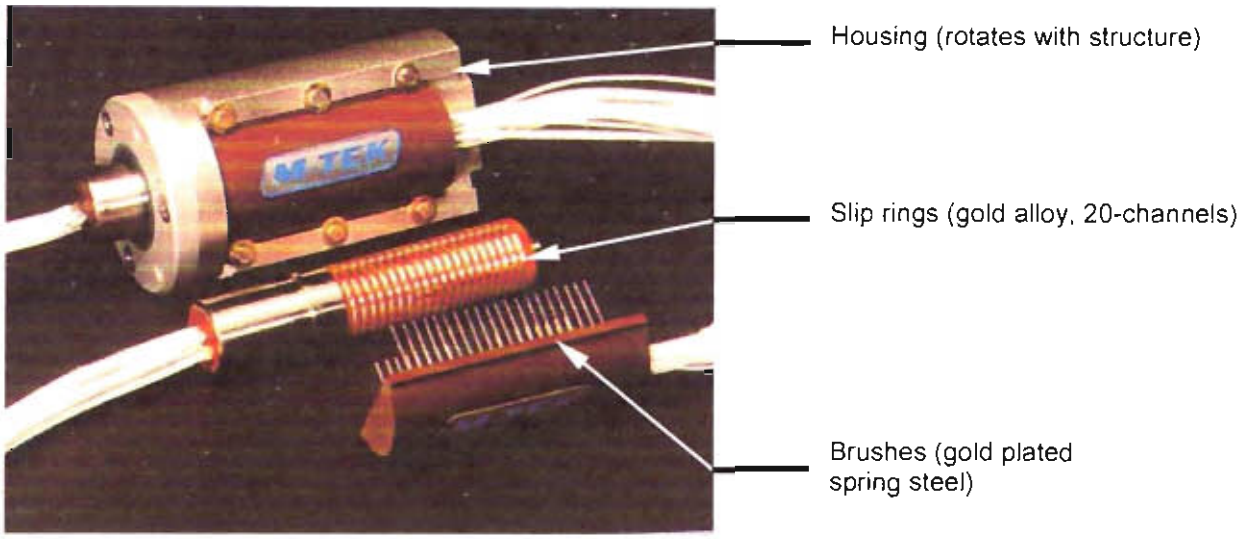

Figure 1.8: The slip ring unit used for transferring data from the rotating transducers to the signal processing unit and personal computer.

1.6 Scope of work

This chapter described an extensive literature study covering:

- Damage detection techniques
- Vibration based damage detection techniques
- Viability of dynamic measurements on a rotating structure such as a fan
- Sensor requirements
- Telemetry requirements

It was found that exhaustive efforts have been made in the field of vibration based damage detection. From these efforts it was apparent that damage could be located and classified provided good quality measurements (repeatable and accurate) was available. Although most applications in industry made it impossible to obtain accurate input forces on structures, the majority of the techniques developed required accurate input data. For an application such as health monitoring of operational structures, especially fan blades, this was not a realistic requirement. Fortunately some methods involving output data had been developed. Time domain techniques offered the best applicable results. Special attention was given to ARMA based techniques, as various researchers have used these techniques to successfully identify modal parameters such as natural frequency.

A great deal of time was spent gathering data on various sensors, especially so-called "smart" sensors. From the vast number of articles on this subject available on the Internet, it seemed reasonable to assume that these sensors are being developed more and more. The integrated sensors used for the deployment of air bags in cars are a good example. These sensors measure the deceleration forces and make a decision as to whether the air bag should be deployed or not within a split second before sending the activation signal to the deployment system. The cost of these sensors have come down to about $10 due to mass production. Wireless sensors are also becoming more and more common and it seems certain that a damage detection technique for fan blades can be developed, knowing that inexpensive transducers are not too far into the future.

Due to the fact that most industries can not afford to make unscheduled maintenance stops, the development of on-line monitoring techniques providing adequate warning of possible failures have become of paramount importance. Failures leading to loss of lives and production can be prevented if these techniques can be developed into reliable and relatively inexpensive solutions.

The feasibility of using vibration-based damage monitoring has been studied in some detail in chapter 1. The next chapter deals with the specific techniques used for damage level monitoring for this project. It became clear at an early stage that it would be necessary to design and build an experimental test structure to facilitate with the development of a damage identification technique. Some of the most important reasons for using an Experimental Fan Blade Damage Simulator (EFBDS) and not the actual fan from industry (such as the FD fan at Majuba) were:

- Most fans in industry can not be switched on and off at will.
- Because of the construction of industrial fans, instrumentation of the blades would have been quite difficult and time consuming.
- The time spend travelling would have been unacceptably much.
- It made sense to develop techniques in an environment that can be controlled to cut down the number of variables that needed to be taken into account.
- In order to test the damage detection techniques the blades would have to be damaged artificially. This would have carried a severe cost and safety penalty if done at a power plant or other industry.
- The minimum of telemetry can be bought because most of the required sensors and measuring equipment are already available in the Gold Fields Dynamics Lab.

After the decision to construct an EFBDS was taken, different concepts were generated, a selection was made and a detailed design done. This also involved the procurement of the necessary telemetry such as the slip ring unit discussed in section 1.5 and the electric motor and control system discussed in chapter 3.

With the EFBDS constructed and assembled, some preliminary measurements were taken followed by a full set of measurements taken at 0, 10, 20, 30 and 40% levels of damage. Statistical techniques were used to determine the required number of data sets that needed to be taken in order to compensate for measuring inaccuracies. All the results found can be seen in Chapter 4. Frequency shifts proved to be a good indicator of blade damage. Time domain damage indicators were also evaluated with a future view for use as features in pattern recognition techniques such as neural networks.

Some of the natural frequencies did not shift by as much as was predicted by the FEMs developed. A postulation that this was due to the global modes of the structure proved to be correct and is discussed in Chapter 5. Final conclusions and recommendations can also be found in Chapter 6.

CHAPTER 2

MODEL IDENTIFICATION STRATEGIES

2.1 Time domain and frequency domain identification

Various methods can be used to identify the natural frequencies present in the Experimental Fan Blade Damage Simulator (EFBDS). The simplest form would be to read the natural frequencies from a power spectral density, or similar frequency domain graph. Since the damage identification method need to be autonomous it was decided early on not to use a technique that depended on a certain amount of human expertise and experience which will certainly be required if a value has to be read of a graph prior to damage identification.

System identification is the field of modelling dynamic systems from experimental data. A schematic representation of a dynamic system can be seen if Figure 2.1. The system is driven by input variables u(t) and disturbances v(t). The user can control u(t) but not v(t). For the EFBDS the inputs are missing. The output signal originates from sensors such as accelerometers and dynamic strain gauges, designed to measure dynamic properties of the system.

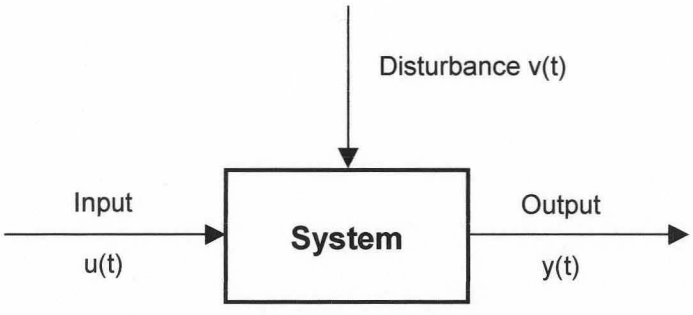

Figure 2.1 Typical example of a dynamic system

Mathematical models of systems are very useful in predicting behaviour of systems and although this is not necessary for this project, it will certainly be of paramount importance when automated detection using neural networks or similar methods are

implemented. Basically, there are two ways to model the EFBDS, mathematical modelling and system identification

- *Mathematical modelling:* This is an analytical approach. Basic laws from physics (such as aerodynamics, Newton's laws etc.) are used to describe the dynamic behaviour of the damage simulator.
- *System Identification:* This is an experimental approach. Some experiments are performed on the system; a model is then fitted to the recorded data by assigning suitable numerical values to its parameters.

Clearly it would have been very difficult to obtain an accurate mathematical model of this particular system due to the many stochastic external forces and complicated boundary conditions. A FEM was constructed that was, in essence, a mathematical model. More detail can be seen in the second part of this chapter.

Various modal identification techniques that require only output data were found in the literature study (Section 1.4). The problem with most of these techniques is that more than one output was required. While this was not an insurmountable problem (the data acquisition equipment used can sample up to four channels at the same time), the actual FD fan at the Majuba power generation fan has 20 blades. Even using one sensor per blade would already result in a huge amount of raw data, not to mention the cost involved (20 blades per fan, twelve fans at plant).

ARMA based curve fitting has been used by various researchers for the identification of modal parameters from output only data (see section 1.4). This algorithm was also readily available as a MATLAB toolbox. A brief description of this model is given below.

ARMAX model

The ARMAX model is short for an ARMA (AutoRegressive Moving Average) with an eXogenous signal (that is a control variable u(t)). A typical description of this model may be found in Torsten *et al. (1989)* and Pandit, (1991) .

Let *y(t)* and *u(t)* be scalar signals and consider the model structure:

$$A(q^{-1})y(t) = B(q^{-1})u(t) + C(q^{-1})e(t) \qquad \textbf{(2.1)}$$

where

$$A(q^{-1}) = 1 + a_1 q^{-1} + \ldots + a_{na} q^{-na}$$
$$B(q^{-1}) = 1 + b_1 q^{-1} + \ldots + b_{nb} q^{-nb} \quad \textbf{(2.2)}$$
$$C(q^{-1}) = 1 + c_1 q^{-1} + \ldots + c_{nc} q^{-nc}$$

The parameter vector is taken as

$$\theta = (a_1 \ \ldots \ a_{na} \quad b_1 \ \ldots \ b_{nb} \quad c_1 \ \ldots \ c_{nc})^T \quad \textbf{(2.3)}$$

The model (2.1) can be written explicitly as the difference equation

$$y(t) = a_1 y(t-1) + \ldots + a_{na} y(t-na) = b_1 u(t-1) + \ldots + b_{nb} u(t-nb) + e(t) + c_1 e(t-1) + \ldots + c_{nc} e(t-nc) \quad \textbf{(2.4)}$$

This model can easily be rewritten in state space format since from (2.1)

$$y(t) = \frac{B(q^{-1})}{A(q^{-1})} u(t) + \frac{C(q^{-1})}{A(q^{-1})} e(t) \quad \textbf{(2.5)}$$

For this structure (2.5),

$$G(q^{-1};\theta) = \frac{B(q^{-1})}{A(q^{-1})}$$
$$H(q^{-1};\theta) = \frac{C(q^{-1})}{A(q^{-1})} \quad \textbf{(2.6)}$$

There are several important special cases for (2.1)

- An autoregressive (AR) model is obtained when *nb*=*nc*=0. In this case a pure time series is modelled, no input signal is assumed to be present. In that case (2.1) reduce to

$$A(q^{-1})y(t) = e(t)$$
$$\theta = (a_1 \ \ldots \ a_{na})^T \quad \textbf{(2.7)}$$

- A moving average (MA) model is obtained when *na*=*nb*=0. Then

$$y(t) = C(q^{-1})e(t)$$
$$\theta = (c_1 \quad \ldots \quad c_{nc})^T \tag{2.8}$$

- An autoregressive moving average (ARMA) model is obtained when *nb*=0. Then

$$A(q^{-1})y(t) = C(q^{-1})e(t)$$
$$\theta = (b_1 \quad \ldots \quad b_{nb})^T \tag{2.9}$$

- Another special case is when *nc*=0. The model structure then becomes

$$A(q^{-1})y(t) = B(q^{-1})u(t) + e(t)$$
$$\theta = (a_1 \quad \ldots \quad a_{na} \quad b_1 \quad \ldots \quad b_{nb})^T \tag{2.10}$$

This is sometimes called an ARX (controlled autoregressive) model.

The AR and ARMAX (reduced to an ARMA model because of the output only data) subroutines were the only models that could be used in the system identification toolbox of MATLAB. The AR model was substantially less expensive computationally but the ARMAX model outperformed the later in terms of accuracy and was chosen instead. Appendix C reviews initial studies done to establish the constraints of the ARMAX model.

2.2 Finite Element Modelling

As described in Chapter 1, the forward frequency problem was often solved with the help of mathematical models of the physical system. Since it is known that only limited success was achieved when frequency shifts has been used to detect damage, it was decided to create a mathematical model to ascertain the viability of using this technique.

Finite element modelling has become a widely used tool in the field of vibration monitoring and damage detection. Various papers make use of FEM only to test damage identification techniques (see Chapter 1). It soon became apparent that the

number of elements used in the mesh, aspect ratio of the elements and element type used, made a substantial difference to the mode shapes corresponding natural frequency. A study to determine the mesh refinement and element type that should be used was therefore undertaken.

2.2.1 Mesh refinement

In order to determine the required mesh refinement to produce accurate results, a simple beam was constructed. In this way the exact natural frequencies could be computed numerically. A summary of the analytical and finite element model results for different meshes and elements can be seen in Table 2.1. The natural frequencies could be analytically calculated as follows:

For free vibration of a uniform beam, the natural frequencies are given by

$$f_n = A_f \sqrt{\frac{EI}{\rho A L^4}} \qquad \textbf{(2.11)}$$

The A_f value change with different boundary conditions. These values were found in Barber (1992).

The methodology to find an analytical formulation such as equation 2.11 can be found in a number of literature sources, Rao (1995) provides a good example.

Interestingly enough, it was not possible to obtain accurate results using first order, 8 node brick elements. Even when a refined, dense mesh was used, the natural frequencies calculated still differed by as much as 15% from the analytically calculated frequencies. The situation deteriorated the higher the natural frequency was. This phenomenon was caused by the inherent stiffness of a first order element. The complex shapes of the actual blades made the use of solid elements desirable. These elements also make the construction of a model simpler.

Results for different mesh refinements and element types can be seen in Tables 2.1 and 2.2. Only in-plane modes were analysed (horizontal and vertical in Figure 2.2).

Basically the 8-node element uses a constant strain integration scheme through the element which causes this element to perform poorly in bending. Since most mode shapes show extensive bending in the vertical or horizontal plane, this made a huge difference when calculating the natural frequencies.

A second order 20-node brick element with mid-side nodes was tested next. This element assumes a linear distribution of strain throughout the element. This allows for an accurate representation of the strain fields in elastic analysis. As a result this element gives almost exact predictions of natural frequencies. Furthermore 27-point Gaussian integration is used for the stiffness calculation, compared to the 8-point Gaussian integration used with the 8-node element.

The reason why the horizontal natural frequencies (see Figure 2.2) were predicted much more accurately with 8-node brick element than the vertical natural frequencies, can be explained as follows: Only about a fifth the amount of beams used through the horizontal cut of the beam were used through the vertical cut. In essence the mesh was more refined in the horizontal direction and it is known that the accuracy of the 8-node beam element increased when the mesh was refined (see Table 2.2).

Table 2.1: Comparison of natural frequencies found for 1m aluminium hinged beam.

Vertical natural frequencies				
Description	**Mode 1**	**Mode 2**	**Mode 3**	**Mode 4**
Analytical values	8.23	52.4	144.3	283.1
8-node, course mesh (760 elements)	13.7	96.9	279.7	551.1
8-node, very fine mesh (4400 elements)	11.3	74.6	211.2	414.8
8-node, good aspect ratio (2000 elements)	8.98	56.2	157.4	308.1
20-node, course mesh (760 elements)	8.23	51.8	144.3	284.6

Table 2.2: Comparison of natural frequencies found for 1m aluminium hinged beam.

Horizontal natural frequencies				
Description	**Mode 1**	**Mode 2**	**Mode 3**	**Mode 4**
Analytical values	74.1	472	1299	2548
8-node, course mesh (760 elements)	70.4	425	1127	2277
8-node, very fine mesh (4400 elements)	70.3	425	1128	2300
8-node, good aspect ratio (2000 elements)	74.0	447	1189	2370
20-node, course mesh (760 elements)	74.1	447	1190	2400

Clearly, it was also of paramount importance that a good aspect ratio was used throughout. Even though a very fine mesh of 4400 elements was used at one stage, a mesh with only half that number of elements gave much closer results to the analytical solution because the aspect ratio was kept within the guidelines of good meshing. The quadratic element was not effected as much by a bad aspect ratio because of the linear distribution of strain used for this element.

A graphical presentation of Table 2.1 and 2.2 can be seen in Figures 2.3 and 2.4 respectively. Clearly a FEM can give grossly inaccurate results if meshing and element choice are not done with care. Predicted natural frequencies were in error by up to 90% when a coarse mesh with a bad aspect ratio was used. This was largely due to the linear strain distribution used for an eight-node brick element. Very accurate predictions regarding natural frequencies could be made even when a coarse mesh with a bad aspect ratio was used and the quadratic element was used.

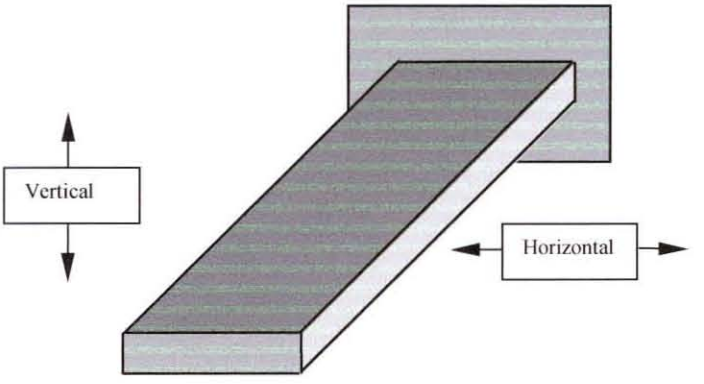

Figure 2.2: Schematic representation of test beam used for FEM testing

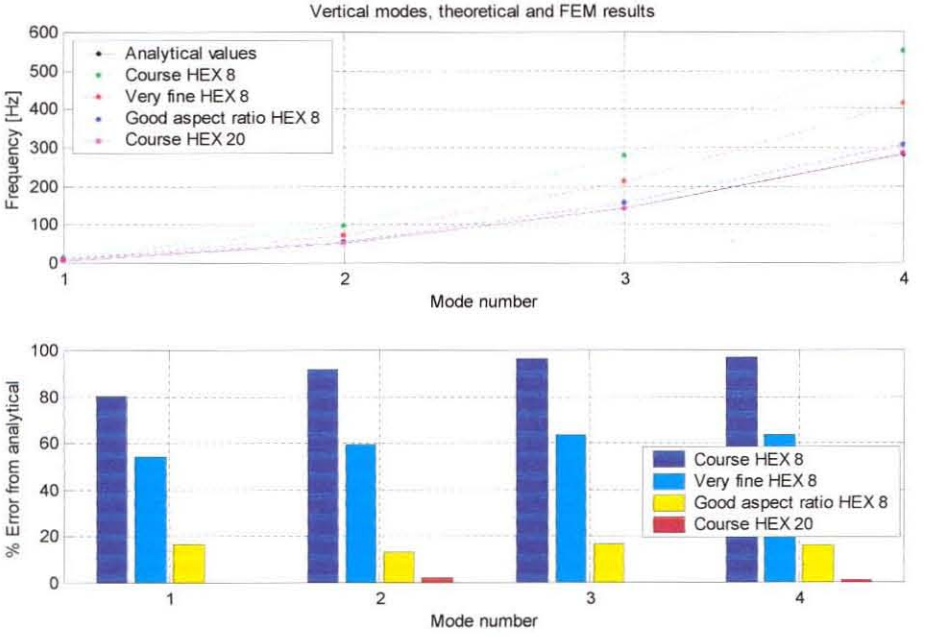

Figure 2.3: Graphical presentation of Table 2.1

The 20-node brick element was substantially more expensive computationally. This was because of the triquadratic interpolation used by the second order element together with the 27 point Gaussian integration for the stiffness of the element. The 8-node brick element use trilinear interpolation functions and 8-point Gaussian integration. In order to get the same accuracy for the mode shape frequencies, the mesh had to be so much refined that computational time actually became unacceptably high and the analysis was stopped before completion.

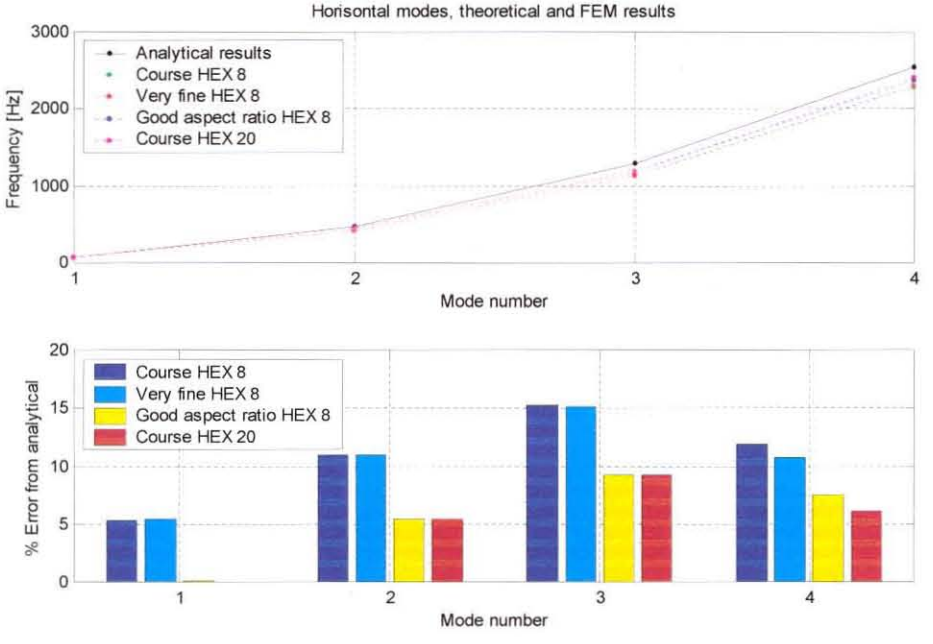

Figure 2.4: Graphical representation of Table 2.2

2.2.2 Modelling of experimental fan blade damage simulator

After guidelines for the accurate modelling of blade like structures had been established, a model of one blade of the experimental fan blade damage simulator was constructed. An important difference between the stationary beams analysed in the previous section and a fan blade, is the centrifugal acceleration imposed on the blade. Fortunately, modern Finite Element (FE) software allows these boundary conditions to be added with relative ease. For accurate results it is however, necessary to use load steps since an iterative approach to finding the updated stiffness matrix for a centrifugal load is used by most software. Five consecutive analyses were therefore performed starting at one fifth the rotational velocity.

As a first attempt, a very simple clamped beam with the same dimension as the actual blade was modelled. Natural frequencies found by means of the FEM are compared to the frequencies found experimentally in Table 2.3. The fifth mode shape can be seen in Figure 2.5.

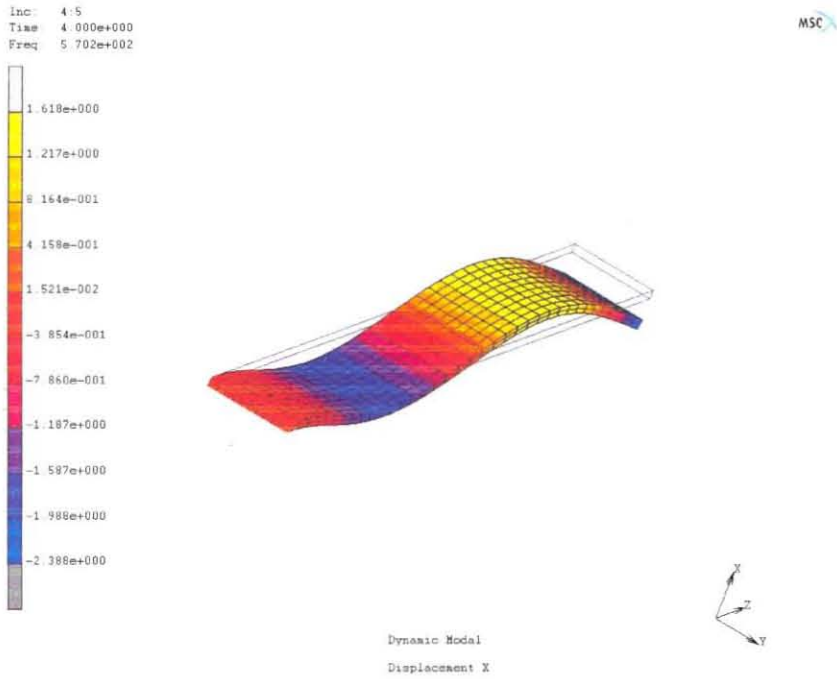

Figure 2.5: Simple FEM used as first iteration.

Table 2.3: First FEM results compared to experimental results.

Mode number	FEM value	Experimental value
1	36.63	33.41
2	205.4	203.3
3	319.6	285.5
4	441.9	447.3
5	572.9	563.5

While reasonable accuracy was obtained, even better overall results were found when the FEM was slightly modified to more accurately resemble the experimental fan blade damage simulator. An example of this model can be seen if Figure 2.6. Results for the natural frequencies found can be seen in Table 2.4.

The purple areas at the base of the blade in Figure 2.6, represent the boundary constraints that was imposed. These nodes were constrained in the x, y and z directions. The experimental and FEM results can be seen in Table 2.4

Table 2.4: More accurate FEM results compared to experimental results.

Mode number	FEM value	Experimental value
1	34.53	33.41
2	202.4	203.3
3	285.2	285.5
4	435.1	447.3
5	562.8	563.5

Fig 2.6: More accurate FEM for fan blade damage simulator.

While some difference still existed between the finite element model and the experimentally obtained results, the prediction was fairly good overall. The results obtained in all Finite Element Analyses (FEA) were at 750 r.p.m. as were the results obtained during experimental measurements. The reason for the inaccuracy of the fourth (first torsional) mode shape were the inconsistency of welds found in the EFBDS. Figure 2.7 shows a close up of the root of the blades used in the EFBDS.

The next step was to introduce artificial damage to the finite element model that would be representative of the damage induced on the EFBDS.

2.2.3 Damage modelling using FEM

During recent years finite element modelling has become a very attractive method for simulating real life systems. This is mostly due to the fact that very fast, relatively inexpensive desktop computers can now be used to run the packages. MSC Marc can for example model the very complicated behaviour of fatigue cracking. While

these modelling tools can never replace experimental measurements and do not give exact answers, it can save a substantial amount of time and money.

In this specific case, the object was not to compute the exact stress concentration and fatigue life of the blade. If this could be done with any degree of accuracy, a monitoring technique would not be necessary, provided no external influences that could damage the blade (such as debris) are present. Due to the nature of the damage induced by a fine hack saw (see Figure 2.7) stress concentration factors and other fatigue information for the material are not required. This method of inducing damage does provide near crack like behaviour for the dynamics of the system (Cawley and Ray 1988). Basically there are three methods with which the damage done to the EFBDS can be modelled:

- Nodes can be untied from each other on the cut surface.
- The modulus of elasticity can be decreased in the neighbouring elements
- Elements can be removed. This requires a very fine mesh however and is not a practical option.

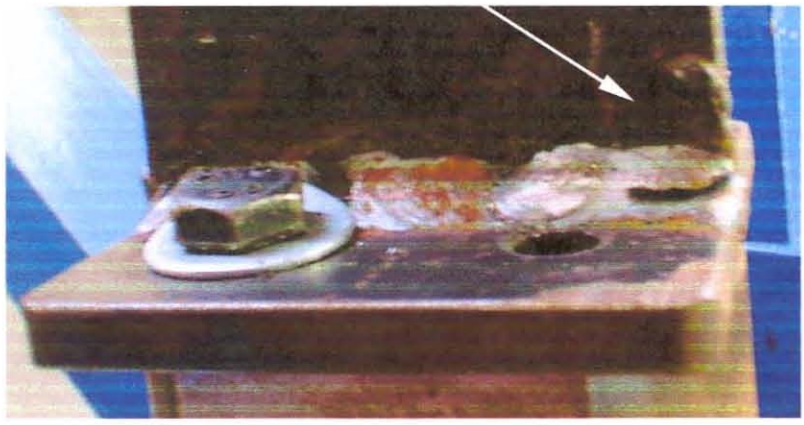

Figure 2.7: 15% Damage inflicted by using a fine hack saw.

The first two options provided simple and effective solutions to the problem. Since the actual damage induced on the EFBDS consisted of using a fine hacksaw to saw through part of the blade at the root, disconnecting the nodes provided an accurate representation of the damage. The exaggerated movement of the FEM model can be seen in Figure 2.8. Disconnecting the nodes allow the faces to move through each other. While it did not model an actual crack well, it was an accurate depiction of EFBDS.

When the modulus of elasticity was adjusted for damage it was found that although the model could be optimised to give very close to the same results as were found

experimentally, the general trend with increasing damage was substantially worse. For the case of modelling an opening and closing crack, this method could work very well since a non-linear modulus of elasticity with a normal modulus in the closing direction and a reduced modulus in the opening direction could be used.

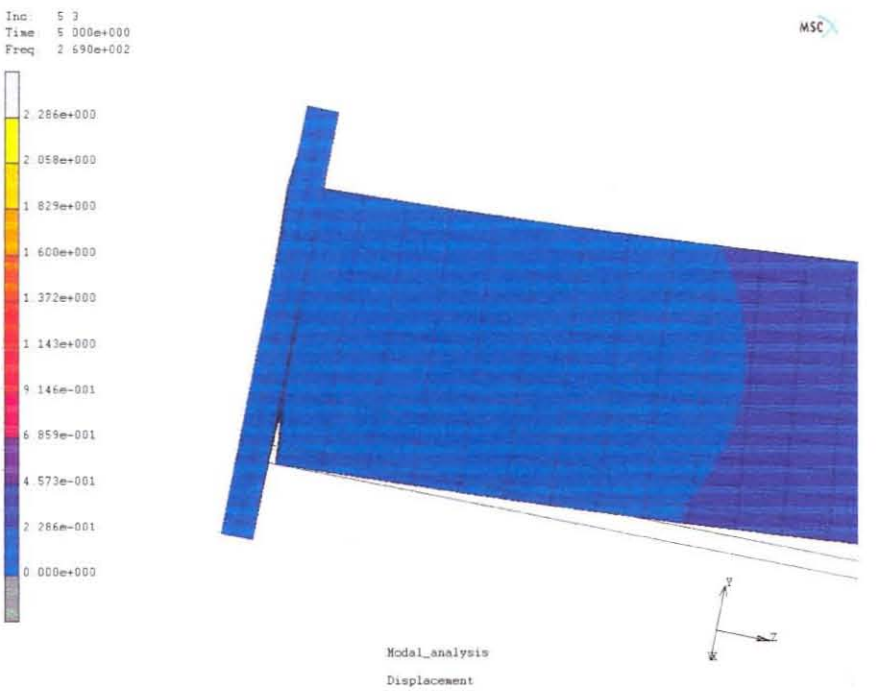

Figure 2.8: Exaggerated movement of FEM model with a 30% crack.

When the model was optimised as far as possible to give results very close to the undamaged experimental frequencies found, nodes were untied and modal extraction performed. The results for various damage levels are shown in Figure 2.9.

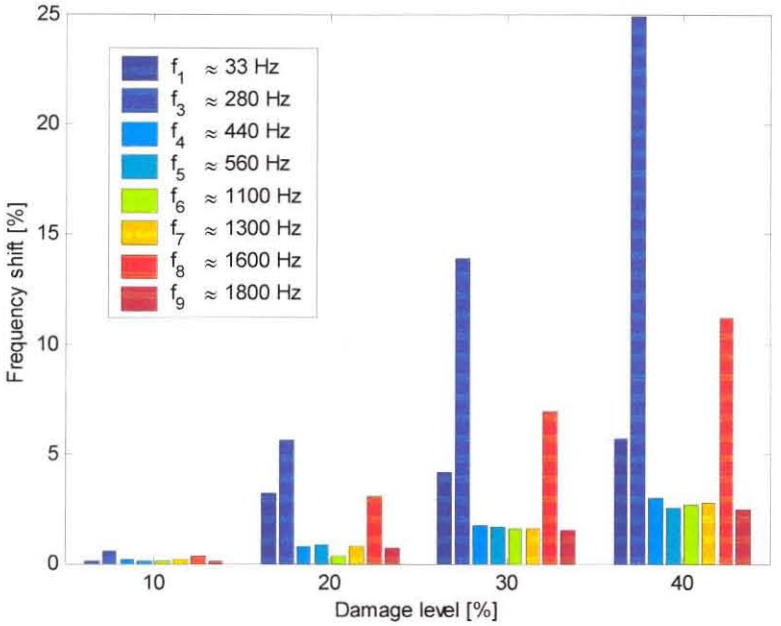

Figure 2.9: FEM results for increasing damage levels at different natural frequencies.

As can be expected, the shift showed an exponential trend as more damage was induced. Although the first frequency seemed to be a relatively good choice, it had to be remembered that a frequency shift of 2.5% means that the frequency change from around 34.5 Hz, to 33.6 Hz. Due to electrical noise, drift and other external influences some measurement error can be expected. Furthermore the resolution with which frequencies were measured was generally about 0.33 Hz due to the discrete nature of peak picking algorithms. This represents a 1% error at 34 Hz but only 0.1% at 280 Hz. The obvious frequency to use would be the one found at 280 Hz.

The second natural frequency showed very little promise as a damage indicator and was not used at all. This turned out to be the case for the EFBDS as well. The experimental results can be seen in Chapter 4.

2.2.4 Results for curved blade

For various reasons described in Chapter 1, it was decided to use an EFBDS to develop a damage detection method. Since this project may be expanded to include the FD and ID fans found at the Majuba power plant, it was decided that a FEM would be used to show that the techniques used for a simple blade on the EFBDS also apply to more complex curved blades which is found more often in practice.

A single blade with very close to the same dimensions as that found on an actual blade on a FD fan was modelled using MSC MARC. The boundary constraints used for this model can be seen in Figure 2.10.

Figure 2.10: Boundary conditions (purple) for the FEM of the FD-fan blade.

The crack can propagate from the trailing edge of the blade or from the leading edge. Both these scenarios were modelled using suitable FEM models. While the computer time for the simple T-blade given in the previous section was typically seven minutes, the curved blade took around 70 minutes. The results for the trailing edge crack can be seen in Table 2.5 and the leading edge in Table 2.6. The reason for choosing 16%, 23% and 33% for the trailing edge and 12%, 21% and 31% for the leading edge is the discrete nature of the FEM. Since nodes were untied to simulate damage and the airfoil section is not symmetrical, different areas are effectively damaged.

Table 2.5: Frequency shifts due to trailing edge cracks.

Mode number	0% damage	16% damage	23% damage	33% damage
1	23.67	23.35	23.17	22.92
2	100.7	96.94	91.49	81.49
3	111.1	106.8	104.1	101.3
4	141.3	140.5	140.1	139.9
5	262.4	259.6	258.7	256.8
6	409.8	407.6	405.8	402.3
7	492.9	488.1	485.8	482.0
8	666.0	652.8	639.8	619.6
9	697.1	691.7	686.9	678.6
10	783.2	777.4	774.3	767.2
11	982.2	975.9	969.9	957.6

Table 2.6: Frequency shifts due to leading edge cracks.

Mode number	0% damage	12% damage	21% damage	31% damage
1	23.67	23.51	23.28	22.86
2	100.7	100.2	99.0	90.64
3	111.1	108.1	103.0	98.83
4	141.3	140.4	139.2	136.7
5	262.4	260.5	258.0	254.7
6	409.8	408.2	405.4	399.9
7	492.9	490.4	487.1	481.6
8	666.0	658.1	646.4	625.3
9	697.1	693.8	688.2	677.9
10	783.2	779.7	775.8	770.0
11	982.2	977.8	970.9	957.0

A comparison of the crack locations can be seen in Figure 2.11.

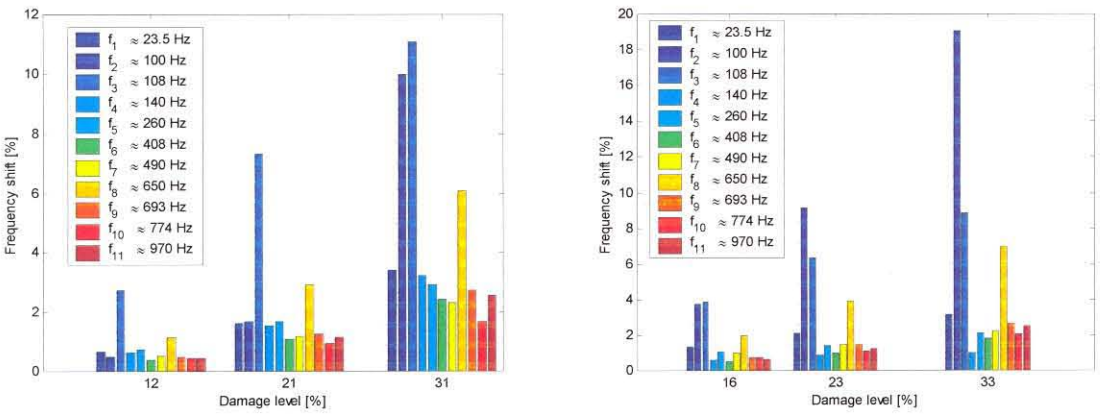

Figure 2.11: The leading edge can be seen on the left while the trailing edge van be seen on the right.

Again, some of the modes were more susceptible to damage than others. The obvious choices here would be the second, third or eighth mode shapes. The accuracy with which the various mode shapes can be measured and the potentially global nature of some of the mode shapes will make it necessary to create a more detailed finite element in conjunction with preliminary measurements on the actual blades to determine the accuracy of the FEM model.

Some of the mode shapes found during the FEA can be seen in Figures 2.12 and 2.13. Because of the airfoil cross-section of the blade, it was not easy to intuitively decide what shapes would be found. The placement of sensors for optimal sensitivity with regard to two or more mode shapes could be done by studying these findings. Chapter 5 deals with the phenomenon of global and local mode shapes.

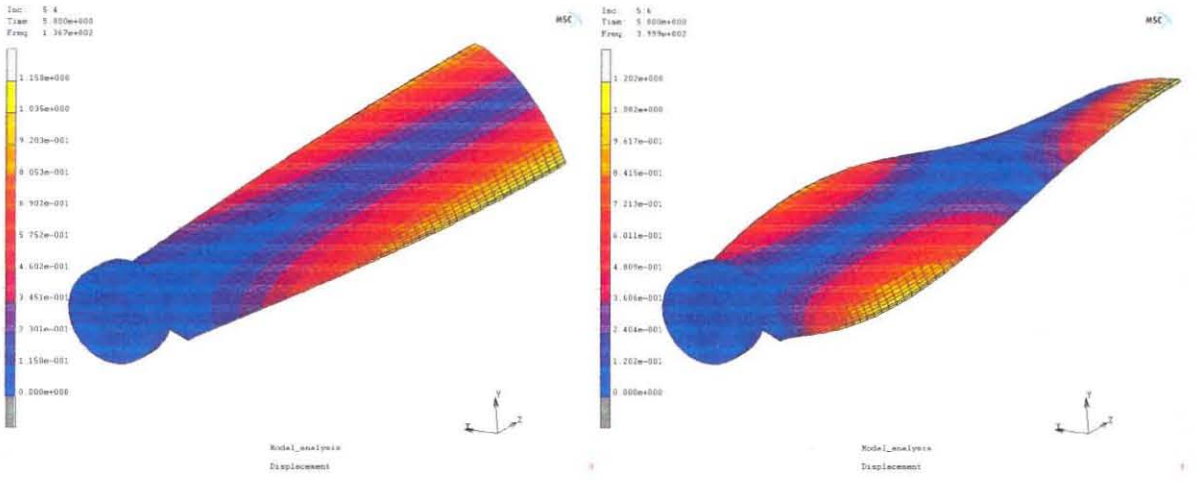

Figure 2.12: The fourth (left) and sixth (right) mode shapes for a curved blade.

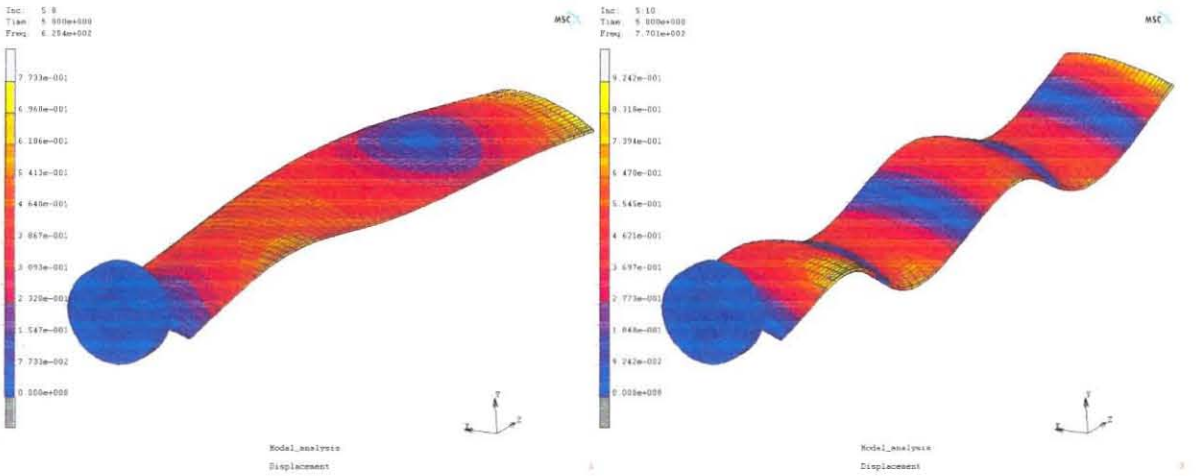

Figure 2.13: The eighth (left) and tenth (right) mode shape for a curved blade.

The contour bands in Figure 2.12 and 2.13 represent scalar displacement of the blade. These displacement plots could be used to determine the optimal location for the placement of accelerometers. This was not necessary for the simple blade used by the EFBDS since both the mode shapes used (first sideways, Figure 2.8 and first torsional) for damage level detection caused maximum strain and movement at the same location. If a high number of frequencies are to be used however, this situation may change and an optimal location can then be found by mathematical optimisation.

2.3 Conclusion

A model identification strategy that would provide modal parameters (natural frequencies) was selected in this chapter. Furthermore a FEM of the fan blade damage simulator used to develop a damage detection technique for fan blades was developed. FEA showed that the frequency shifts due to simulated damage should be significant enough to detect using natural frequencies only as a damage indicator.

It was also found that FEM packages such as MSC MARC gave very good correlation with both analytical results and experimental results. A model that closely resembles the blades found on the FD fan at the Majuba power generation plant was also developed. This model showed similar trends regarding frequency shifts with increasing levels of damage. The following were the most interesting:

- Although the asymmetric nature of the airfoil section does not lend itself to a sideways mode shape, the nearest comparable mode shape was also very sensitive to damage.
- Sensitivity differed depending on whether the crack was introduced on the leading or trailing edge, this could complicate experimental classification of damage.
- Because the actual FD blades are physically larger than the EFBDS blades, the natural frequencies are a lot lower. This implies that a lower sampling frequency can be used. A lower sampling frequency means less data needs to be processed and lower order ARMAX models can be used.

Provided good experimental results could be found, there was every reason to believe that a damage detection technique for fan blades could be developed both for the EFBDS and actual fan blades in industry.

CHAPTER 3

EXPERIMENTAL FAN BLADE DAMAGE SIMULATOR

As discussed in Chapter 1, it became clear at an early stage that it would be necessary to design and build an experimental test structure to facilitate the development of a damage identification technique. Cost and safety aspects make it impractical to develop such a technique on a fan in industry. The design and construction of the EFBDS from scratch took time, effort and a large amount of the available funds, but provided an excellent tool for the development of a damage identification technique. There would also not have been any way to know exactly what was required for a successful identification to be done. As mentioned in Chapter 1, a scanning laser vibrometer would be an ideal sensor, the cost of around 80 000 US $ was prohibitive however.

3.1 Design issues

In order for a technique, that can be used on fans such as FD fans, to be developed, the most important design aspect would be that results obtained from the experimental fan must be representative of FD fans. The EFBDS had to comply with the following specifications:

- Only ambient agitation should be used to excite the system.
- The blades should be attached to the structure in a similar way as that used on the FD fans.
- Variable speed should be available to proof that the technique works at any rotational speed. The EFBDS is roughly one fourth the size of an ID fan and the dynamics of blades change due to centrifugal acceleration. Different dynamics can be simulated by using different rotational speeds.
- The fan blades should have roughly the same aspect ratio as the existing blades.
- Should provide for growth in future research.

It was recognised at an early stage that it would not be possible to develop a damage detection technique and implement it on the actual structure within the time con-

straints of a masters degree. For this reason the simulator was given a modular design to facilitate further research.

3.2 Concepts and selection

3.2.1 Blade attachment

One of the most important aspects of the axial flow fans used at Majuba are the variable pitch blades used. Because of this arrangement, the hub is not a simple construction and takes up a relatively large percentage of the total diameter. Various methods for attaching blades with variable pitch were looked at. The most important and practical concepts are discussed below.

Wedge blocks

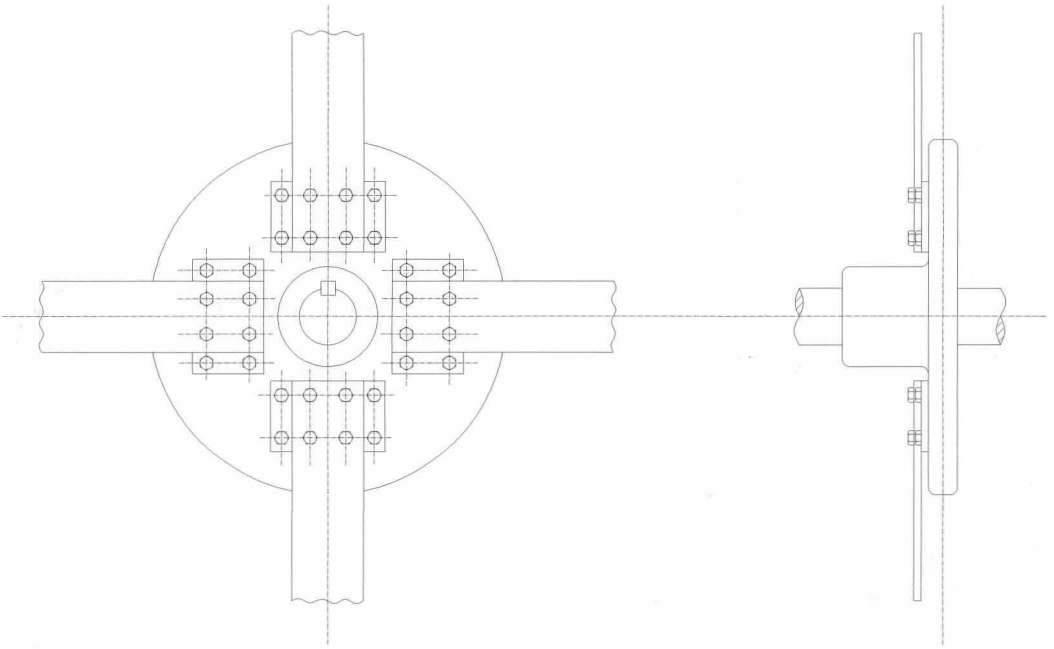

Figure 3.1: Wedge block schematic assembly drawing

The first method considered for adjusting the pitch of the blade made use of different wedge blocks. Each block would then represent a specific pitch. A schematic representation of the hub- and blade interface can be seen in Figure 3.1.

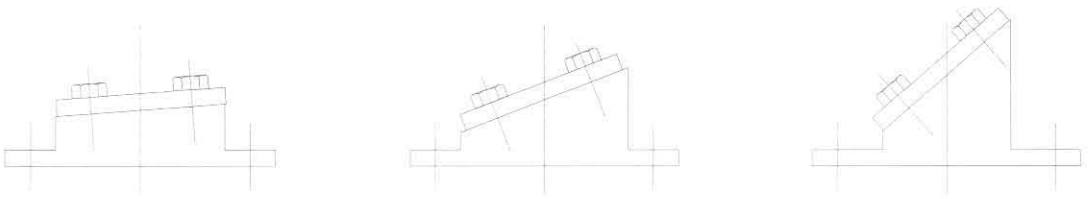

Figure 3.2: Different pitch angle configurations for the wedge block concept

Examples of the different wedge blocks that would be required can be seen in Figure 3.2.

Advantages of this concept was:

- Simple construction and machining.
- Relatively simple to change the pitch.
- All blades will have the same pitch angle.

Disadvantages was:

- A whole range of wedge blocks needed to be manufactured.
- Limited number of pitch angles available.
- Due to the space the wedge blocks occupied, the number of blades would probably have been restricted to four at most.
- The shear forces on the bolts that attached the blade to the hub may result in inaccurate frequency measurements at different fan speeds. Furthermore it did not represent the actual fan blades well.

Clamped blades

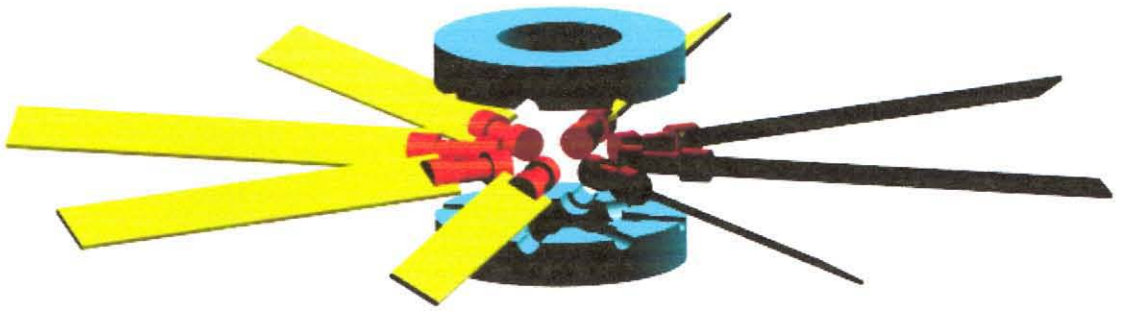

Figure 3.3: Clamped blades schematic concept drawing

To get around the problems of the wedge block concepts, the next concept looked at, was optimised for using the minimum space to hold blades, while offering a very wide range of pitch angles. A schematic three-dimensional representation of this concept can be seen in Figure 3.3. Some sort of indexing mechanism would off-course have to be employed to ensure that all the blades were at the same pitch for a particular measurement.

Advantages:

- More compact, can accommodate more blades if necessary.
- The blade attachment can be made to represent the actual fan blades more accurately.

Disadvantages:

- Very difficult to assemble and machine this concept.
- Some sort of an indexing mechanism would have been necessary to ensure the blades were all at the same pitch.

This concept presented a much more realistic approach for the fan blade damage simulator. The final development model was therefore an extension of this concept.

Inserted blades

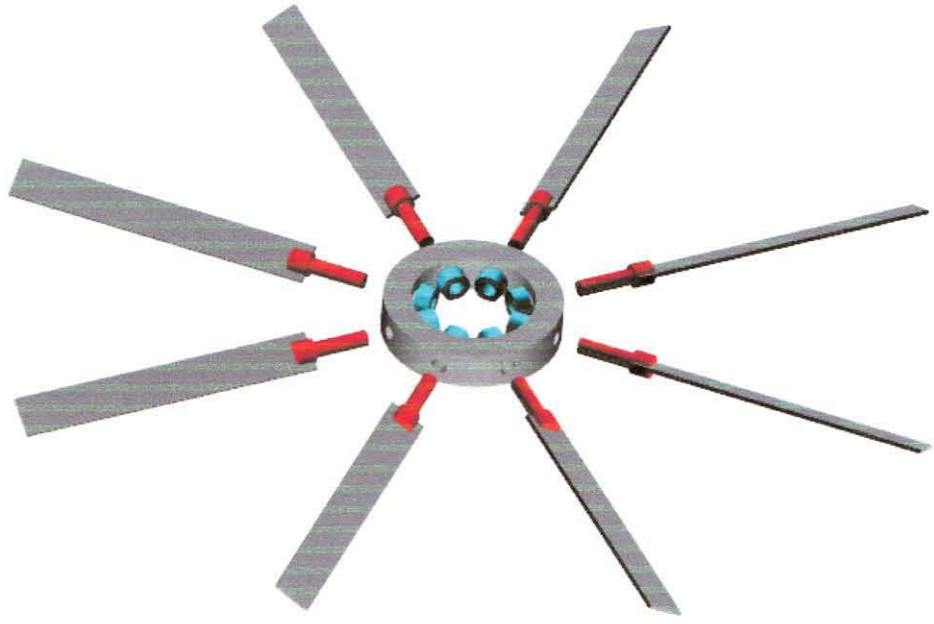

Figure 3.4: Inserted blades concepts

By keeping the blade seat interface as simple as possible to manufacture without loosing the advantages of the above concept, a concept using a solid ring with inserted blades was developed.

Clearly an indexing mechanism would also be needed for this interface. Since the blades can be inserted one at a time, this should not be a big problem.

Advantages:

- Compact, can accommodate more blades as necessary.
- Very close to the method used to fix the blades on the FD fan at Majuba.
- Relatively easy to change the pitch of the blades.
- Machining and assembly easier than clamped blades concept.

Disadvantages:

- Indexing mechanism will be necessary.
- All the force due to centrifugal acceleration has to be carried by the bolt and nut.

In the end this concept was developed into a final design for the interface between the blades and the hub. The final design can be seen in the section 3.3. of this chapter.

3.2.2 Drive design

To make it possible for the fan to be tested in an easily accessible location, it was decided not to use three-phase power. As a result the choice of a speed controlled electrical motor was limited to around 1.5 kW. More detail on the electric motor and speed control unit as well as the reasons for these choices follow in the next section.

The model was planned to be about a quarter scale model. To check whether the 1.5 kW motor would be adequate a simple calculation was done to calculate the amount of power 8 blades rotating at around 750 r.p.m. would absorb.

The following assumptions were made:

- Force on the blade was only due to the conservation of momentum
- Since air leak around the edges of the blade and a component flows in a radial direction along the blade the force was taken as around 60% of the computed force. This Figure corresponds to the efficiency of a fan with straight, simple blades (Osborne, (1977)).

- Compressibility of air was not taken into account.
- Blades do not influence one another.

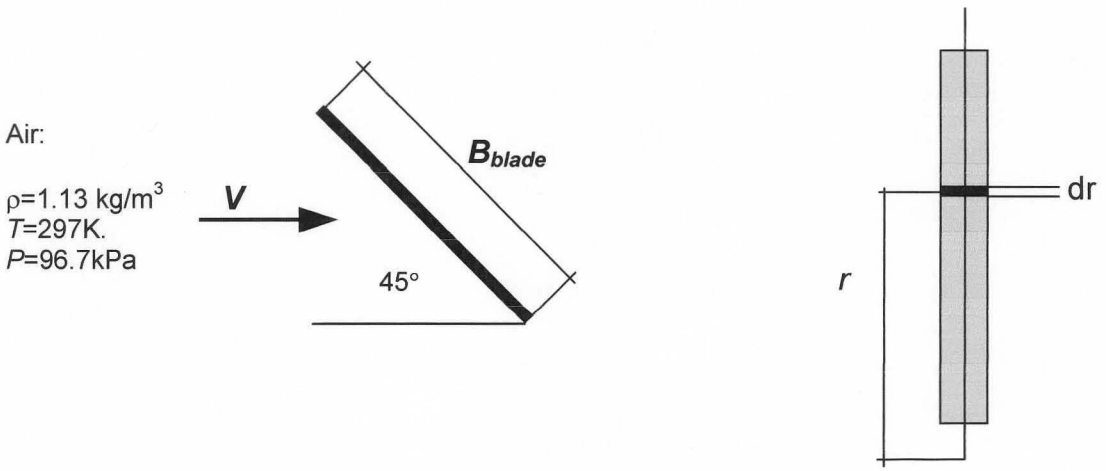

Figure 3.5: Schematic of simple blade moving through air

With reference to Figure 3.5 the mass flow of air was calculated as

$$\begin{aligned} M_{air} &= \rho A v \\ &= \rho \omega r B_{Blade} \sin 45^{o} \, dr \end{aligned} \tag{3.1}$$

$$\rho = 1.13 kg / m^{3}$$
$$A = (B_{blade}) \sin(45^{o}) dr$$
$$v = \omega \cdot r$$

The force acting on a finite section of the blade *dr* can then be calculated as

$$\begin{aligned} F_{Blade} &= M_{air} v \eta \\ &= \eta \rho \omega^{2} r^{2} B_{Blade} \sin 45^{o} \, dr \end{aligned} \tag{3.2}$$

The total moment on the shaft due to a single blade can then be calculated as

$$\begin{aligned} M_{shaft} &= F_{Blade} d \\ &= \eta \rho \omega^{2} r^{2} B_{Blade} \sin 45^{o} \, dr \int_{\text{Blade root radius}}^{\text{Blade tip radius}} r^{3} dr \end{aligned} \tag{3.3}$$

The power absorbed by a blade can then be calculated at 750 r.p.m. (ω=78.54 rad/s)

$$\begin{aligned} P_{Blade} &= M_{blade}\omega \\ &= \eta\rho\omega^3 B_{Blade} \sin 45^o \left[\frac{r^4}{4}\Big|_{0.15}^{0.485}\right] \\ &= 159W \,/\, blade \end{aligned} \qquad \textbf{(3.4)}$$

For eight blades this equates to 1.253 kW. A 1.5 kW motor would therefore be adequate. For reasons of simplicity and flexibility it was decided to use a belt drive. The main reasons were:

- The frame design was simplified since alignment of the motor with the shaft of the fan was not as important as it would have been with an inline shaft connection.
- The speed ratio between the motor (1450 r.p.m.) and the fan (750 r.p.m.) can easily be adjusted by using different pulley sizes.
- Centre of gravity of the structure is lower and a more sTable structure was the result.

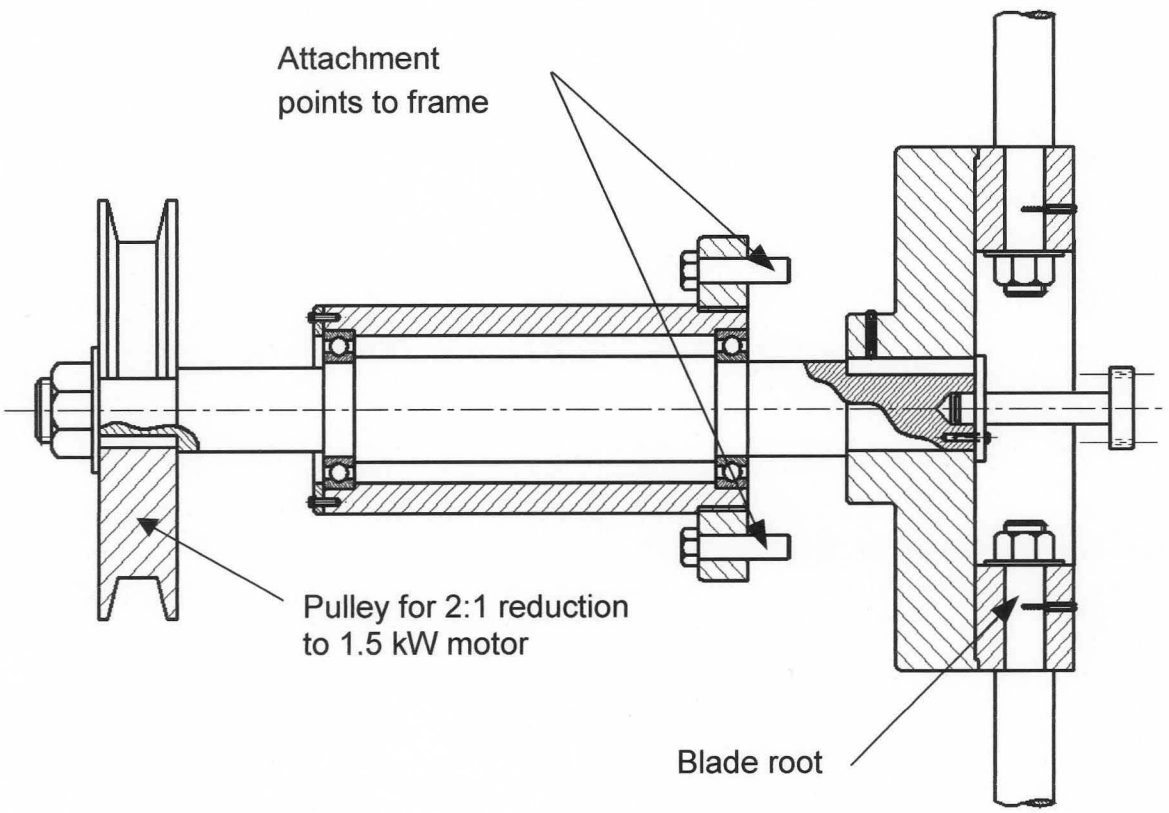

Figure 3.6: Final concept configuration before design refinements had been implemented

The fan belt- and bearing design was done according to the manufacturer's catalogues.

3.2.3 Final design

With the general layout of the fan and the methods for attaching blades decided on, various small changes had to be made to facilitate the manufacturing of the components. A schematic representation of experimental fan blade damage simulator can be seen in Figure 3.7.

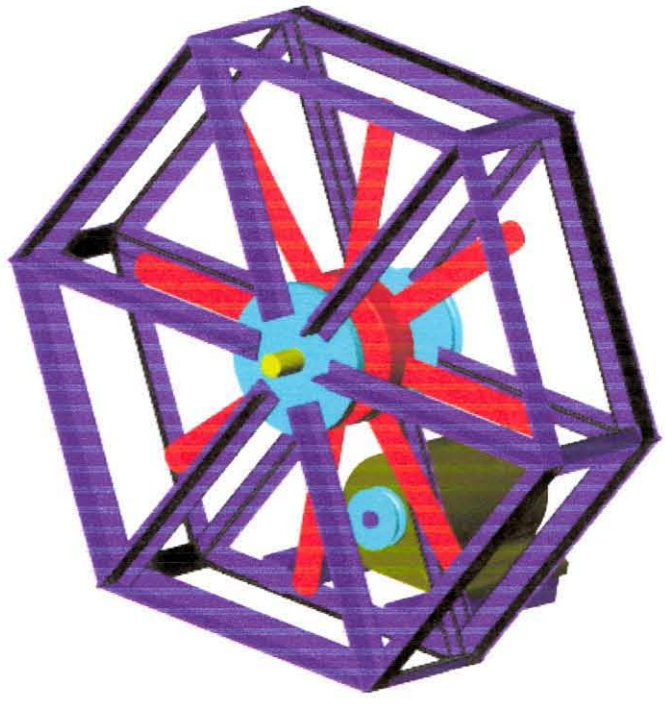

Figure 3.7: Schematic drawing of the final design of the fan

Most of the detailed manufacturing drawings are not included in this thesis since it had no real relevance on the outcome of the experiments. The blade seats and attachment to the hub are of some importance however and is shown in Figure 3.8 and 3.9.

With reference to Appendix B, it can be seen that the interface decided on was very similar to the actual fan found at the Majuba power plant. Because of the ability to change the pitch of the blade, the stiffness of the rotational axis around which the pitch was adjusted is not as high as the stiffness in the translation directions.

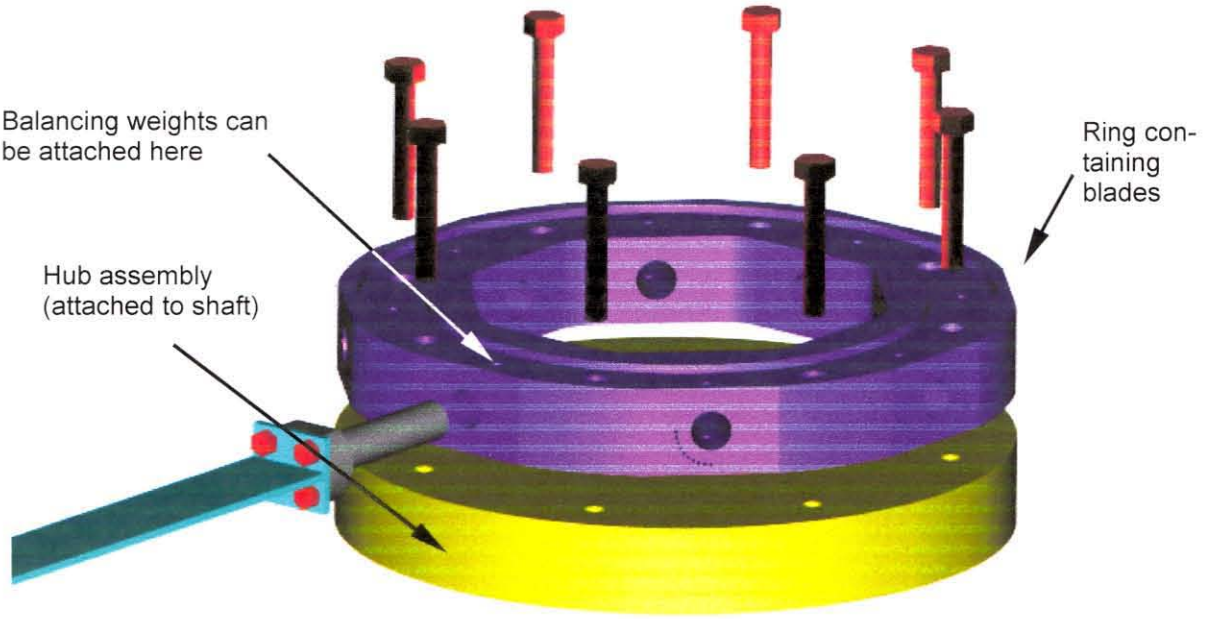

Figure 3.8: 3D representation of blade, hub interface

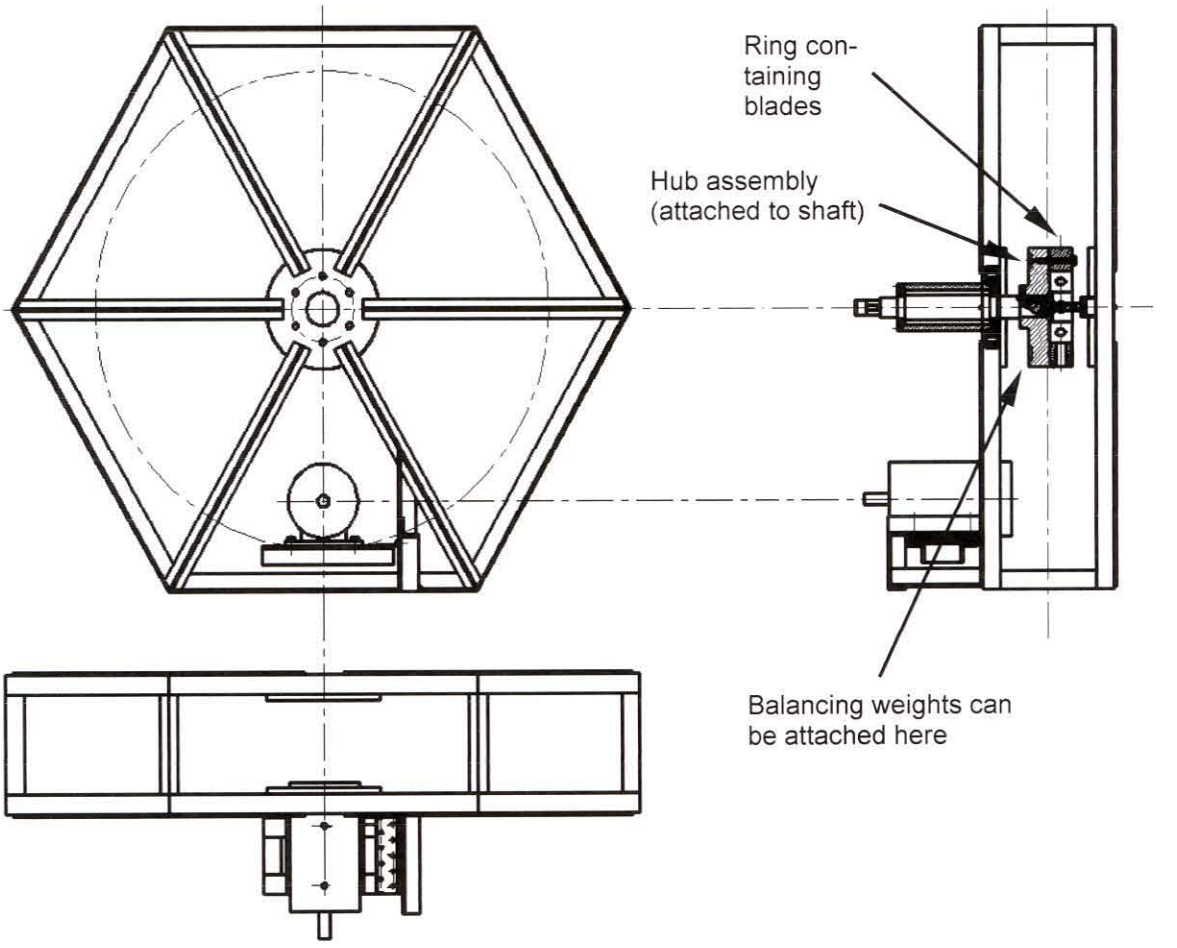

Figure 3.9: Assembled drawing (Blades excluded)

3.3 Manufactured fan blade damage simulator

As mentioned earlier in this chapter, the decision to install the EFBDS in an easily accessible location limited the power supply to single phase 220 V. While DC motors with a 1.5 kW rating do exist and excellent speed control can be applied to the motors, the total cost was approximately three times higher than an induction motor with an electronic speed control unit. The specifications for the speed controller can be seen in Table 3.1. The speed controller can run of a single phase 220 V supply. By varying the output frequency of the three-phases provided by the controller, the rotational speed of the induction motor can be selected.

The speed control unit used to control the three phase 1.5 kW electric motor can be seen in Figure 3.15.

Table 3.1: Specifications of speed controller

AC Tech Variable Speed AC Drive SF 100 series	
Storage Temperature	-20°C to 70°C
Ambient Operating Temperature	0°C to 50°C
Ambient Humidity	< 95% (non-condensing)
Maximum Altitude	3300ft (1000m) above sea level
Input Line Voltages	208/240 Vac
Input Voltage Tolerance	+10%, -15%
Input Frequency Tolerance	48Hz to 62Hz
Output Wave Form	Sine Coded PWM
Output Frequency	0-240Hz
Service Factor	1.00
Efficiency	Up to 98%
Power Factor	0.96 or better
Overload Current Capacity	150% for 60 seconds, 180% for 30 seconds.
Speed Reference Follower	0-10 VDC, 4-20mA
Control Voltage	15 VDC
Power Supply for Auxiliary Relays	50 mA @ 12 VDC
Analog Outputs	0-10 VDC proportional to frequency or load
Digital Outputs	Open collector outputs: 50 mA @ 30 VDC

Before measurements could be taken on the EFBDS, the ring containing the blade seats had to be aligned with the hub assembly (see Figures 3.8 and 3.9). Balancing surfaces provided on the hub assembly proved unnecessary as the first rotational frequency fell well below the first natural frequency and was filtered out using a high pass filter. In addition, the unbalance was relatively little and did not appear to influence measurements significantly.

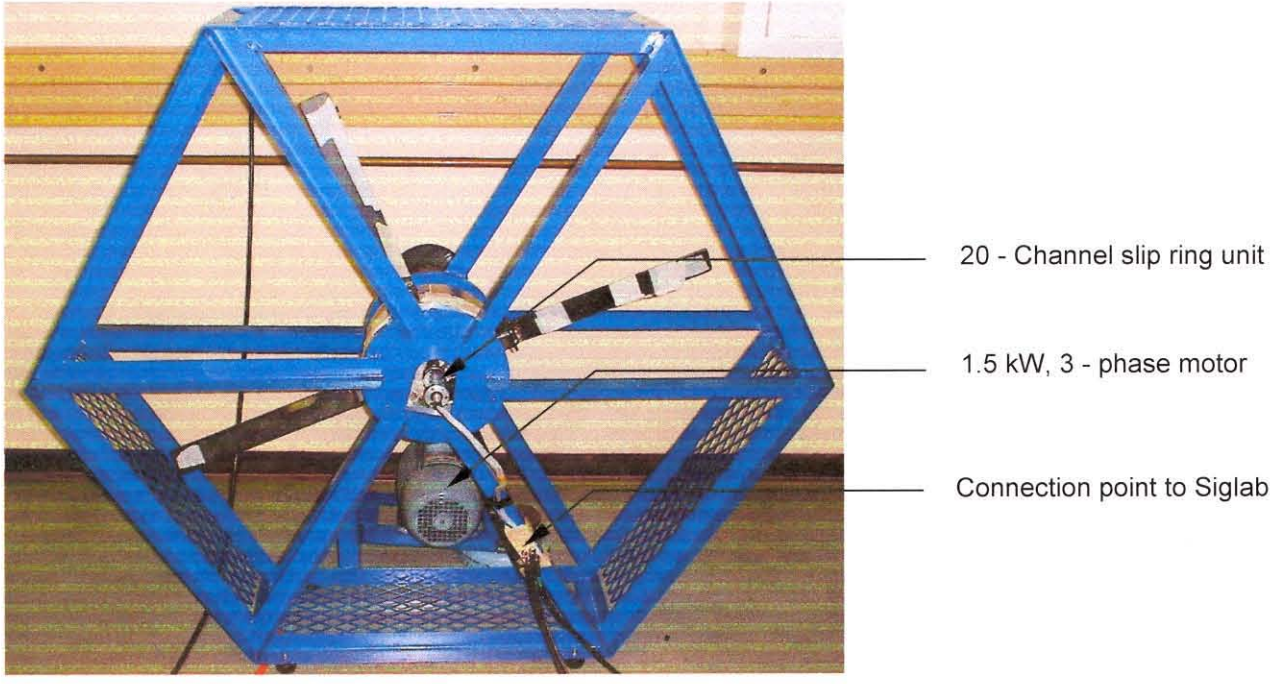

Figure 3.10: Experimental fan blade damage simulator

The completed experimental fan blade damage simulator can be seen in Figures 3.10 through 3.14.

Figure 3.11: Side view

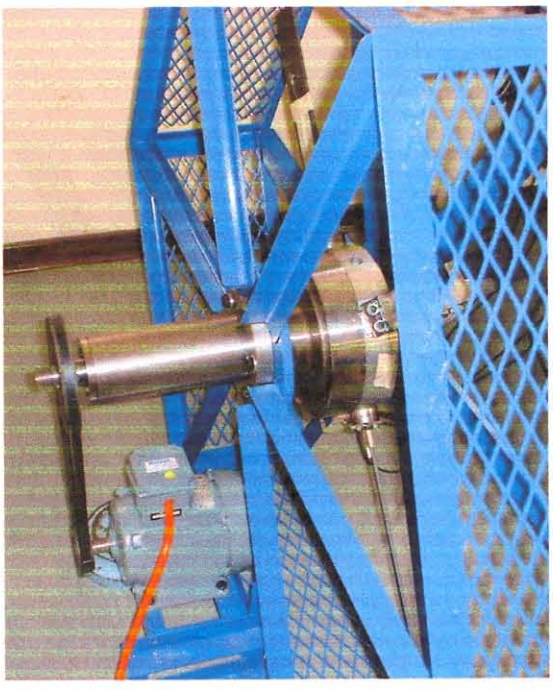

Figure 3.12: Rear view

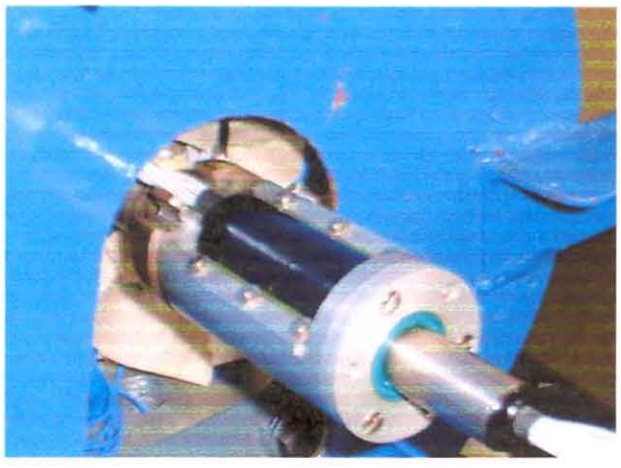

Figure 3.13: Close up of 20 – channel slip ring unit

Figure 3.14: Close up of the blade seat and attachment

The method with which the blades were attached to the blade seats can clearly be seen in Figure 3.14. This was a good simulation of the way in which the actual fan blades at Majuba are attached. Figure 3.13 show the 20–channel slip ring unit. Specifications can be seen in Table 3.2. The unit made use of gold alloy brushes and slip rings to transfer power to the various transducers and measure the output.

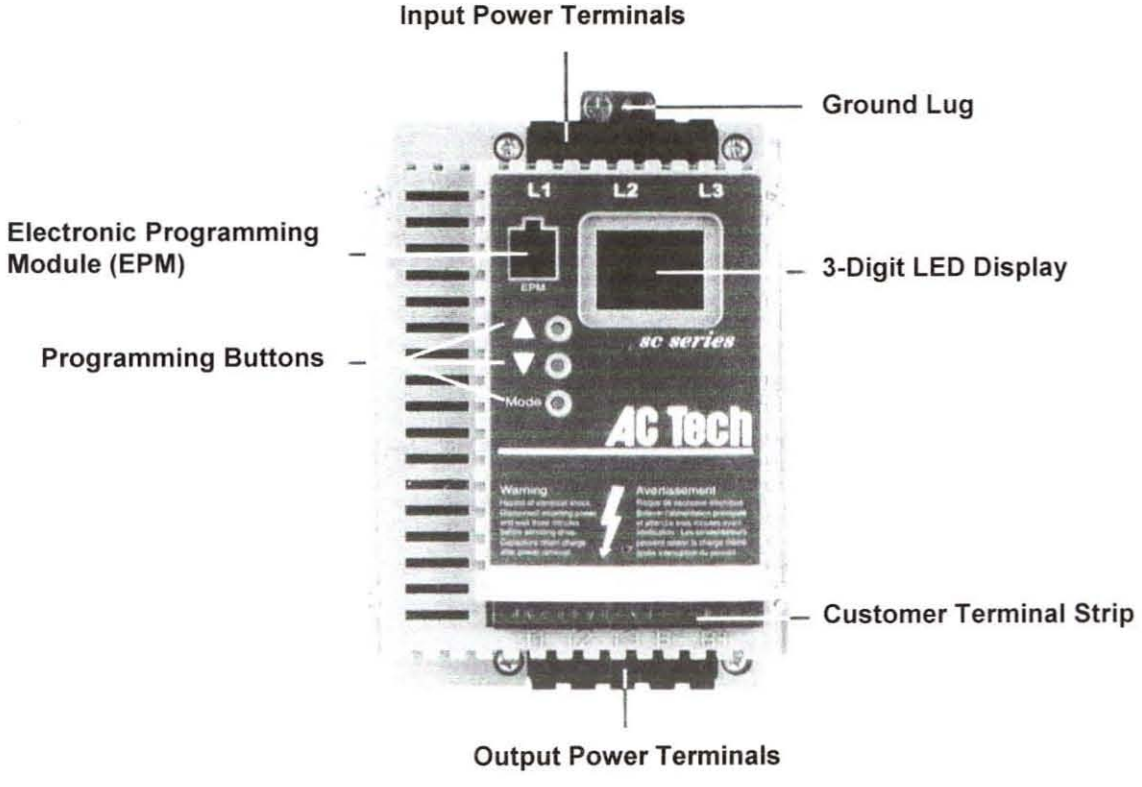

Figure 3.15: The speed controller used for the 1.5 kW 3-phase motor

Table 3.2: Specifications of the 20 – channel slipring unit

C-series slip rings (C-20)	
Current (continuous)	2.6A per circuit
Current (peak)	4A per circuit for 10 seconds
Voltage	200 VDC
Insulation resistance	> 200 MΩ at 500 VDC
Contact resistance	< 20 mΩ
Recommended maximum speed	600 r.p.m.
Life	12 million revolutions minimum
Rings	Hard gold plated.
Brushes	Gold alloy covered spring steel.
Wire	Teflon coated
Sealing	IP:64
Surface treatment	Clear anodize

Permission was granted by the manufacturers to use the unit at 750 r.p.m. and they claimed that speeds of up to 1200 r.p.m. should not cause a significant increase in resistance or wear. The minimum operational time expected can thus be calculated as approximately 260 hours. The brushes and rings can be re-plated with gold alloy should it be required.

3.4 Conclusion

The EFBDS performed very well throughout the experimental testing phase and due to the modular designs, further development should not be a problem. The experimental results obtained are presented in the next chapter.

CHAPTER 4

FAN BLADE DAMAGE DETECTION

4.1 Introduction

From the results obtained in Chapter 2 with the FEM of various blade models, it was clear that it is viable to detect damage using one sensor per blade (possibly less) by making use of the shift of natural frequencies due to structural changes. The purpose of the EFBDS was to verify these findings experimentally, using a model that simulates the conditions that will be found on an actual fan as described in Chapter 3. This chapter concentrate on the measurements taken from the EFBDS and the results obtained.

A brief description of the experimental conditions, sensors and processors used is given. The next step was to look at the effect of certain variables such as rotation speed, blade pitch and sensor type and location. Thereafter the signal conditioning and reasons for the conditioning, the measurement period and number of measurements was studied. This was evaluated by looking at the feature extraction results obtained from ARMA models. As described in Chapter 1 it was important that a specific natural frequency could be determined accurately and repeatedly. The main reason for this being the relatively small shifts of frequency for low levels of damage and the need to distinguish between measurement inaccuracies and shifts due to damage. With these variables fixed, different levels of damage was induced to the structure to ascertain the selection criteria and classification structure.

Time domain damage indicators such as Root Mean Square (rms) values, Kurtosis, Crest factors and variance were also evaluated as a possible means of damage identification with future work that may include neural networks in mind.

The only remaining step was then to compare the predictions of the finite element model to the experimental results found with the EFBDS. This included updating of the finite element model if necessary.

4.2 Experimental conditions

The following measurement equipment were used for all experimental measurements:

Table 4.1: Description of measurement equipment

Name	Description
1 x PCB 100 mV/g Accelerometer	353B65
1 x PCB 10mV/g Accelerometer	352C22 Shear accelerometer.
2 x PCB strain gauges.	740B02 piezoelectric strain gauge.
1 x Siglab	Model 20-22 Signal analyser
4 x Signal conditioners	480E09 Battery-powered signal conditioners
1 x Personal Computer.	Pentium ™ 200MMX, 64M RAM.

4.2.1 Placement of sensors

Two different types of sensors were used. The first sensor type used, was a piezoelectric accelerometer, while the second sensor type was a piezoelectric strain gauge. Because of the different physical measurements these sensors make, the optimal location of measurement is not always the same.

The finite element model provided valuable insight regarding the placement of the sensors at a position where the third and fourth mode shapes cause maximum strain or acceleration, depending on which type of sensor was used. To find a suiTable location for the accelerometer, an analysis was done to give a displacement plot of the third and fourth modes shapes. These plots can be seen in Figure 4.1 and 4.2.

As can be expected, it is better to place the accelerometer as far out towards the tip of the blade as possible. Because the fourth mode shape is a torsional mode, the nodal points (position of zero movement) lie along the middle of the blade. It was necessary to offset the sensor to the left or right side of the centreline of the blade to make sure this mode can be measured as indicated in Figure 4.1. In the same way, the maximum strain occurs at the root of the blade. Again, the sensor should be offset from the centreline to measure the fourth mode shape.

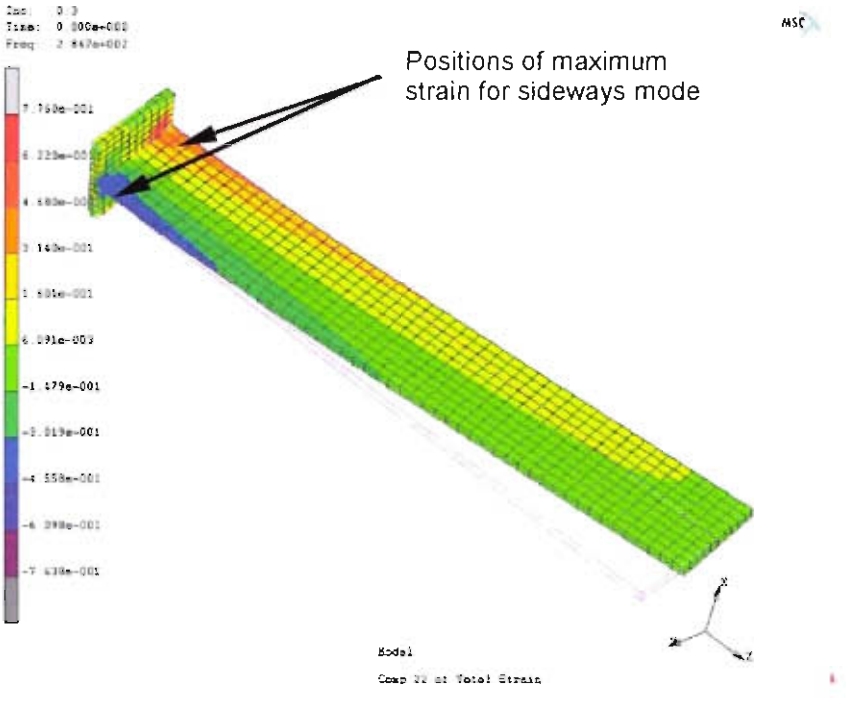

Figure 4.1: Optimal strain location in the y-y direction for third mode shape

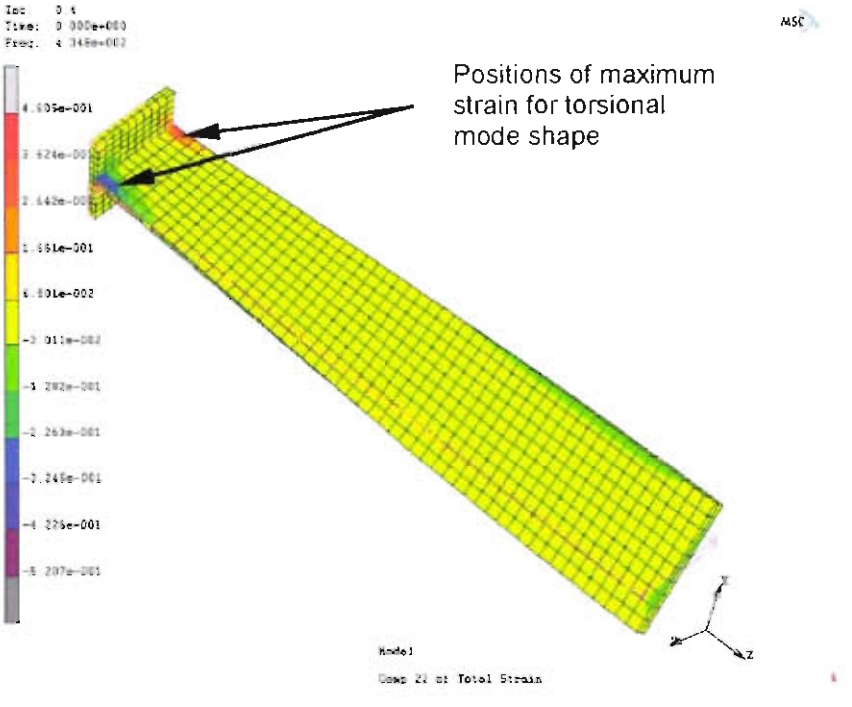

Figure 4.2: Optimal strain location for the fourth mode shape

4.2.2 Typical results obtained

To test the ability of the ARMA model to correctly identify model parameters and get some idea of what settings should be used for this algorithm, a simple aluminium cantilever beam was analysed. An electromagnetic exciter was used to provide stochastic input to the system and only output data from an accelerometer was measured for use with the ARMA algorithm. The details of the tests conducted can be seen in Appendix C.

As can be expected, the Power Spectral Density (PSD) found on the blades is not as well defined as those found on a stationary cantilever beam. In particular, the blade pass frequency and its harmonics was very prominent. Furthermore, the speed control system of the three phase electrical motor caused further electromagnetic noise. Even though the resulting PSD was less than ideal, repeaTable results could be obtained by ARMA curve fits. An example of an ARMA fit for an accelerometer can be seen in Figure 4.3, while Figure 4.4 shows a typical piezoelectric strain gauge fit.

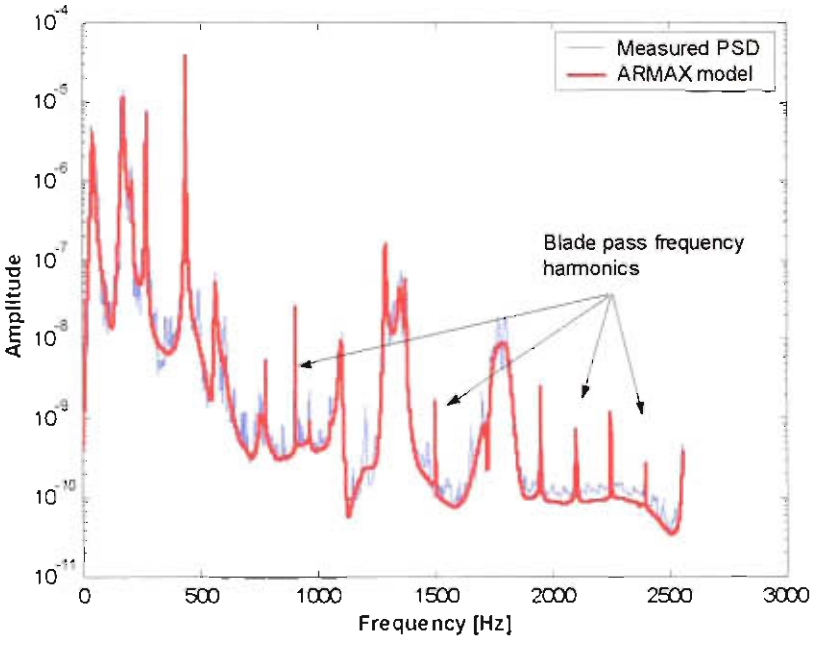

Figure 4.3: Typical ARMA fit to accelerometer data, note blade pass frequency harmonics

As can be expected the blade pass frequency harmonics result in a very narrow band excitation, while the natural frequencies result in a broader band, higher power distribution. Natural frequencies can be seen at around 200 Hz, 280 Hz, 440 Hz, 560 Hz, 1100 Hz, 1340 Hz and 1800 Hz. The peak at 75 Hz corresponds to the blade pass frequency. The rotational velocity for this measurement case was

750 r.p.m., translating to 12.5 Hz. Due to the six stationary support beams of the structure, the blade pass frequency will then be at 75 Hz.

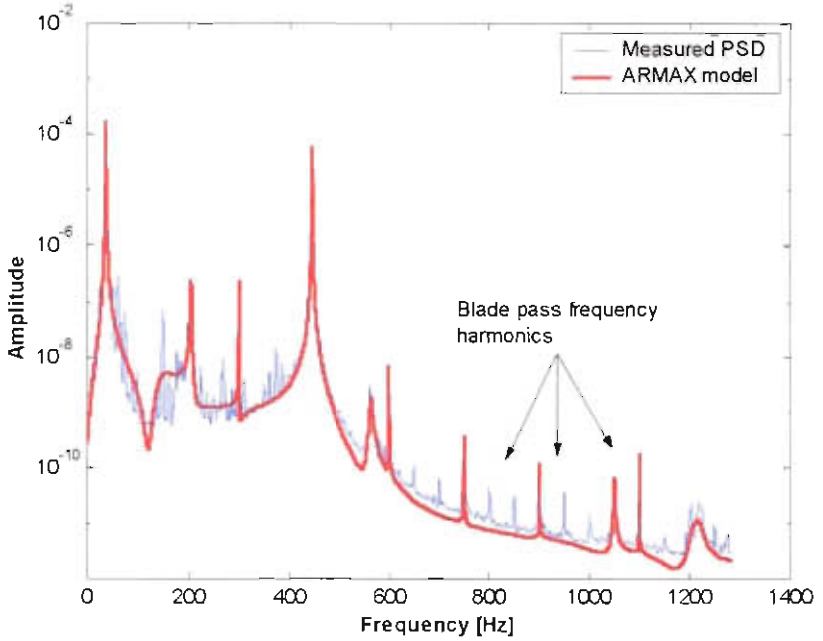

Figure 4.4: Typical ARMA model fit to piezoelectric strain gauge, note blade pass frequency harmonics

For the measurement in Figure 4.4 the distance between these excitation peaks on the x-axis (frequency) was found to be approximately 45 Hz. This corresponds to 6 times the rotational speed (in this case 450 r.p.m.). This was again due to the six stationary support structures found on the EFBDS (see Chapter 3).

Although these harmonic frequencies make it necessary to fit a higher order ARMA model in order to make sure all the natural frequencies are found, it was possible to work with the data obtained. A blade pass frequency can be expected on an actual fan, and the technique for the detection of damage developed, must be robust enough to handle these various noise sources found in the spectrum.

Another source of noise was the speed control system used for the three-phase motor. This caused a broad band noise floor to be present. To demonstrate the effect this noise has on the spectrum a 4 s measurement was taken at 600 r.p.m. and compared to a 4 s measurement taken just after the controller was shut down at 750 r.p.m. The results can be seen in Figure 4.5 on the next page.

As can be seen, the effects of the blade pass frequency were also greatly reduced. The fan loose momentum quite quickly because of air resistance and thus the blade pass frequency change rapidly from around 75Hz to 45Hz (4s at 18° pitch angle).

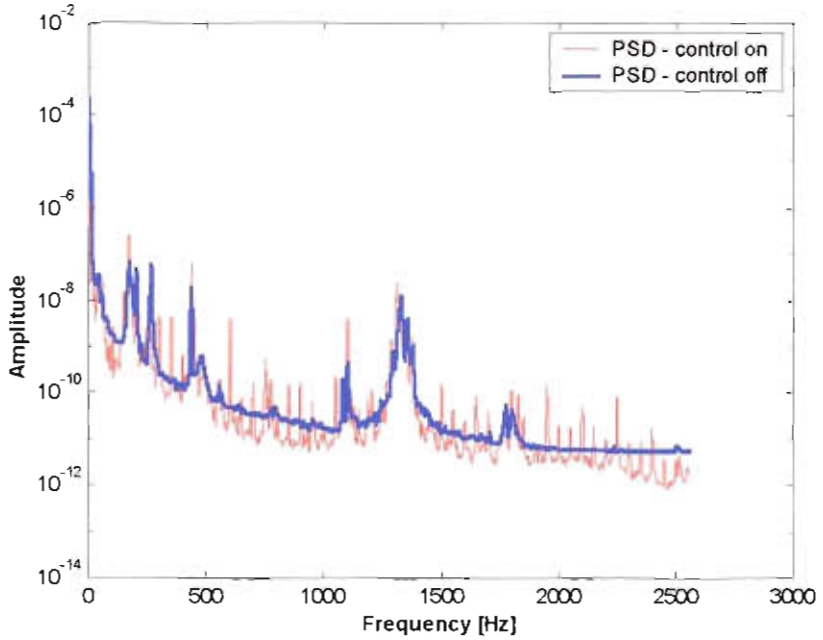

Figure 4.5: PSD with speed controller operating (red), and coasting to stop (blue).

While measurements taken during run-downs were substantially cleaner and required a lower order ARMA model for an accepTable fit, it was not really practical since an actual fan is not switched off unless maintenance is required. Furthermore almost any fan will have a blade pass frequency in practice and any technique developed for the detection of damage in fan blades should be able to cope with such noise.

Another variable of the EFBDS was pitch of the blades. Figure 4.6 shows a spectrogram of channel 2, taken at 500 Hz sampling frequency at pitches of 0°, 27° and 45°. Clearly energy input (and response) get higher with increasing pitch. The blade pass frequencies also became more prominent with increasing pitch. Figure 4.7 shows the ARMAX fits and the general noise level of measured PSDs at different pitch levels. If too little stochastic excitation was present (0° pitch), the natural frequencies did not get excited enough to stand out clearly from electric and other noise. While the second and fourth natural frequencies were not very sensitive to the pitch angle, the third was very sensitive. FEA results confirmed that the second mode shape is very sensitive to pitch angle. The blade pitch angle was therefore locked at 18° for all subsequent measurements so as not affect measurements.

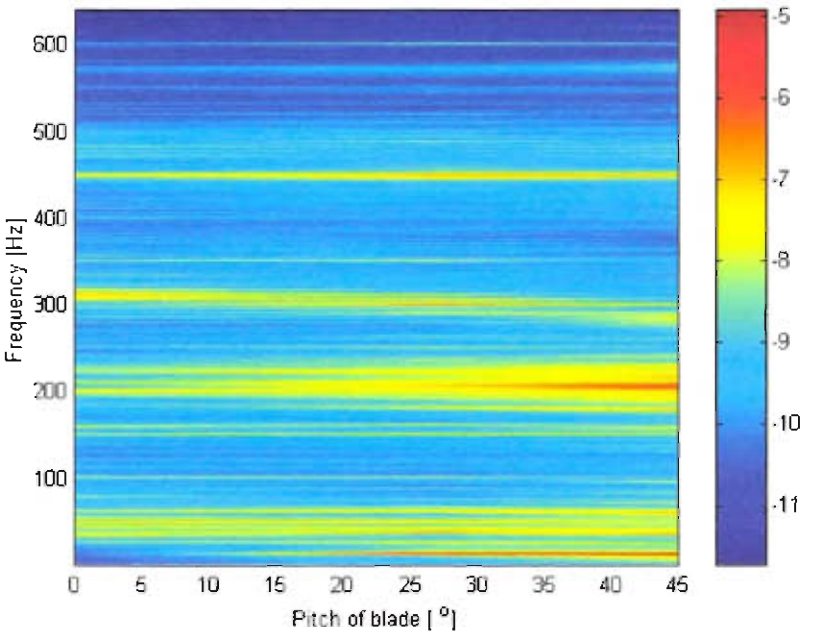

Figure 4.6: Spectrogram showing increase of response with increasing blade pitch

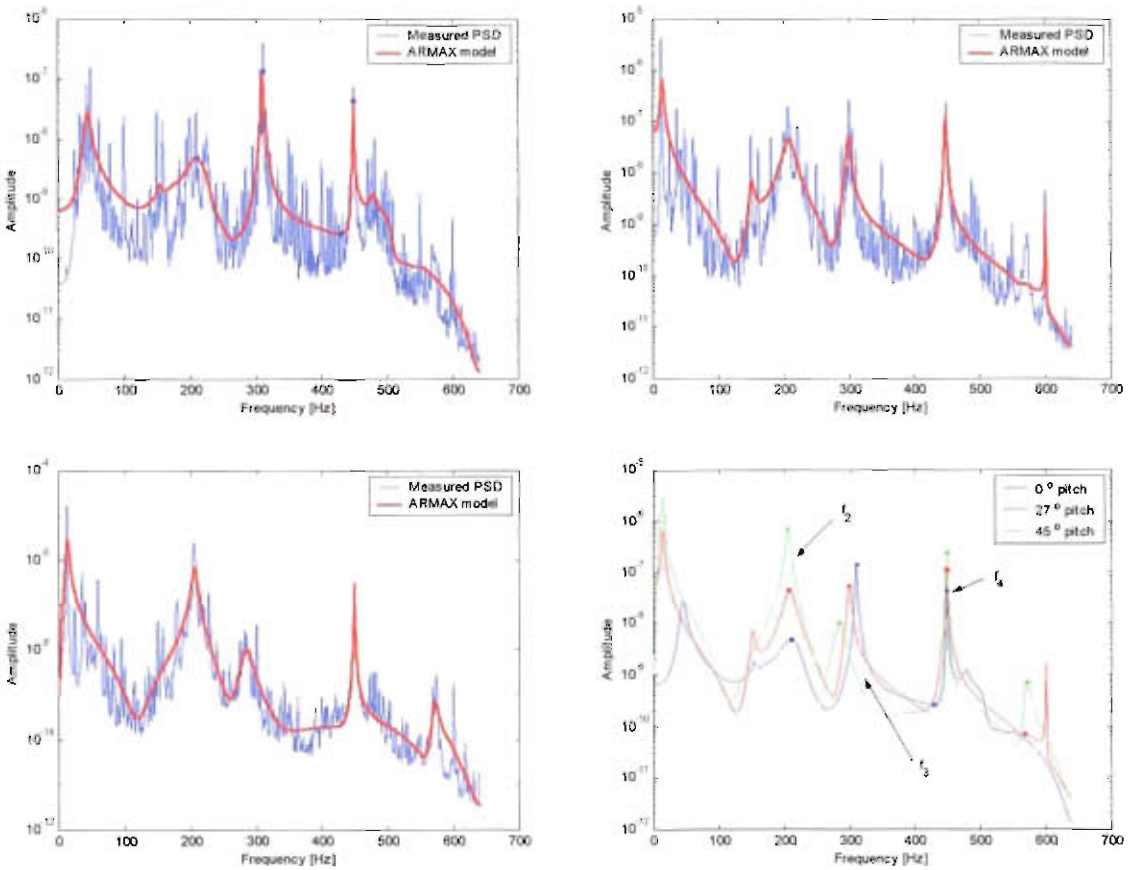

Figure 4.7: Top left at 0°, top right at 27°, bottom left at 45°, bottom right, comparison

4.3 Experimental results

The ARMA model algorithm used time signal data as input although this algorithm eventually fitted a polynomial through a power spectral density plot for modal parameter extraction purposes.

4.3.1 Processing of raw data

An example of a 2 s measurement, sampled at 500 Hz can be seen in Figure 4.8. The most apparent characteristic of this measurement was the one times rotational frequency sine wave found because of imbalance in the system. A six times rotation frequency is superimposed on this signal, followed by al the other frequencies present in this system. Since the first natural frequency was found to be around 33 Hz during the finite element analysis, it was decided to high pass filter the signal from 25 Hz. The filtered signal can be seen in Figure 4.9.

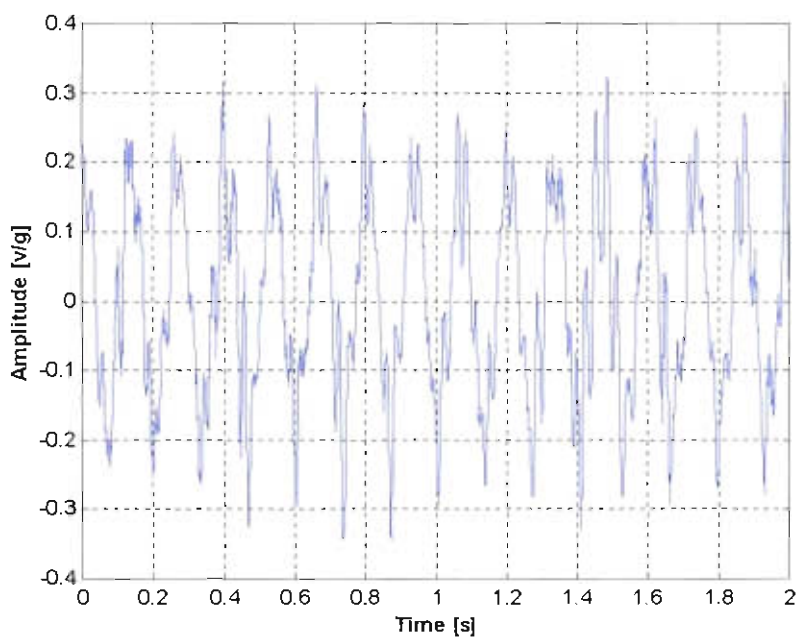

Figure 4.8: Example of the typical time data measurement (f_s was 500Hz).

The primary reason for filtering the signal was to lower the order of the ARMA model required to fit an accurate polynomial. Since the first natural frequency that could be measured accurately and showed relatively high sensitivity to damage was found at around 280 Hz, filtering below 200 Hz was also implemented. The ARMA algorithm struggled to fit repeaTable curves through the resulting power spectral density how-

ever and the order of the model could not be decreased as a result. It was thus decided not to filter to such a high frequency.

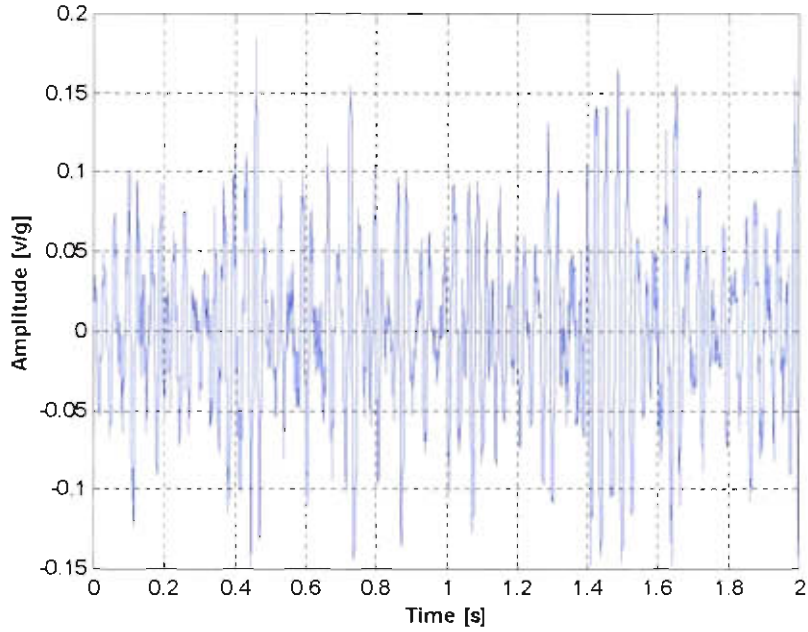

Figure 4.9: The filtered signal, note change of maximum amplitude

4.3.2 Determination of required order for ARMAX curve fits

As discussed in Appendix C, a certain minimum model order was necessary for the ARMAX model. The pole-zero plots for a number of typical measurements can be in Figure 4.10 for 500 Hz sampling, Figure 4.11 for 1000 Hz sampling frequency and Figure 4.12 for 2000 Hz sampling frequency.

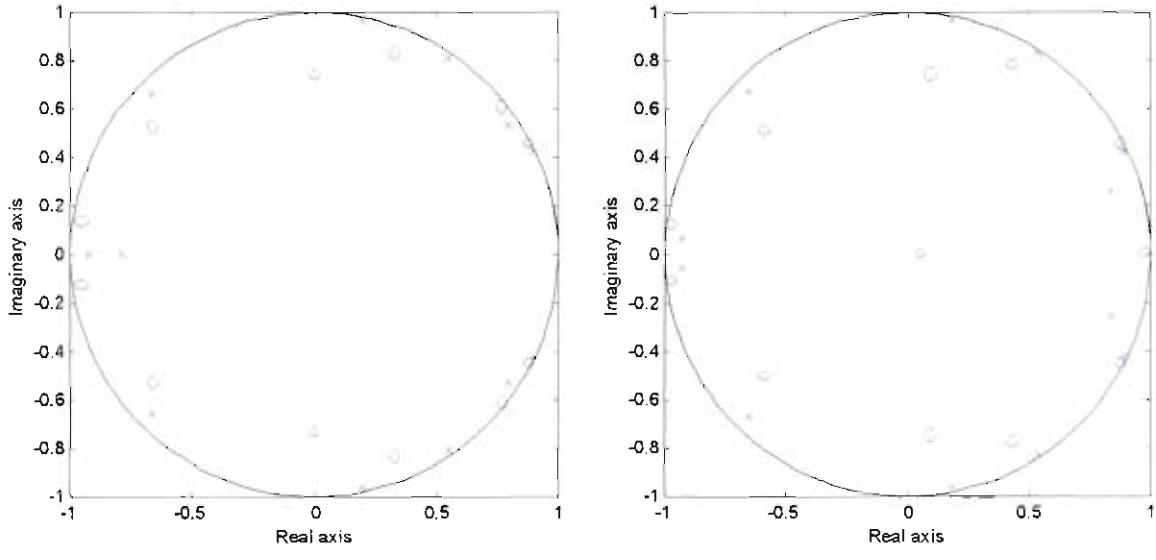

Figure 4.10: Pole-zero plot for a 2 s (left) and 4 s fit (right)

It was clear that a few near redundant poles were present (proximity of poles and zeros). Appendix C deals with the implication of this phenomenon in more detail. Due to the high level of noise (blade pass frequency and electromagnetic) this was necessary to ensure all the natural frequencies were picked up.

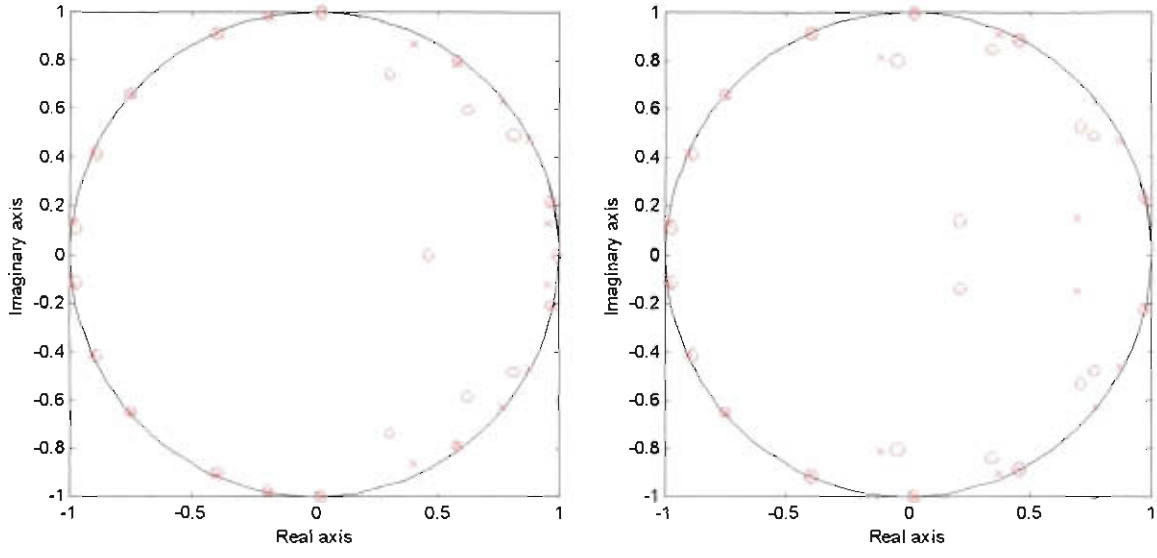

Figure 4.11: Pole-zero plot for a 2 s (left) and 4 s fit (right)

Clearly the number of redundant poles increased dramatically for higher sampling frequencies. The reason for this can be clearly seen in Figures 4.13 and 4.14.

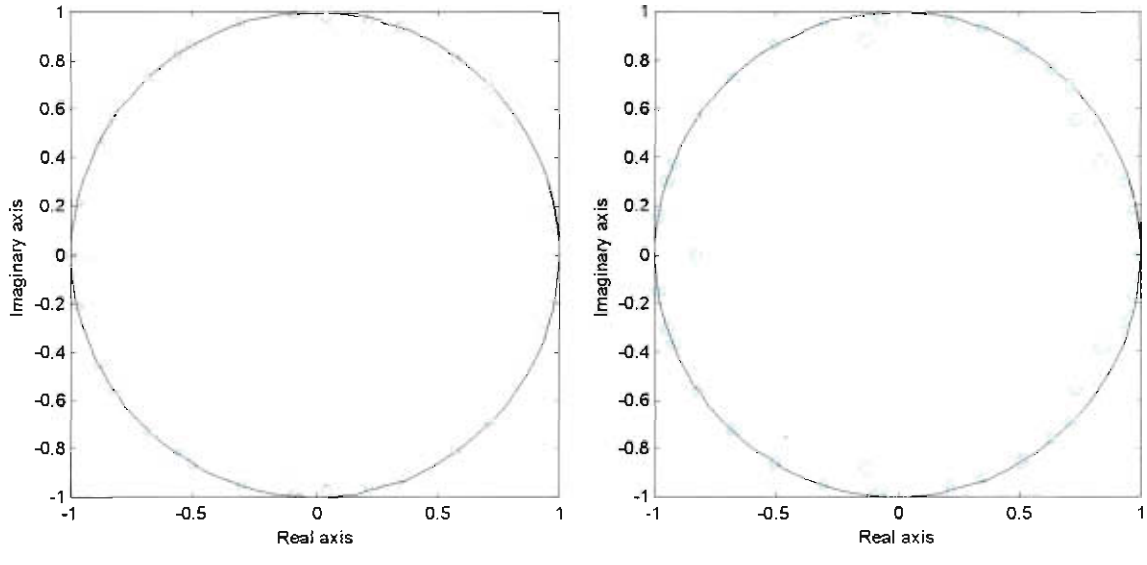

Figure 4.12: Pole-zero plot for a 2 s (left) and 4 s fit (right)

The higher order was necessary because of dominating effect of the noise spectrum from around 600 Hz and up.

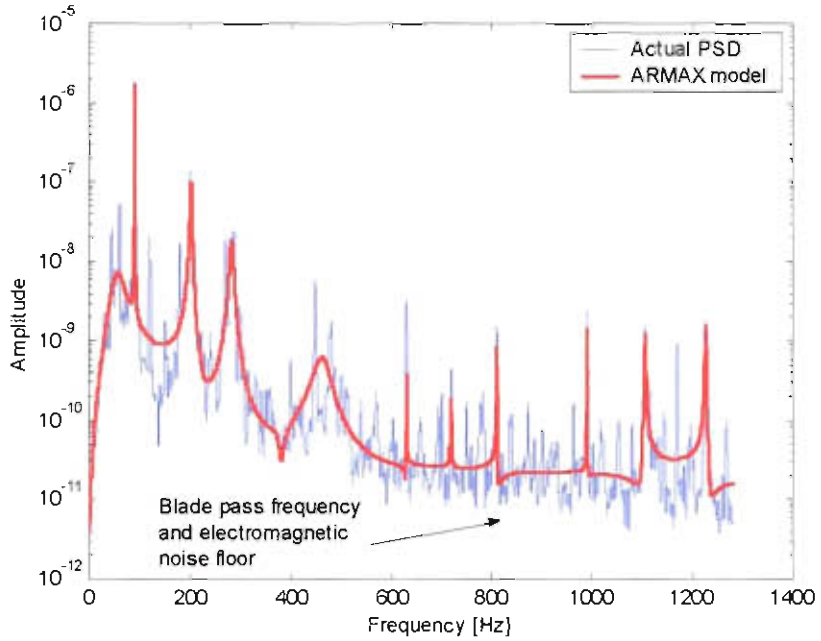

Figure 4.13. Reason for high number of redundant poles and zeros (1000 Hz sampling frequency)

Both of these PSDs were four second samples taken with the 10mV/g accelerometer and represent the worst-case data found during the experimentation phase. Even though these data sets were clearly far from ideal, reliable and repeaTable results could be obtained with the ARMAX algorithm used. A peak picking algorithm was used to identify the natural frequencies.

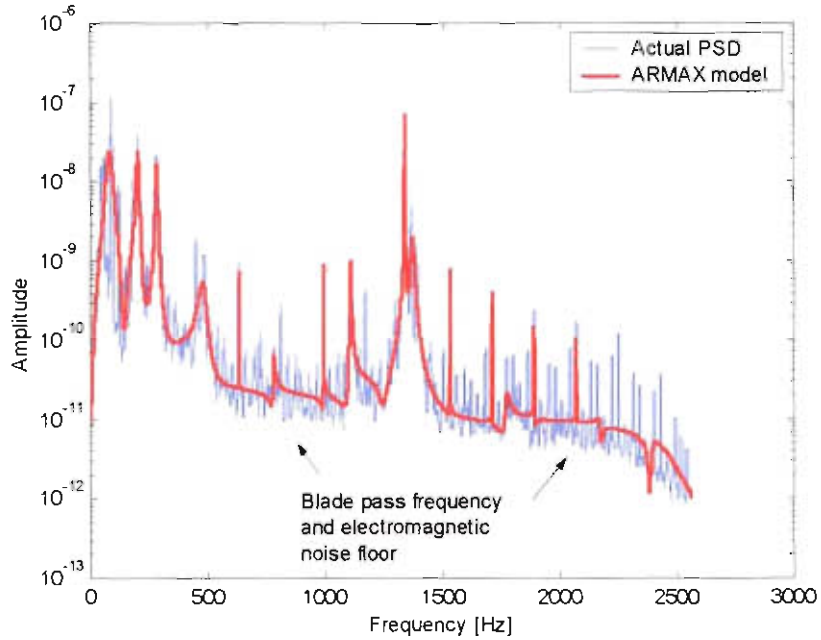

Figure 4.14. Reason for high number of redundant poles and zeros (2000 Hz sampling frequency)

In the end, the order of the model was determined not as much by minimising the number of redundant poles and zeros but by the ability of the ARMAX algorithm to find all the relevant peaks that represented the natural frequencies of the structure. This was only accomplished if the order was increased beyond a certain point. For 500 Hz, a 12^{th} order fit was necessary while 24^{th} and 48^{th} order fits were necessary for the 1000 Hz and 2000 Hz sampling frequency, samples.

4.3.3 Determination of measurement number and length

It was very difficult, if not impossible, to compute the period of time domain data that will be required for an accurate model beforehand. Because the shifts in natural frequencies found for various damage levels are so small, it was very important that natural frequencies could be found repeatedly in an even smaller band of uncertainty. Since the frequency may shift by as little as 0.3% for 10% damage, the error of the measured frequency must then be less than half this shift to ensure accurate classification of the damage level at that frequency. From work done earlier on a simple hinged beam to evaluate the ARMA modelling technique, a rough estimate on the period of measurement and number of measurements was made.

After these initial measurements had been used to compute models, the results could be used in a statistical analysis to make a better estimate of the amount of measurements that would be needed for a certain accuracy to be obtained. Since long time signals combined with high order ARMA models increased computer time dramatically (Appendix C, Tables C.5 and C.6), it was important to minimise the number of measurements and the measurement time.

One method that can be used is confidence intervals (Bendat and Piersol, 1967). If a variable *x(k)* is normally distributed (it will be in this case) with an average value of μ_x and an unknown variance, the sampling distribution for the mean sample $\bar{x}$ will look as follows :

$$\frac{\bar{x} - \mu_x \sqrt{N}}{s} = t_n \qquad \text{n = N - 1} \qquad \textbf{(4.1)}$$

In this case t_n has a normal distribution with n=N-1 degrees of freedom, where N is the number of elements in the sample data set. A probability statement for the sample mean $\bar{x}$ prior to collection of the sample can then be made.

$$Prob\left[\bar{x} > \left(\frac{st_n}{\sqrt{N}}\right) + \mu_x\right] = \alpha \qquad \textbf{(4.2)}$$

For a general case of a normally distributed random variable with an unknown mean value and variance, the probability statement can be obtained from Equation 4.1 as follows.

$$Prob\left[t_{n;1-\alpha/2} < \frac{(\bar{x} - \mu_x)\sqrt{N}}{s} \leq t_{n;\alpha/2}\right] = 1 - \alpha \qquad n = N\text{-}1 \qquad \textbf{(4.3)}$$

Since a certain amount of data has already been collected, the values $\bar{x}$ and s are known. Therefore the above probability statement no longer apply since the quantity $(\bar{x} - \mu_x)\sqrt{N}/s$ either falls into the noted limits (0 or 1) or not. After a sample has been collected the probability statement thus changes as follows.

$$Prob\left[t_{n;1-\alpha/2} < \frac{(\bar{x} - \mu_x)\sqrt{N}}{s} \leq t_{n;\alpha/2}\right] = \begin{Bmatrix} 0 \\ 1 \end{Bmatrix} \qquad \textbf{(4.4)}$$

It is usually not known whether the correct probability is zero or unity. As the value of α becomes small (the interval between $t_{n;1-\alpha/2}$ and $t_{n;\alpha/2}$ becomes larger) the probability is more likely to be unity than zero. If a lot of samples sets were collected and $\bar{x}$ and s computed for each sample, the value in Equation 4.3 should fall within the noted interval for about 1-α of the samples. A statement can thus be made concerning the interval where the quantity $(\bar{x} - \mu_x)\sqrt{N}/s$ would be found with a small degree of uncertainty. These statements are called confidence statements, while the interval associated with this statement is known as the confidence interval. For the case of a mean value estimate, a confidence interval can be established for the mean value μ_x based upon the sample values $\bar{x}$ and s by rearranging the terms in Equation 4.3 as follows.

$$\left[\left(\bar{x} - \frac{st_{n;\alpha/2}}{\sqrt{N}}\right) \leq \mu_x < \bar{x} + \frac{st_{n;\alpha/2}}{\sqrt{N}}\right] \qquad n = N - 1 \qquad \textbf{(4.5)}$$

because $t_{n;1-\alpha/2} = -t_{n;\alpha/2}$. Thus, the true mean value μ_x falls within the stated interval with a confidence of (1- α)100 percent.

As a first iteration, eight, 2 s and four, 4 s measurements were taken for the frequency around 280 Hz. Table 4.1 shows the frequencies.

Table 4.1: Typical third mode frequencies found during a measurement run

Example of 3rd natural frequencies found (2 s samples)				**Example of 3rd natural frequencies found (4 s samples)**	
283.90	283.90	285.09	281.91	279.93	279.74
285.30	285.09	283.70	284.69	280.72	280.52

By using Equation 4.5 in conjunction with the $t_{n;\alpha}$ values found in Bendat and Piersol (1967) and data set found in Table 4.1:

$$\left[\left(\bar{x} - \frac{st_{n;\alpha/2}}{\sqrt{N}}\right) \leq \mu_x < \bar{x} + \frac{st_{n;\alpha/2}}{\sqrt{N}}\right] \qquad n = N - 1$$

furthermore:

$\bar{x}$	=	284.20	
$t_{24;\alpha/2}$	=	2.807	(Bendat and Piersol, 1967 with α=0.995)
s	=	1.12	

Thus one can predict with a 99.5% confidence that the mean value will fall between

$$[282.96 \leq \mu_x < 285.43]$$

This meant a maximum error of 0.87% between sets of measurements and did not fall within the accuracy requirements since a frequency shift of around 0.8% was expected for 5% damage.

Similarly the 99.5% confidence interval for four, 4 s samples can be calculated as

$$[279.57 \leq \mu_x < 280.88]$$

This means a maximum error of 0.47% which was considerably better than the two second samples. Since these were obviously still not accurate enough results, the

data points were increased to 24 for the 2 s samples and 12 for the 4 s intervals. These data sets can be seen in Table 4.2.

Table 4.2: Typical third mode frequencies found during a measurement run

Example of 3rd natural frequencies found (2 s samples)				Example of 3rd natural frequencies found (4 s samples)	
283.90	283.50	283.90	284.89	280.52	279.93
283.90	283.70	283.50	284.89	280.52	280.33
281.91	284.69	284.69	285.09	280.72	280.13
284.29	283.70	284.49	283.70	279.93	280.52
284.29	284.69	284.89	285.30	279.93	279.93
283.10	284.69	283.70	285.09	279.74	279.74

Again using Equation 4.5 in conjunction with the $t_{n;\alpha}$ values found in Bendat and Piersol, 1967 and data set found in Table 4.2:

$$[283.73 \leq \mu_x < 284.63]$$

This meant a maximum error of 0.32% between sets of measurements and felt within the accuracy requirements since a frequency shift of around 0.8% was expected for 5% damage.

For 12, 4 s measurements, the 99.5 % confidence interval for the mean value can be calculated in the same way as:

$$[279.88 \leq \mu_x < 280.44]$$

That meant a maximum error of 0.2%. Since this was better than the 24 measurements, and requires roughly the same computational time, it was better to choose 12 sets of 4 seconds.
The fourth mode was also of interest. Since this mode shifted significantly less, it was necessary to check whether 24, 2 s or 12, 4 s measurements were enough.

The data for the fourth mode can be seen in Table 4.3.

Table 4.3: Example of fourt[illegible]ies found during test run

Example of 4th natural frequencies found (2 s samples)				Example of 4th natural frequencies found (4 s samples)	
446.65	447.28	446.97	446.97	446.97	446.97
446.65	447.28	447.28	446.97	447.28	446.97
446.97	447.59	446.97	446.65	447.28	446.97
446.97	447.28	446.65	447.28	446.97	447.28
446.97	447.28	447.28	446.97	446.97	447.28
446.97	446.97	446.97	446.65	446.97	446.97

Again using the same technique the mean of a measurement set will fall in the range

$$[446.87 \leq \mu_x < 446.87]$$

with a maximum error of 0.07% which was exceptional. For the 12 measurements of 4 s the confidence interval was found to be

$$[446.95 \leq \mu_x < 447.20]$$

giving a maximum error of 0.06%. It is therefore clear that 12, 4 s measurements should give accurate enough results, in order to do damage identification.

Not surprisingly, longer samples of time data gave more accurate results and less were required to achieve an average frequency with a high level of confidence. This was due to the fact that the ARMAX algorithm makes use of a PSD that will be more accurate the longer the length of the time signal used as input. Ideally, an infinitely long time signal would be used which will result in a perfect PSD. This would lead to a perfect fit and the frequency should then not appear to move around a little between measurements. The specific algorithm used was very Random Access Memory (RAM) intensive and long time signals resulted in unrealistic CPU times.

Further experimentation with longer samples was not viable, given the time constraints of the project, but can certainly be looked at in more detail if a decision is made in future to use this technique without modification on actual blades in industry. The confidence interval statistical approach gave a mathematically solid method to determine the number of measurements necessary for a specific sampling length.

4.4 Damage detection measurements

With all the preliminary work done regarding sensor placement, measurement length, signal processing, model fitting and feature extraction, a full set of measurements was taken on a blade.

4.4.1 Measurement system used on the EFBDS

For the damage detection measurements the blade that was to be damaged was instrumented with two piezoelectric strain gauges and one accelerometer. Since the Siglab analyser allows four channels, the remaining channel was used to instrument a different blade to test the ability of the method to predict damage on a specific blade. The location and orientation of the sensors can be seen in Figure 4.15.

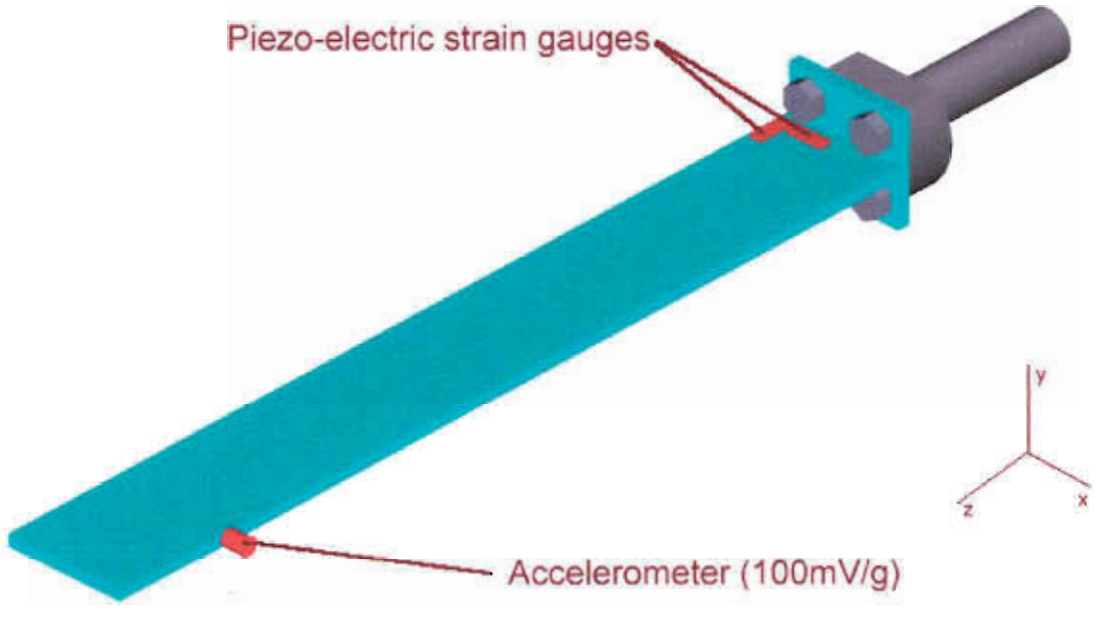

Figure 4.15: Location of sensors on the blade to be damaged

The accelerometer on the undamaged blade was located in the same position as the accelerometer on the blade to be damaged. As discussed in section 4.2.1, both the x-x and the z-z direction show promise for a strain gauge, both were therefore instrumented. The channel numbers can be seen in Table 4.4 along with the calibration values of the sensors associated with each channel.

Table 4.4: Sensor channel and description

Channel number	Sensor type	Sensor sensitivity.
1	Accelerometer (undamaged blade)	103.2mV/g
2	Accelerometer (damaged blade)	9.82mV/g
3	Piezoelectric strain gauge. (x-x)	50mV/μE ± 20%
4	Piezoelectric strain gauge. (z-z)	50mV/μE ± 20%

After a reference set of measurements had been taken, damage was introduced in increments of 10% up to 40%. The damage was introduced by using a thin saw blade and cutting from one side only into the root of the blade.

4.4.2 Result of curve fits

From the finite element work done, the amount by which the frequency should shift is known. The resulting curve fits by the ARMA algorithm for channel 3 with a 500 Hz sampling frequency is shown at various damage levels in Figure 4.16.

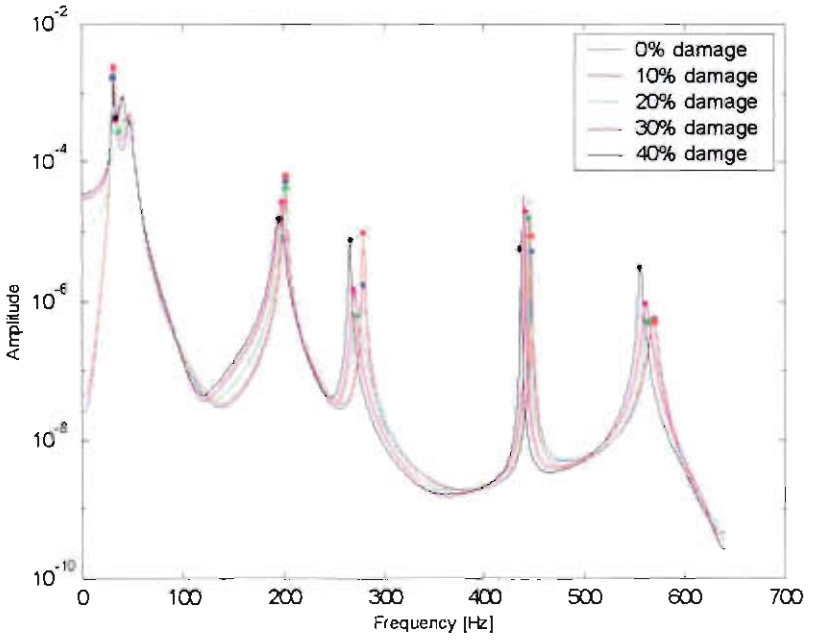

Figure 4.16: ARMA curve fits for channel 3, 500 Hz sampling frequency

It is quite clear that a progressive shift of the natural frequencies can be seen with increasing levels of damage. A waterfall plot of the actual PSDs for the various stages of damage can be seen in Figure 4.17, with a spectrogram of the same set of

measurements in Figure 4.18. The spectrogram in Figure 4.19 shows the ARMAX curve fits.

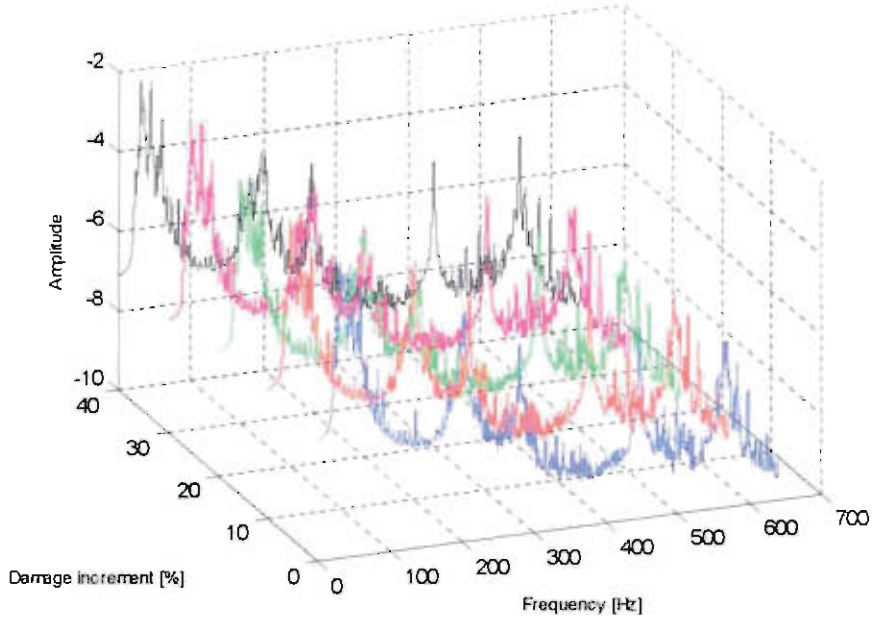

Figure 4.17: Waterfall plot of channel 3, 500 Hz sampling frequency

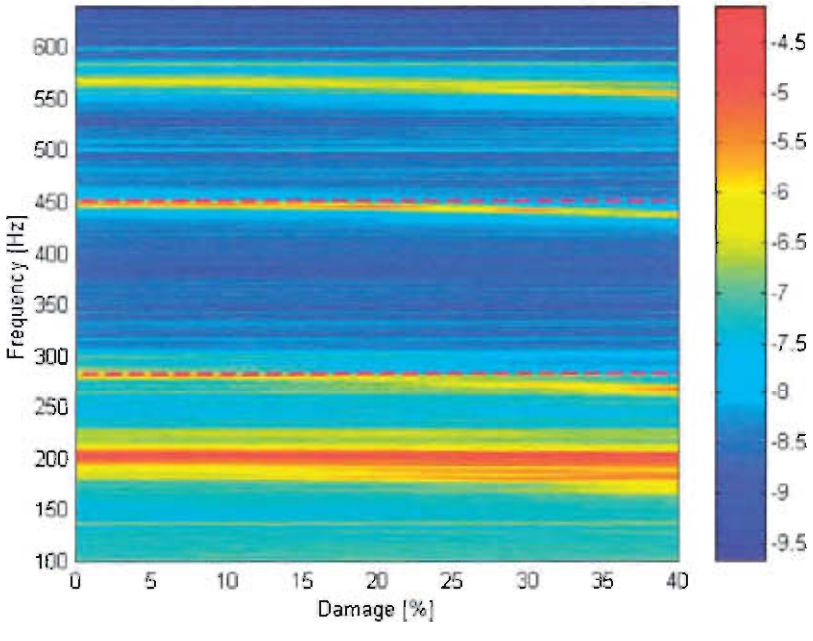

Figure 4.18: Spectrogram showing the frequency shifts with increasing damage

The data in Figure 4.16 to Figure 4.19 is the average of twelve measurement sets of four seconds each. It can thus be stated with a 99.5% confidence that the average of these frequency values will have a measurement error of less than 0.2% for the frequency around 280 Hz, and less than 0.06% for the frequency found around 440 Hz.

Although not very clear in Figure 4.18, the noise floor increases (see Figure 4.17), with increasing levels of damage. This makes physical sense, since the blade cross sectional area gets progressively less, the resultant stress and strain due to the stochastic inputs on the blade should increase (or decrease depending on location of strain gauge relative to crack). This trend can also be seen in the spectrogram plot of the ARMAX curve fits found in Figure 4.19.

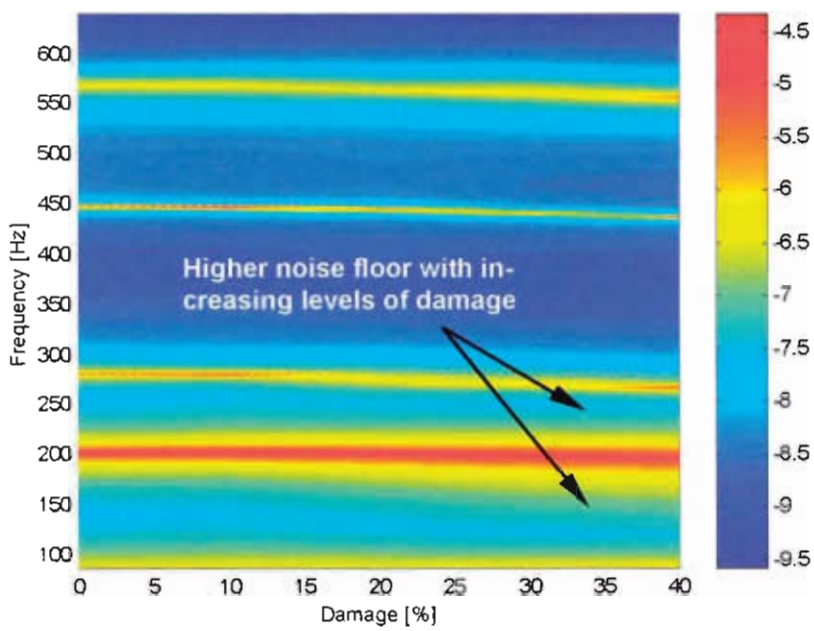

Figure 4.19: Spectrogram of the ARMAX curve fits with increasing levels of damage

The results for a few selected channels and different sampling frequencies are given in appendix D. Table D.1 shows typical results from different channels and taken at different rotational speeds and sampling frequencies for the third natural frequency.

Table D.2 in Appendix D shows the same channels and operating conditions but for the fourth mode shape natural frequency.

It was readily apparent that measurable and significant frequency shifts did take place with increasing damage.

From these examples of measured data, it was apparent that the experimental fan blade damage detector experienced a measurable frequency shift with increasing values of damage. Also immediately obvious was that the frequency shifts for the fourth mode shape was far less than the shifts predicted by the finite element model (see Figure 4.20).

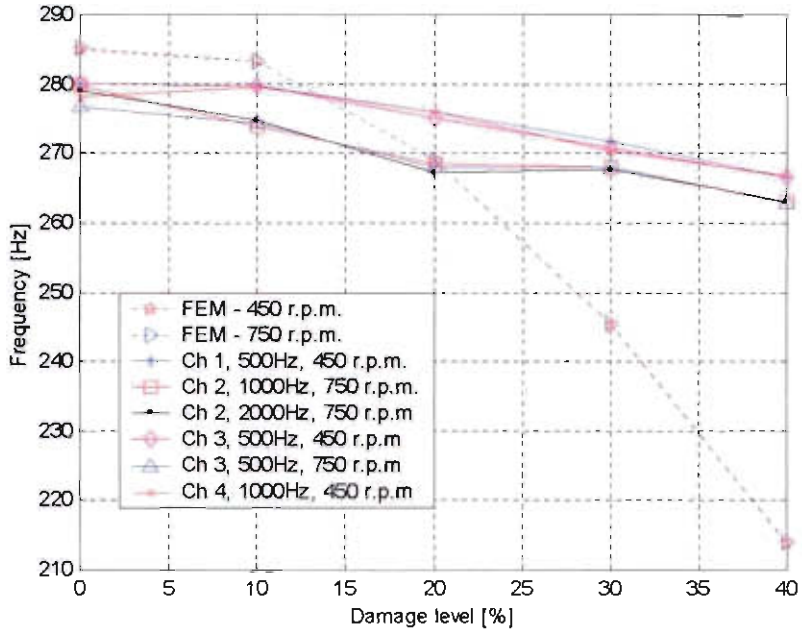

Figure 4.20: Variation of 3rd natural frequency with increasing damage. All samples were 4 s long

The graphs showing the frequency shift per damage increment were directly compiled from the measured data and can be found in Appendix D. Although the general trend of the shifts are the same, the experimental measurements were less sensitive to damage than the finite element model of a single blade predicted. The natural frequency corresponding to the fifth mode shape showed much better correlation however.

As can be seen from Figure 4.20, the measurements sampled at 500 Hz, tended to be more consistent than the measurements sampled at higher frequencies. The reason for this was that the ARMA curve fits, work better when there are less peaks and valleys to find and more consistent fits can be achieved. At higher frequency a large number of redundant poles and zeros need to be used because of the blade pass frequency harmonics and electrical noise. The percentage frequency shift can be seen in Figure 4.21.

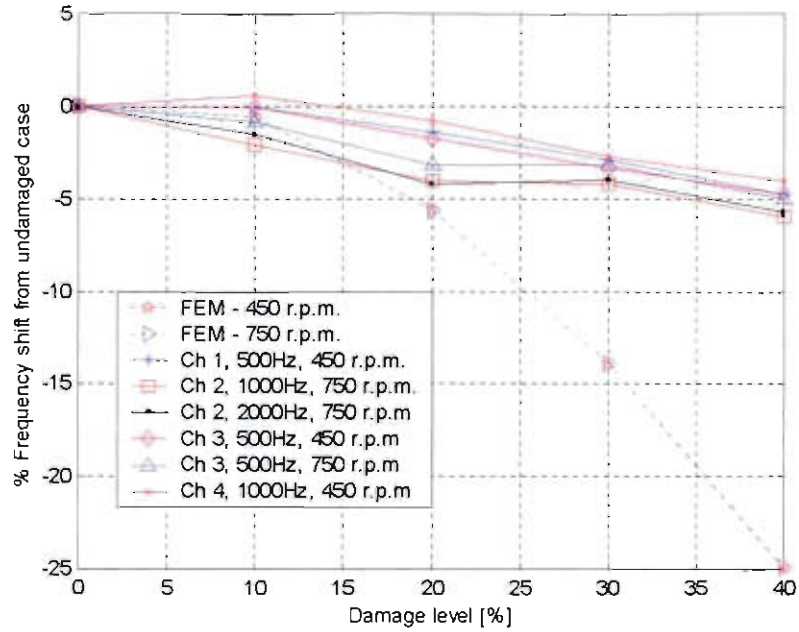

Figure 4.21: Percentage shift from the original undamaged frequency. (280 Hz)

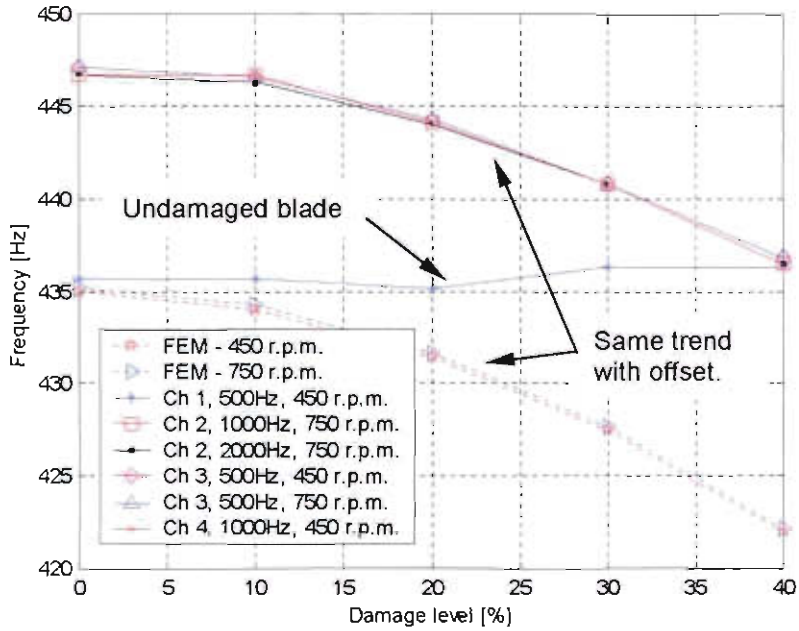

Figure 4.22: Increasing damage levels for the 4th natural frequency

The decrease in the 4th natural frequency can be seen with increasing damage levels in Figure 4.22. The offset of a few Hertz between measurement taken from the un-damaged blade and the damaged blade was not a cause for concern. It was to be expected that the blades would not have the same stiffness at the root of the blade due to the weld used. From FEM it was clear that both the sideways mode shapes

(x-x direction) and the torsional mode shapes were very sensitive to boundary conditions at the root of the blade.

The most significant feature of this mode shape was the lack of shift of the undamaged blade. Although this measurement was influenced to a small extent with increasing levels of damage, no clear pattern could be discerned and the blade would have been classified as healthy.

The percentage change in natural frequencies can be seen in Figure 4.23. Clearly a very good relationship existed between the experimental measurements and the shift predicted by the FEM model for this particular mode shape.

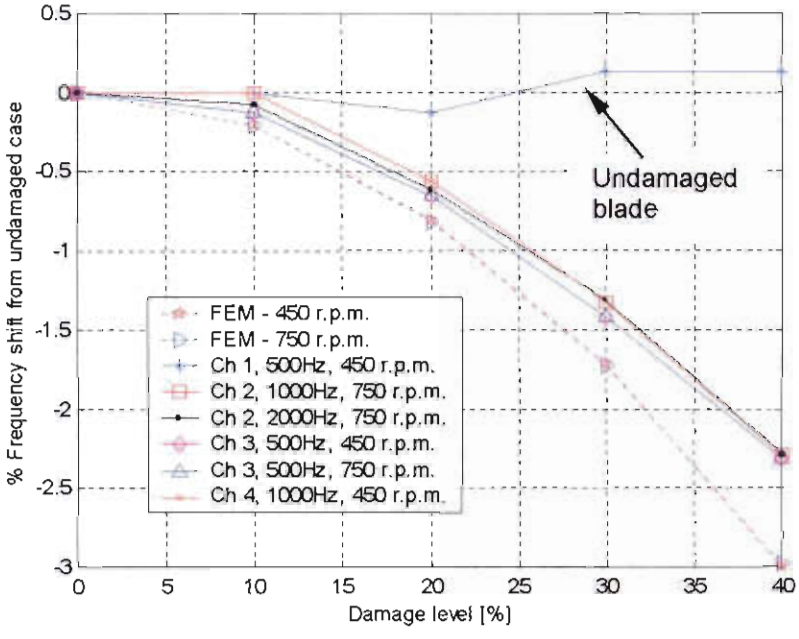

Figure 4.23: Percentage shift of frequency for the fourth mode shape

Although the fourth mode shape showed excellent correlation with predicted FEM results, the third mode shape was not as sensitive to damage as predicted. It was still more sensitive than the fourth mode shape though.

From these results is was clear that further investigation into the discrepancies between the FEM model and the experimental results would have to be done. Chapter 5 deals with this phenomenon.

4.4.3 Time domain damage indicators

Because of the continuing nature of this project with a view to practical implementation on a fan in industry (most likely the FD and ID fans at Majuba), it was decided to investigate other parameters that can be used as features for pattern recognition techniques such as neural networks. Various single values can be calculated for a time signal to give some indication of damage (or other changes). Some of the most important are listed in Heyns (1999).

A. Root mean square (rms)

The *rms* value of a function x(t) over an interval T can be calculated as:

$$X_{rms} = \sqrt{\frac{\int_0^T x(t)^2 dt}{T}} \qquad \textbf{(4.6)}$$

This indicator gives a good indication of changes involving overall peak levels in a signal.

B. Crest factor

This is the ratio of the peak value found to the *rms* level

$$CF = \frac{X_{max}}{X_{rms}} \qquad \textbf{(4.7)}$$

C. Kurtosis

The kurtosis is the fourth statistical moment of a distribution. This value is widely used in machinery diagnostics, particularly for rolling element bearings.

$$kurtosis = \frac{1}{\sigma^4 T}\int_0^T x^4 dt \qquad \textbf{(4.8)}$$

D. Variance and standard deviation

If the mean value is defined as μ_x the variance of data is given by

$$\sigma_x^2 = \lim_{T \to \infty} \frac{1}{T} \int_0^T [x(t) - \mu_x]^2 \, dt$$

The positive square root of the variance is called the standard deviation.

Some examples of the values found can be seen in Figure 4.24 (**V**ariance), Figure 4.25 (*rms*), Figure 4.26 (Kurtosis) and Figure 4.27 (Crest factor)

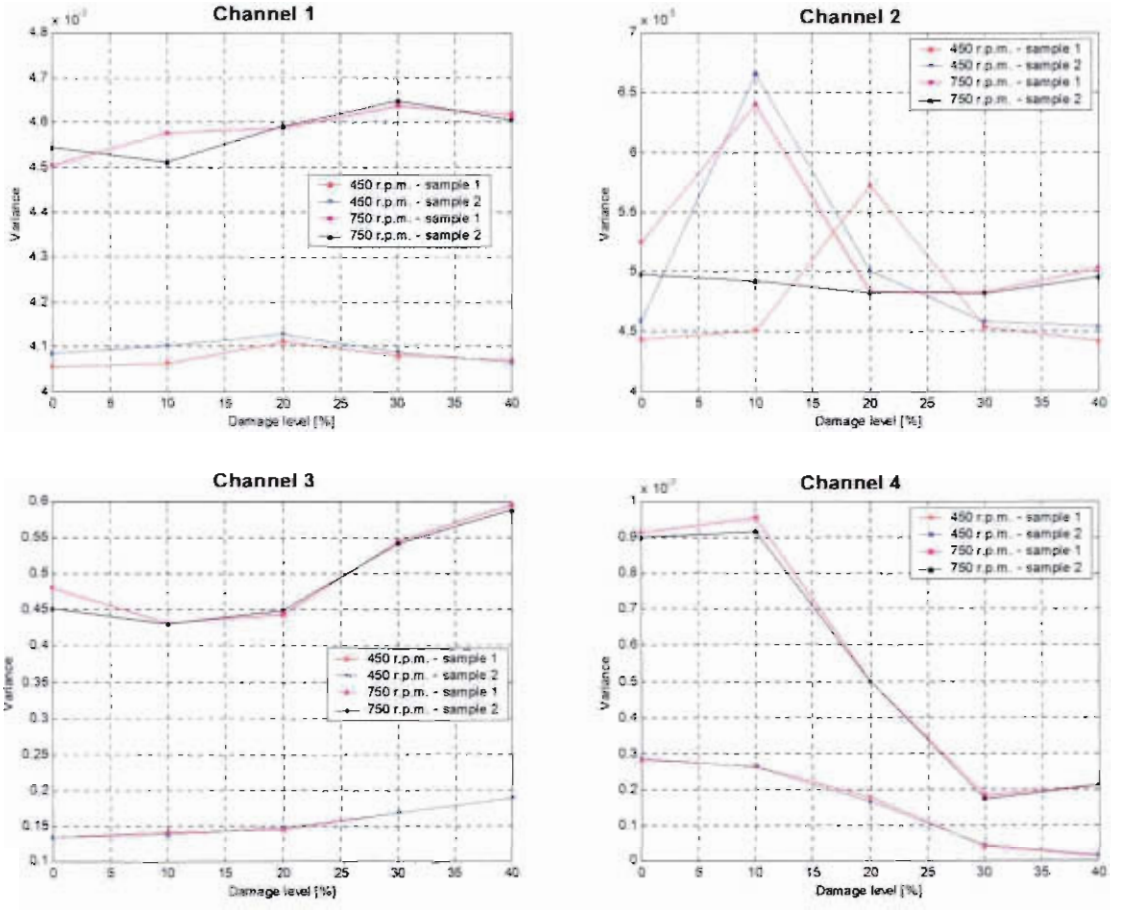

Figure 4.24: Variance plots for channel 1 through 4

Higher rotational speed caused higher stresses in the blade and this could be seen in the higher magnitude values found. Quite clearly the accelerometer channels (1,2) did not measure significantly different signals for increasing levels of damage. This was expected since the movement of the blade will not change significantly with increasing damage. The strain channels (3,4) did show an increase for lower rotational

velocities. This was also expected since the area of undamaged blade (on which the sensor was placed) decreased and the strain therefore increased,.

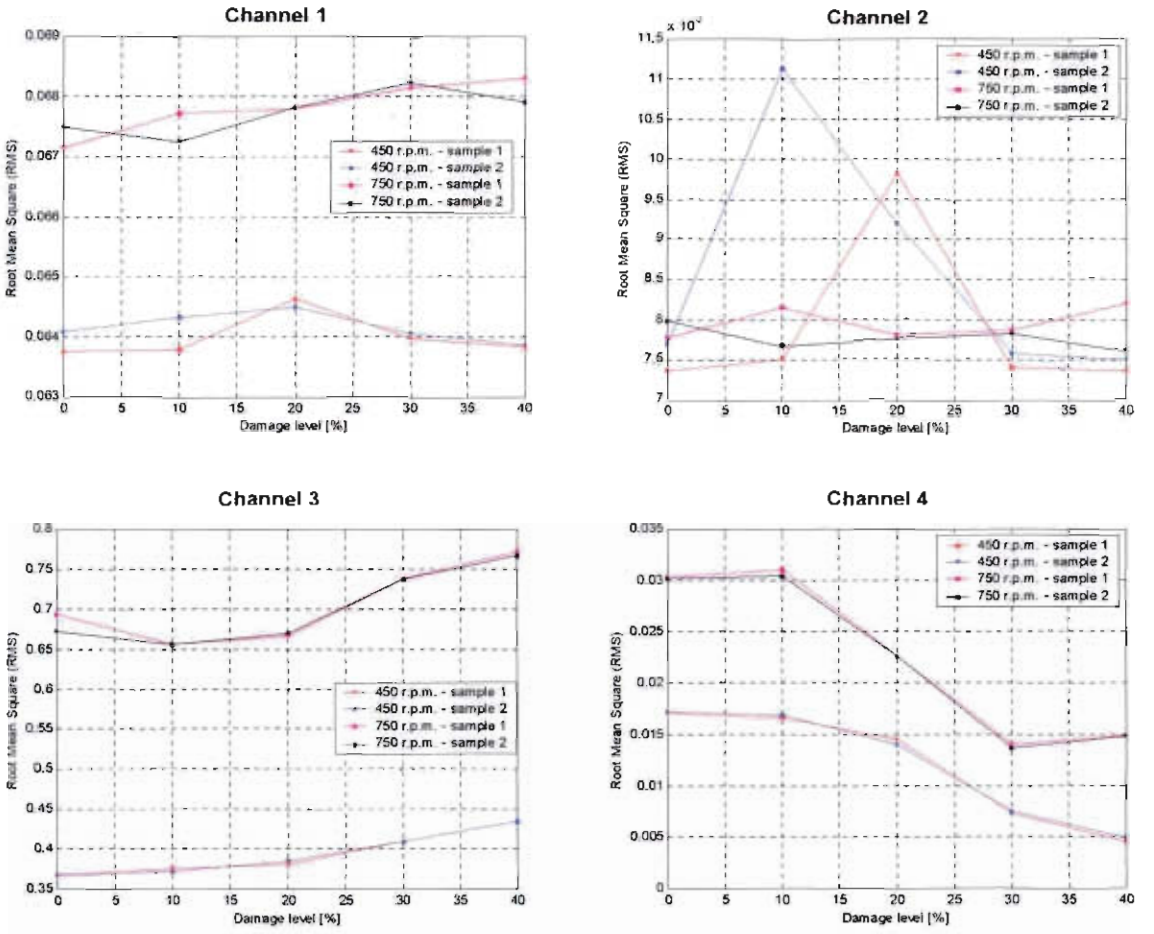

Figure 4.25: Root mean square plots for channel 1 through 4

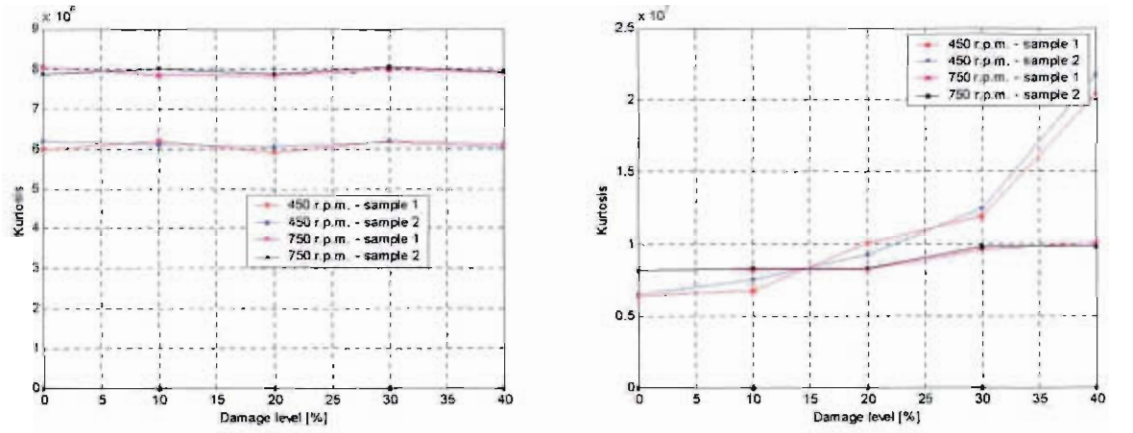

Figure 4.26: Kurtosis plots for channel 3(left) and channel 4(right)

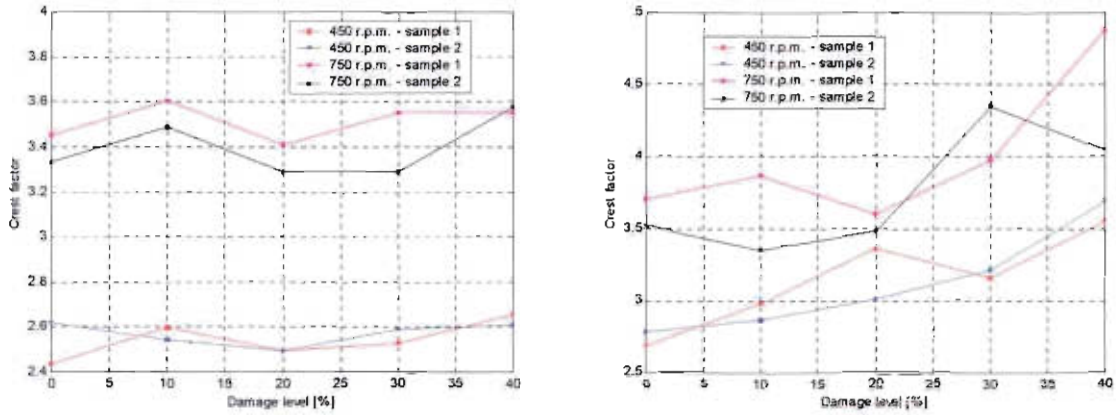

Figure 4.27: Crest factor plots for channel 3(left) and channel 4(right)

Clearly only some of the strain gauge measurements can be used with some success as a damage indicator at specific operational conditions. A better option would probably be to use these time domain indicators in conjunction with the ARMAX models to predict the amount of damage on a blade. This could make very good features for use in Self Organising Maps (SOM) or neural networks.

4.5 Conclusions

Although the ARMAX algorithm used made use of time domain data to generate a polynomial model, the end result was frequency domain parameters. The shift of natural frequencies proved to be a good damage indicator when the approximate location of damage is known. As discussed in Chapter 1, cracks will typically only originate at the root of fan blades because of the location of maximum stress. The results obtained are especially good if results of various researchers over the years (as discussed in Chapter 1) are taken into account.

Some discrepancies were found between the FEM and experimental results for the third mode shape. This phenomenon was investigated in Chapter 5.

Time domain damage indicators did not provide a clear indication or trend with increasing levels of damage for most operating conditions and sensors. If only some of these values are used as features in a pattern recognition algorithm such as a neural network it may further improve the prediction accuracy, especially if a whole range of features (more features were discovered in Chapter 5) are used.

CHAPTER 5

THE EFFECT OF GLOBAL AND LOCAL MODES

5.1 Introduction

Due to the discrepancies found between the frequency shifts of some mode shapes the FEM predicted and the actual measured shifts, it was decided to investigate further. It was postulated that the most likely cause for this phenomenon was that the measured frequencies corresponded to global dynamics of the structure. This would mean that the frequency shift might actually be less than predicted by what would be a "local" mode shape of a single blade modelled by the FEM.

The rest of this chapter is devoted to the development of an additional FEM to gain a better understanding of the global behaviour of the system. Furthermore the results obtained from this new model were compared to the measured results.

5.2 The need for extended FEM modelling in systems

The results when using the natural frequency around 280 Hz can be found in Chapter 4. While a readily measurable shift of frequency was found with increasing amounts of damage, the shift was nowhere near as much as expected. At around 40% damage the shift was found to be around 6% compared to the predicted shift of 25%. The reason for this behaviour can be seen in Figure 5.1. While a whole range of different peaks can be found around 270 Hz, the ARMA model did an averaged curve fit. As a result the different peaks were not picked up. This specific power spectral density plot was done for the instrumented, damaged blade with a 1000 Hz sampling frequency and a 4 s sample.

The most likely reason for this behaviour was that this mode was global. This means that the other three fan blades also take part at slightly different local frequencies. As a result these modes are superimposed on each other to give a much more complex behaviour than could be expected from a single blade.

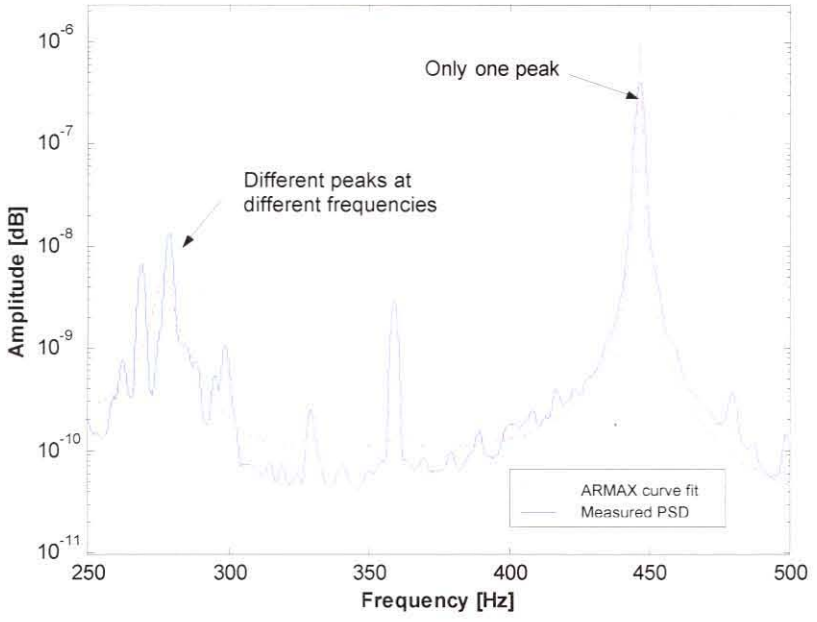

Fig 5.1: Experimental comparison of the third and fourth natural frequencies

Further proof for this hypothesis could be found in the fact that an instrumented, undamaged blade also showed frequency shifts at most of the natural frequencies with increasing amounts of damage (see Figure 5.2).

In sharp contrast with the third natural frequency, the fourth natural frequency produced a very well defined peak at one frequency only. This peak also stayed at virtually the same position on the undamaged blade as can be seen in Figure 5.2. It was to be expected that higher frequencies are more likely to be local mode shapes.

Also readily apparent in Figure 5.2 was the fact that different mode shapes had different sensitivities to the rest of the test structure.

To gain a better understanding of the behaviour of the complete system a simplified finite element model of the hub and blade interface was created. Another possibility would have been to perform a modal analysis on the system. The finite element model approach was preferred due to the following reasons:

- A modal analysis can not be done while the fan is operating. The force input on the system need to be measured and this was realistic only if a modal exciter and force transducer were used.
- The mass of the accelerometer moving from the tip of the blade to the root with different measurements could make a significant difference on the measurements.

- Due to time constraints, only a limited number of measurement points per blade would have been made, reducing the accuracy even further.
- The finite element model was more flexible in terms of inducing damage and provided information about higher mode shapes and symmetrical modes.

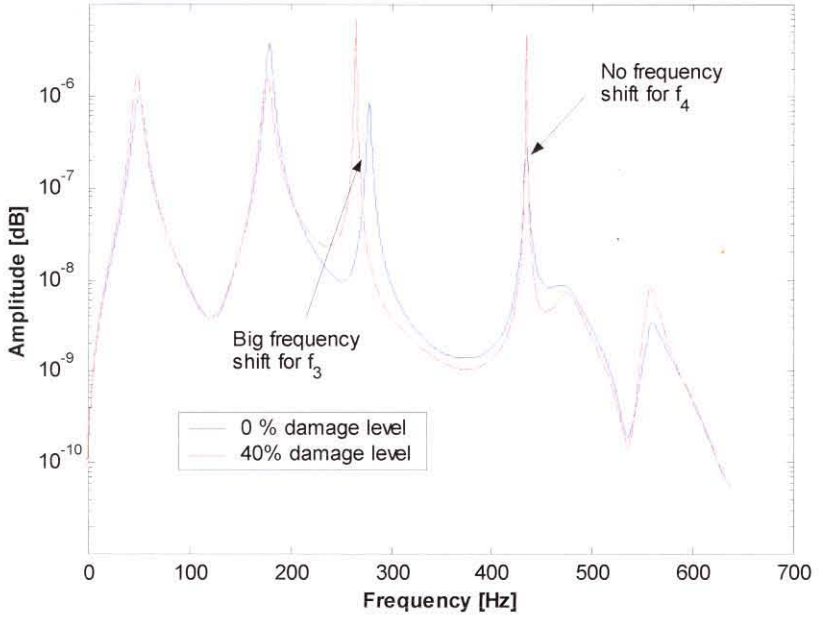

Figure 5.2: ARMA curve fits to undamaged instrumented blade

The finite element model can be seen in Figure 5.3. While it was not an exact representation of the experimental fan blade damage simulator it adequately explained the different shift of frequencies observed during experimental measurements and analysis. Note that the blade seat ring was modelled as aluminium since the experimental fan blade damage simulator was machined from aluminium.

The undamaged mode shapes in the region of 280 Hz can be seen in Figure 5.4. Even for the undamaged case, the first sideways mode shapes differed significantly from each other. It also explains the peak at 294 Hz (see Figure 5.1). Due to the fact that the whole system resonated, these different mode shapes around 280 Hz would have influenced the dynamic behaviour of all the blades. The four mode shapes in the region of 280 Hz for the damaged case can be seen in Figure 5.5. Periodic structures such as a fan, exhibit mode localisation. This can be seen in the top right of Figure 5.5. Only the damaged blade take part in this mode shape.

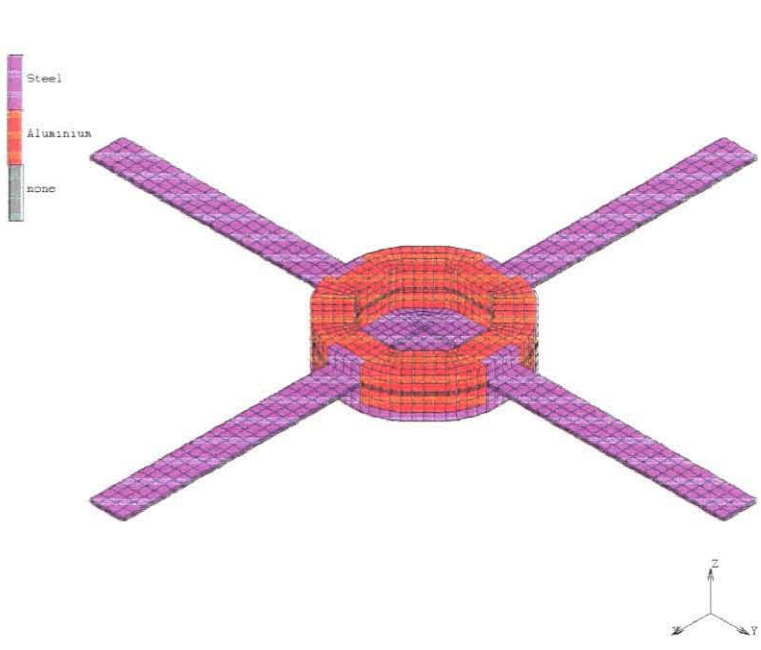

Figure 5.3: The extended finite element model

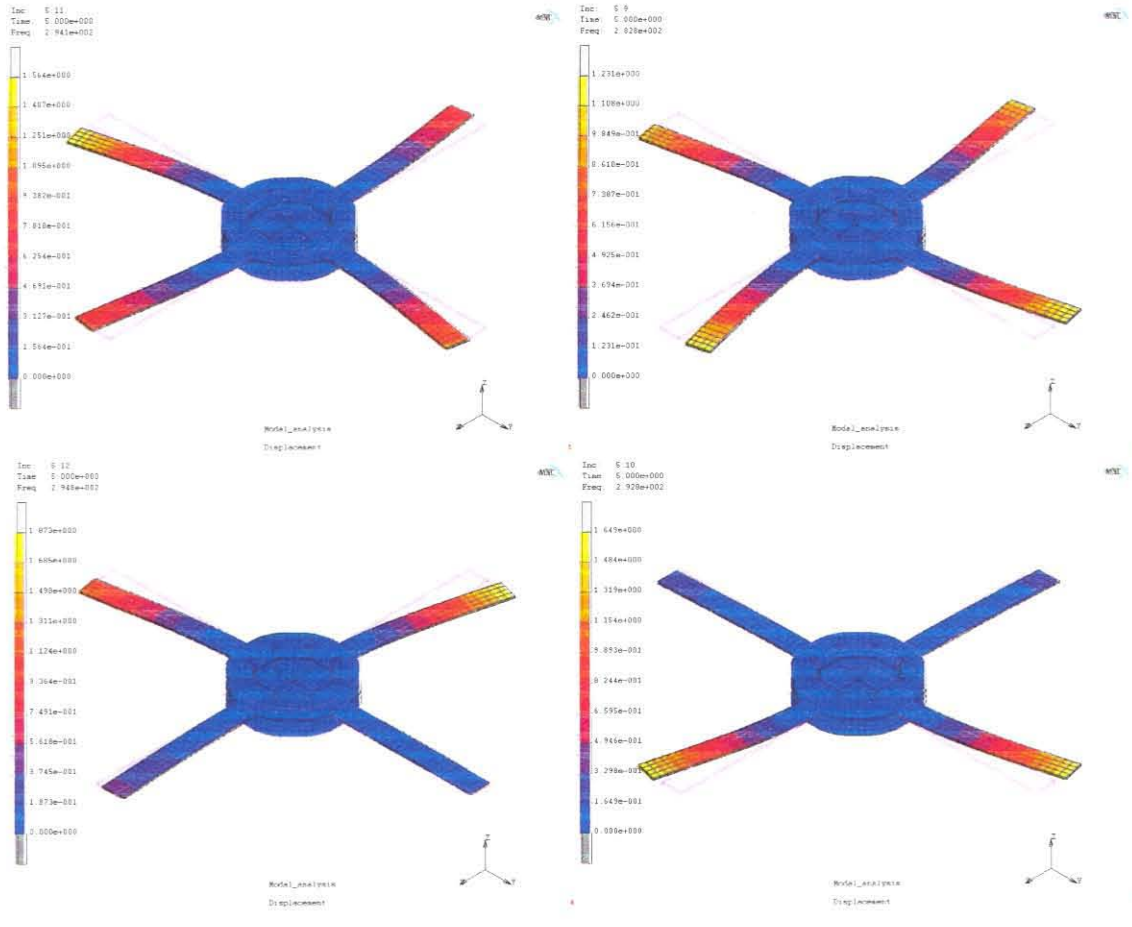

Figure 5.4: Four mode shapes found in the region of the third natural frequency (f ≈ 290Hz)

The frequency values found for the four mode shapes in the region of the third natural frequency (Figure 5.4) can be seen in Table 5.1 (listed clockwise from the top left).

Table 5.1: Comparison at the third mode shape

Undamaged case	25 % Damage case
294.1 Hz	293.7
282.0 Hz.	267.4
292.8 Hz	286.7
294.8 Hz	294.8

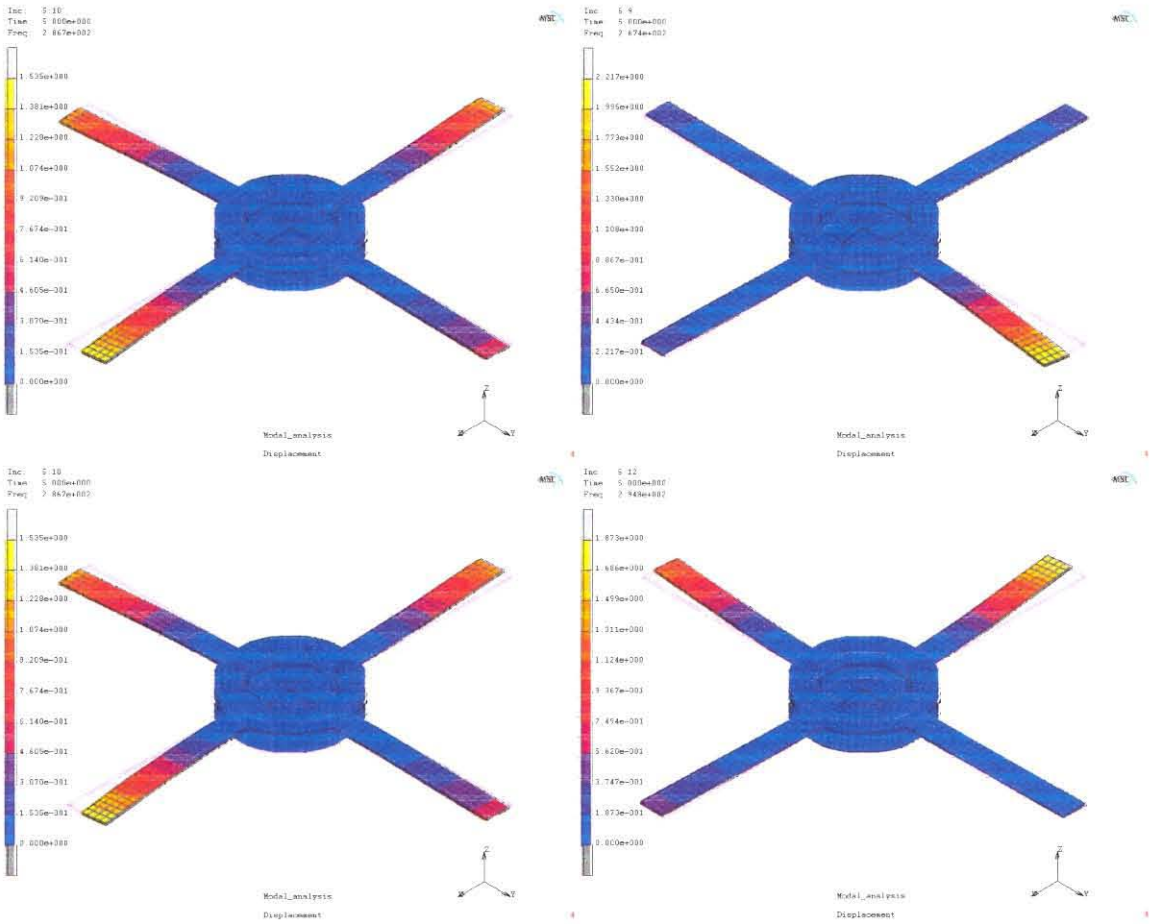

Figure 5.5: The four mode shapes after damage had been induced on one blade.

The fourth mode shape (first torsional) can be seen in Figure 5.6 on the next page. This mode shape provided excellent local damage indicators. The four modes shown here were for the undamaged case. The undamaged case was compared to the damaged case in Table 5.2 (From the top left, clockwise in Figure 5.4). The damaged case can be seen in Figure 5.7

Table 5.2: Comparison at the fourth mode shape

Undamaged case	25 % Damage case
433.4 Hz	429.3
433.6Hz.	433.5
433.8 Hz	433.6
434.0 Hz	433.9

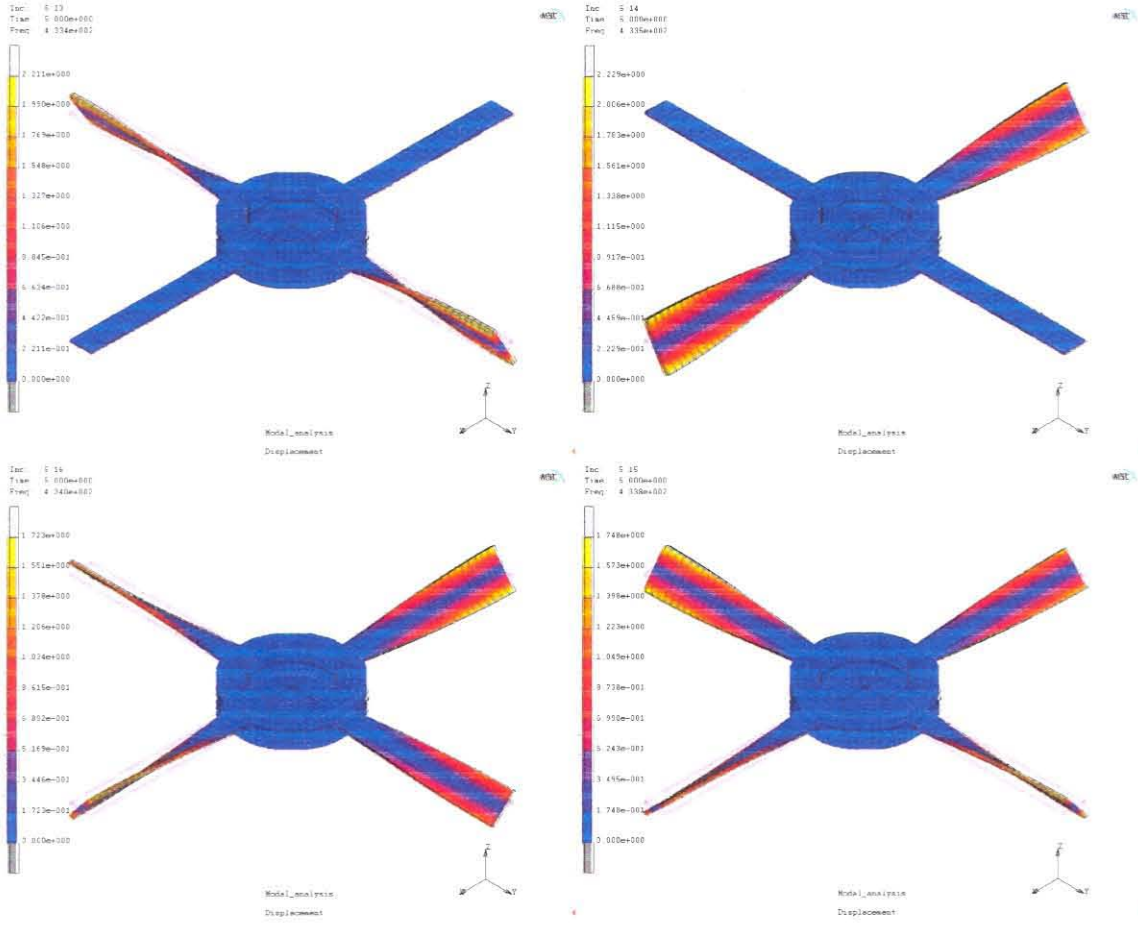

Figure 5.6: The four modes shapes found in the region of f ± 433Hz.

Although this mode shape did not shift by as much as the third natural frequency, the local nature of the mode shape made it much better suited to this problem.

The biggest problem with the third natural frequency in this system was that a whole range of frequencies can be found (see Table 2.4 and fig 2.12). Experimental results confirmed the results found by the finite element analysis. While this frequency can still be useful as a global damage indicator, it was doubtful whether experimental

measurements, and even more importantly, ARMA curve fits could be done accurately enough to monitor all the modes in the region of the third natural frequency.

A further advantage of the torsional mode shapes was the fact that all the natural frequencies found were virtually the same and would therefore be significantly easier to measure accurately and repeatedly.

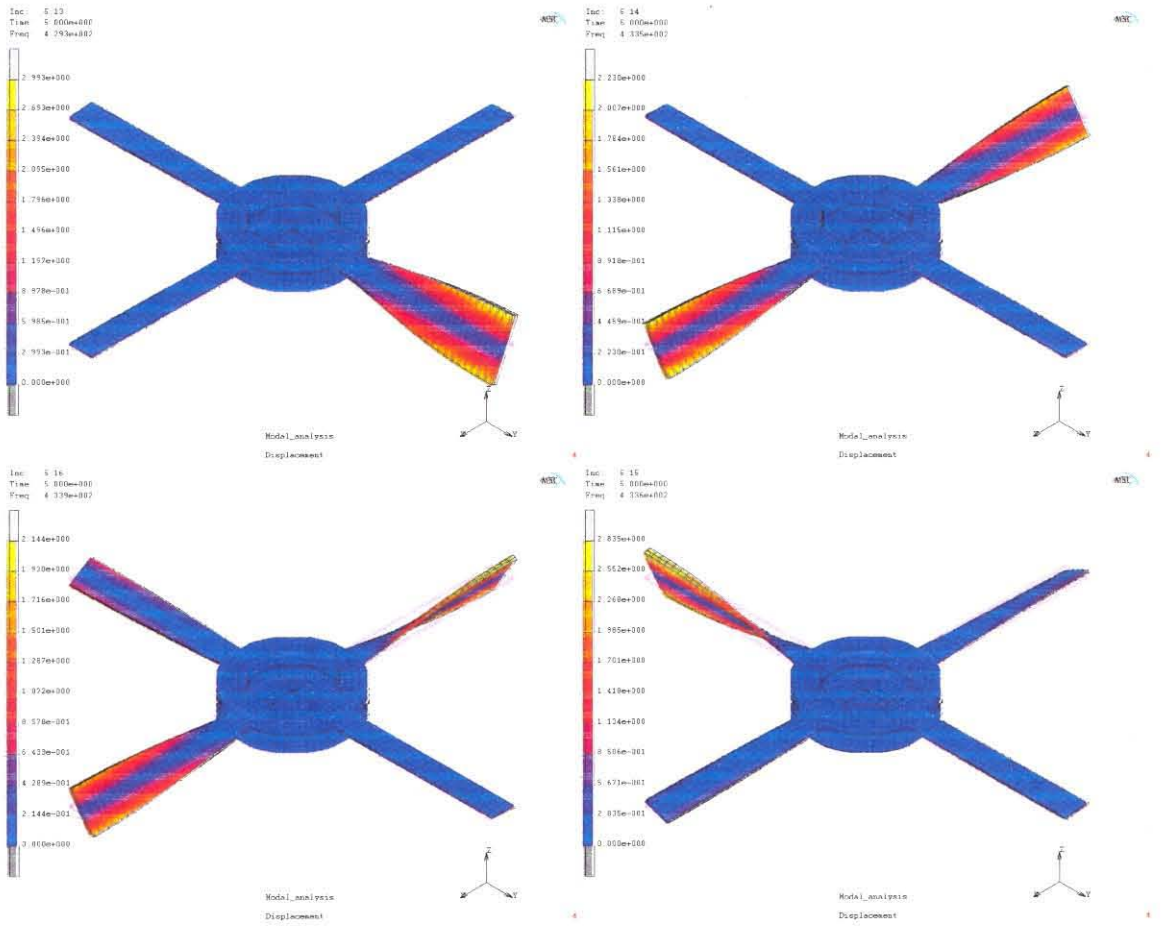

Fig 5.7: The mode shapes after damaged had been induced

As this extended FEM model adequately explained the deviation of FEM results from the results found experimentally, the model was not refined to represent an exact match to the experimental results. For this project the model was used to show correlation between experimental and FEM results. If a simplified laboratory based fan blade damage simulator can be modelled accurately, it is not unreasonable to assume that damage can be detected by using the same technique on the actual fan

5.3 Effects of eight blades

It was also decided to investigate the effect of even more blades on the mode shapes and natural frequencies of a bladed structure. For this purpose, an identical model to the one used in section 5.2 (except for doubling the number of blades to eight) was used. Some of the resultant mode shapes in the region of 280 Hz can be seen in Figure 5.8. Table 5.3 gives the eight natural frequencies found around 280 Hz, while Table 5.4 gives the frequencies found around 433 Hz.

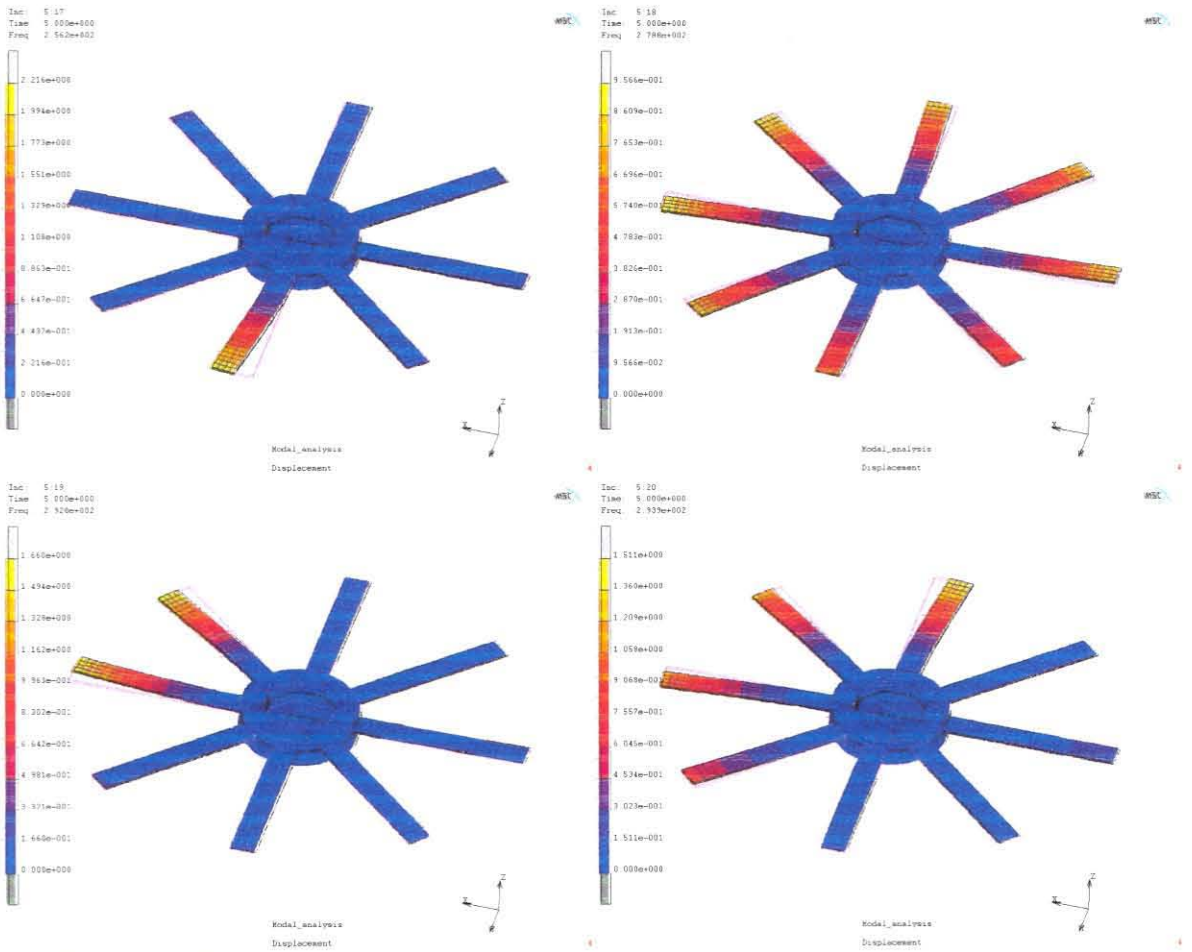

Figure 5.8: Four of the mode shapes and natural frequencies found in the region of 280 Hz

Table 5.3: Comparison at the third mode shape.

Undamaged case		25 % Damage case	
269.278	295.019	256.245	295.019
282.033	295.096	278.758	295.095
292.768	296.358	292.767	296.355
293.904	305.989	293.901	304.982

Table 5.4: Comparison at the fourth mode shape.

Undamaged case		25 % Damage case	
429.527	433.794	424.7	433.793
429.577	433.897	429.527	433.896
433.301	434.227	433.044	434.227
433.040	434.435	433.293	434.435

The results showed that an even greater variety of frequencies now emerge around the "base" frequency. Even so, the first torsional mode shape still provided good local damage indicators.

5.4 Conclusions

The following important aspects were observed:

- Even structures such as the experimental fan blade damage simulator that consists of a very rigid (relative to the blades), inner structure still show a predominantly global dynamic behaviour.
- Global modes provide global damage indicators of structure. This means that the shift of frequency may be smaller than predicted due to the fact that the damage was less relative to the whole structure, than predicted by a local modal.
- Local mode shapes could still be found, it seemed as though torsional mode shapes tended to be more local in nature.
- It will be necessary to do extended FEA on a global structure, in conjunction with preliminary measurements of the FD fan at Majuba, to choose a mode that will provide accurate damage classification.
- By using pattern recognition techniques such as neural networks this complex interaction between the blades may emerge as good features for damage level detection.
- The interaction between different blades may also be used to reduce the required number of sensors to less than one per blade.

CHAPTER 6

CONCLUSIONS AND RECOMMENDATIONS FOR FUTURE RESEARCH

6.1 Introduction

This chapter deals with the final conclusions regarding key aspects of this project. Recommendations for future research are also made. The following issues are considered:

- The use of FEM to help determine the feasibility of vibration based damage detection on an actual structure (the EFBDS in this case)
- The viability of using frequency changes for damage detection in blade structures where the location of damage is usually known
- The practical implementation of the developed techniques with specific emphasis on sensor and telemetry requirements

Recommendations are made regarding further development of the damage detection method, along with areas that needs further research.

6.2 Conclusions

6.2.1 Use of FEM for feasibility study

Rapid progress in computer technology and software has led to the situation where powerful packages such as MSC Marc can be used on desktop systems. This made it possible to study the effect of damage on the dynamics of a structure such as a blade prior to constructing an experimental test structure. From this analysis it could clearly be seen that certain mode shapes were more susceptible to damage than others. These findings correlated well with findings during a literature study. It was also found that the type of element used was extremely important. Higher order elements gave superior accuracy although they were computationally more expensive. First order solid elements are not a real proposition due to their poor performance in bending. Since most mode shapes have some element of bending, results provided

by first order solid elements were found to be unacceptable even for simple structures.

After the results from the EFBDS were compared to the predictions made by making use of a FEM, certain modes were found to exhibit different behaviour to the predictions made by the FEM. After careful consideration it was postulated that this was most likely due to global dynamics of the structure not taken into account by the simplified FEM used initially. After an extended FEM model was constructed, all discrepancies between the initial model and the EFBDS could be explained (chapter 5 deals with these findings in detail).

Clearly, while FEA is certainly a powerful and valuable tool, very careful consideration regarding assumptions and boundary conditions have to be made. Provided this is done, FEA can be used with great success not only to study the feasibility of damage detection but also to determine optimal sensor location and number.

6.2.2 Frequency changes as damage indicator on fan blades

From the results obtained with the EFBDS, it is clear that damage can be accurately detected at levels as low as 10% using one sensor per blade only. During routine maintenance at the Majuba power plant, damage levels of up to 70% were found on some blades that were still operating. Sufficient warning for future maintenance would therefore be given if 10% damage can be detected accurately.

The frequency changes were more consistent damage indicators than time domain indicators such as variance, Crest factors, Kurtosis, *rms* levels, etc.

The ARMAX model used in conjunctions with peak picking provided accurate enough natural frequency values for damage identification. This algorithm needs little user input and experience once it has been set up for specific data sets and an automated on line damage detection method could therefore be developed.

The amount of data that needs to be processed did prove to be fairly high as did the CPU time. This is not an insurmountable problem as a set of measurements can be taken at specified intervals, leaving ample time for processing of the data.

6.2.3 Practical implementation of on-line technique

Any technique developed for damage detection will be of little use if it cannot be implemented on a structure, other than an experimental test structure. The practical implementation of the on-line, vibration based, damage detection method was therefore of paramount importance throughout the project. A considerable amount of time was spent in search of sensor and telemetry technology for this application. The most significant problem for this application is the transfer of data from sensors mounted on a rotating fan blade to a processing unit. Alternatively an integrated sensor will do the processing and send only a result to a monitoring station. Be that as it may, some form of wireless transfer will probably required. Slip rings are usually not easy to install on an existing structure and due the contact between a stationary brush and the rotating structure, a certain amount of wear is inevitable. Bluetooth technology should become readily available within the next two years. This is a standard for the wireless transfer of data between various portable devices and manufacturers of sensors are also looking into this technology.

Due the advent of MEMS, wireless sensors and smart sensors have already been developed and this trend seems set to continue. These smart sensors are already being used in applications such as air bag deployment in the automotive industry.

6.3 Recommendations

6.2.1 Further development of FEM

It was made clear from the outset that this is a long term project. The initial findings are very encouraging and on-line, vibration based damage detection on structures such as fan blades has proved to be a viable means of damage level indication. The next stage would probably be to develop a more detailed FEM of the fan on which the technique will first be tested in industry (probably the FD fan at Majuba). Because of global and local mode shapes, it may make sense to develop a simplified FEM of the complete system. Higher order elements should be used even though computational time is higher.

6.3.2 Sensors and telemetry

Some preliminary measurements will have to be taken on the FD fan. This will be necessary to verify the FEM results and confirm that frequencies can be measured accurately and repeatedly. Due to the installation it will be possible to use fairly conventional sensors for these measurements as the fan are switched on and off at fairly regular intervals for peak power demand although this may change in future. Data can be stored and downloaded when the fan is switched off without the need for (expensive) wireless equipment. Further studies regarding the implementation will be a high priority.

Since the EFBDS already exist, it will make sense to use it to fine-tune the technique. Possible improvements to the technique are described in the next section. The simple plate type blades can be substituted with curved blades easily due to the modular design of the EFBDS.

6.3.3. Further development of detection technique

As mentioned in Chapters 4 and 5, the damage level indicators developed during this project should make good features when used in a pattern recognition algorithm such as neural networks or self-organising maps. The complex interaction between the different blades may not show any clear pattern by just looking at it, but these algorithms may well make it possible to use these features as indicators of damage levels on other blades and make instrumentation of all the blades unnecessary.

6.4 Epilogue

A technique for the on-line detection of damage in fan blades was developed. As a first step in the development of an on-line monitoring system for use on industrial fans, it showed that vibration based damage detection can be developed as a reliable and relatively inexpensive method of damage level indication. The method was shown to give good results even when time signals were polluted by blade pass frequencies and harmonics, as well as high levels of electrical noise. The next step would be to develop this method to such an extent that it can be integrated into existing fans. The large amount of research being done in the field of on-line condition monitoring shows that these methods will eventually become standard on any new equipment

REFERENCES

Agneni A., Balis Crema L., Mastroddi F., Damage detection from truncated frequency response functions. *COST F3 Conference on System identification and Structural Health Monitoring*, Madrid, 2000

Allemang, R.J., Brown, D.L. A Correlation Coefficient for Modal Vector Analysis. *Proceedings of 1st IMAC*, Orlando, Florida, USA, 1982.

Andersen P., Kirkegaard. P.H. Brincker R. Structural time domain identification toolbox. User's guide. *Instituttet for Bygningsteknik, Aalborg Universitet*, 1997.

Balis Crema L., Mastroddi F., Beneditte L. A spatial modal identification by using FRF data. *Proceedings of the 15th IMAC Conference*, pp. 1284-1291, 1997.

Balis Crema L., Matroddi F. A direct approach for updating and damage detection by using FRF data. *Proceedings of ISMA 23*, Vol 1., pp43-50, 1998

Barber A., Handbook of noise and vibration control 6th Edition. Elsevier Advanced Technology, 1992.

Beckwith T.G., Marangoni R.D., Lienhard J.H. Mechanical measurements, fifth edition. Addison-Wesley Publishing company, pp.282-285, July 1993.

Bendat J.S., Piersol A.G. Measurement and analysis of random data, John Wiley & Sons, 1967.

Cawley, P., A comparison of the natural frequency changes produced by cracks and slots, *Journal of Vibration, Acoustics, Stress and Reliability in Design*, New York: American Society of Mechanical Engineers, 1988.

Cawley, P., Adams, R.D. The location of defects in structures from measurements of natural frequencies, *Journal of Strain Analysis*, Vol 14, No. 2, pp. 49-57, 1979.

Cobb R.G., Liebst B.S. Structural damage identification using minimal sensor information. *Proceedings of International Conference on Identification in Engineering Systems*, Swansea, pp. 275-284, 1996.

Colonnelo A., Morassi A. Hearing cracks in a vibrating rod. Proceedings of ISMA 23, 1998

Corbelli A., Mastroddi F., Gennaretti M. Damage detection for helicopter rotor blades in operative condtions. *Proceedings of ISMA 25*, pp179-186, 2000.

Doebling S.W., Farrar C.R., Prime M.B., Shevitz D.W. Damage identification and health monitoring of structural and mechanical systems from changes in their vibration characteristics: a literature review, *Los Alamos National Laboratory Report LA-13070-MS*, 1996

Dos Santos J.M.C., Zimmerman D.C. Damage detection in complex structures using component mode synthesis and residual modal force vector. *Proceedings of the 14th IMAC*, Vol. 2, pp. 1299-1305, 1996

Felber A.J., Ventura C.E. Frequency domain analysis of the ambient vibration data of the Queensborough bridge main span. *Proceedings of the 14th IMAC*, pp. 459-465, 1996.

Friswell M.I., Penny J.E.T. Is damage location using vibration measurements practical. *EUROMECH 365 International Workshop: DAMAS 97, Structural Damage Assessment using Advanced Signal Processing Procedures*, Sheffield, UK, www.swan.ac.uk/mecheng/staff/mfriswell/PDF_Files/DAMAS97.html,1997

Friswell M.I., Penny J.E.T. The use of vibration data and model updating to detect damage. Dynamics, *Control and Vibration Research Group, U.K*, 1996 D04618.

Fritzen C.P. Jennewein D., Buchen D. Model based damage detection from vibration data. *Proceeding of ISMA 21*, pp. 1017-1031, 1996

Hermans L., Van der Auweraer H., Matheleu L., Coppens D. Modal parameter extraction from in-operation data. *Proceedings of the 16th IMAC*, pp. 531-539, 1998.

Heyns P.S. Modal testing with natural excitation using a time series approach. *Research and Development Journal*, pp. 34-39, 1995

Joon-Ho K., Hyuck-Soo J., Chong-Won L. Applications of the modal assurance criteria for detecting and locating structural faults.

Klein K. Guigné J.Y., Swamidas A.S.J. Monitoring of change in modal parameters with fatigue. *Proceedings of the 12th IMAC*, Honolulu, Hawaii, Vol.2, pp. 1792-1800, 1994.

Ko, J.M., Wong C.W., Lam H.F. Damage detection in steel-framed structures by vibration measurement approach. *Proceedings of the 12th IMAC*, pp. 280-286, 1994.

Kriel C.J., Heyns P.S. Damage identification on piping systems using on-line monitoring of dynamic properties. *Proceedings of the 16th IMAC*, pp. 482-488, 1998.

Liang Z., Huang T.J., Lee G.C. A study on damage dynamics by using modal energy transfer. *Proceeding of the 15th IMAC*, pp. 1339-1345, 1997

Lomenzo R.A., Barker A.J., Wicks A.L. Laser vibrometry system for rotating bladed disks. *Proceeding of the 17th IMAC*, pp.277-282, 1999.

Maddux, G.E. Work plan for high cycle fatigue instrumentation subtask. WPAFB Document, 1997.

Mastroddi F. Beneditti L. A generalization of spatial model identification by using FRF data. *ESA Conference on Spacecraft Structures, Materials and Mechanical Testing*, The Netherlands, SP-386, pp. 1319-1326, 1996.

Mastroddi F. Identification and damage detection using FRF experimental data with applications to a wing structure. *Proceedings of ISMA 25*, pp. 209-216, 2000.

Osbrone W.C. Fans 2nd Edition, pp. 46-47. Pergamon Press, 1977.

Peeters B., Wahabb M.A., De Roeck G., De Vissher J., De Wilde W.P., Ndambi J.M., Vantomme J. Evaluation of structural damage by dynamic system identification. *Proceeding of ISMA 21*,pp. 1349-1361, 1996

Penny J.E.T., Wilson, D., Friswell M.I. Damage location in structures using vibration data. *Proceeding of the 11th IMAC*, Kissimee, Florida, USA, pp. 861-867, 1993.

Pereira J.A., Heylen W., Lammens S., Sas P. Model updating and failure detection based on experimental FRFs: case study on a space frame structure. *Proceedings of ISMA 19*, Vol. II, pp. 669-681,1994

Pandit S.M. Modal and spectrum analysis: data dependant systems in state space. John Wiley & Sons, 1991.

Ratcliffe C.P. Damage detection using a modified laplacian operator on mode shape data. *Journal of Sound and Vibration*, pp. 505-517, 1997.

Salawu O.S., Williams C. Damage location using vibration mode shapes. *Proceedings of the 12th IMAC*, Vol. 1, pp. 933-939, 1994.

Schulz M.J., Naser A.S., Pai P.F. Health monitoring of helicopter rotor systems. *http://www.psu.edu/dept/rcoe/ppt/health.html*, 1997.

Shi Z.Y., Law S.S., Zhang L.M. Two stages damage detection in structure based on modal data. *Proceedings of the 15th IMAC*, Vol. 1, pp. 665-671, 1997

e Silva, J.M.M., de Araújo Gomes, A.J.M.Crack Identification of simple structural elements through the use of natural frequency variations: the inverse problem. *Proceedings of the 12th IMAC*, Vol.2, pp. 1728-1735, 1994.

Sohn H., Farrar C.R. Time series analyses for locating damage sources in vibration systems. *Proceedings of ISMA 25*, p187-191, 2000.

Springer W.T., Reznicek A. The prediction of the natural frequency shifts for a cantilevered L-section beam due to the presence of a crack. *Proceedings of the 12th IMAC*, Honolulu, Hawaii, Vol.1,pp 889-897, 1994.

Sundaresan M.J., Schulz M.J., Hill J., Wheater E.A., Ferguson F., Pai P.F. Damage Detection on a Wind Turbine Blade Section. *Proceeding of the 17th IMAC*, pp. 1359-1365, 1999.

Söderström T, Stoica P. System identification, Prentice Hall, 1989.

Williams C., Salawu O.S. Damping as damage indication parameter. *Proceedings of the 15th IMAC*. Vol. 2, pp. 1531-1536, 1997.

Williams E.J., Contursi D., Messina A. Damage detection and localization using natural frequency sensitivity. *International Conference on Identification in Engineering Systems*, Swansea, UK pp. 368-376, 1995.

Williams, E.J., Messina, A., Payne, B.S. A frequency-change correlation approach to damage detection, *Proceedings of the 15th IMAC*, Vol 3, pp. 652-657, 1997.

Wolff P.J., Patrick, A.M., Experimental and finite element investigation of blade cracking in a scrubber fan model. *Proceedings of the 7th IMAC*, Vol.1, pp.119-123, 1989.

Yoo S.H., Kwak H.K., Kim B.S. Detection and location of a crack in a plate using modal analysis. *Proceedings of the 10th IMAC* , pp. 1902-1908, 1992.

APPENDIX A

SENSORS

A.1 Piezoelectric accelerometer

Table A.1: Specifications of the miniature (M352C22) and lightweight (M353B65) accelerometer used

Decription	Units	M352C22	353B65
Voltage sensitivity	mV/ms^{-2}	10	100
Frequency range (±5%)	Hz	5 to 8000	1 t o10000
Resonant frequency	kHz	>32	>70
Amplitude range	$\pm m/s^2$ pk	500	50
Mechanical shock limits	$\pm m/s^2$ pk	0.0015	0.007
Temperature range	°C	-31 to +121	-31 to 121
Amplitude linearity	%	±1	±1
Transverse sensitivity	%	<5	<5
Base strain sensitivity	$m/s^2/\mu_\varepsilon$	<0.05	<0.002
Excitation voltage	VDC	18 to 30	18 to 30
Constant current excitation	mA	2 to 20	2 to 20
Discharge time constant	second	>0.3	>0.5
Sensing element	type	ceramic	quartz
Weight	gram	0.5	2

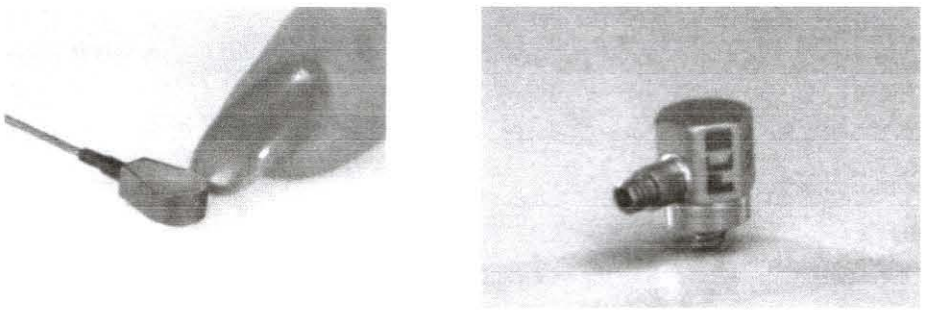

Figure A.1: Miniature (left) and lightweight (right) accelerometer available.

These are just two of the many types of accelerometers available of the shelf. The miniature accelerometer cost around R5000 and will work very well for this application. The lightweight accelerometer provides better sensitivity and also worked adequately for this application. Specifications can be seen in table A.1.

A.2 Piezoelectric strain gauge

Fig A.2: The PCB piezoelectric strain gauges used on the EFBDS.

The piezoelectric strain gauges are ideal sensors for the measurement of system dynamics. The very low weight and profile makes for easy attachment with adhesives and minimal turbulence in fan systems. Due to the position of maximum strain being at the root of the blade, these sensors are also not subjected to maximum flow velocities, a problem for accelerometers. Specifications can be seen in table A.2.

*Table A.2: Specifications for piezoelectric strain gauge (*740B02)

Description	Value
Sensitivity (±20 %)	50 mV/μ E
Amplitude range	100 peak/μ E
Broadband resolution (1 Hz to 10 kHz)	0.6 μ E
Frequency range	0.5 to 100 000 Hz
Operating temperature range	-53 to +121 °C
Output bias	9to 13 VDC
Cable, 3m length supplied	Integral Coaxial
Weight	0,5 grams
Size (Width x Length x Height)	5,1 x 15,2 x 1,8 mm

APPENDIX B

Work drawing of Majuba fan blade

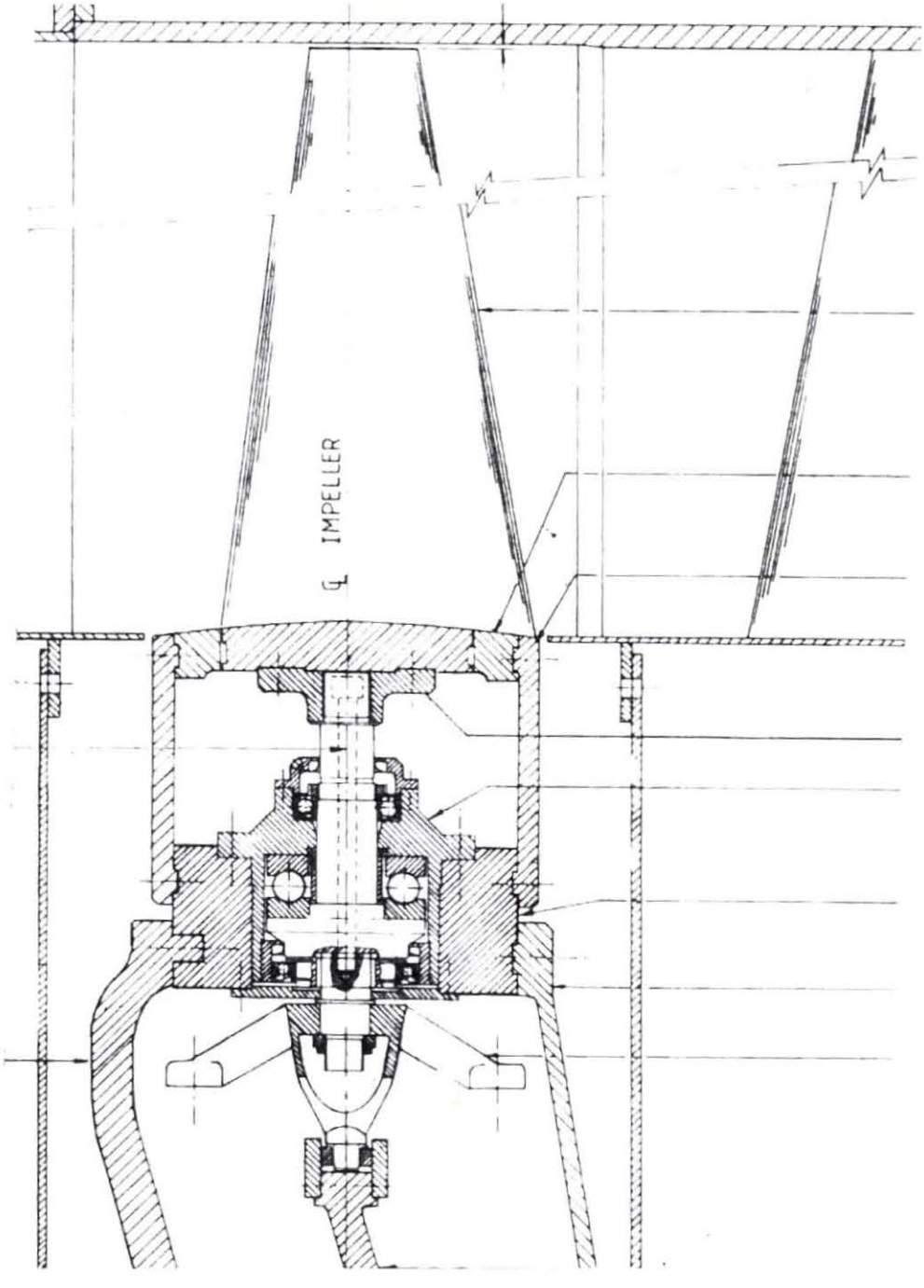

Fig B.1: Section drawing of one of the fan blades of the FD fan at Majuba

APPENDIX C

INVESTIGATION OF ARMAX MODELLING TECHNIQUE

C.1 Experimental test structure

To evaluate the effectiveness of using an ARMAX model to determine natural frequencies of a system, a simple aluminium cantilever beam was used. A schematic of the experimental test set-up can be seen in figure C.1.

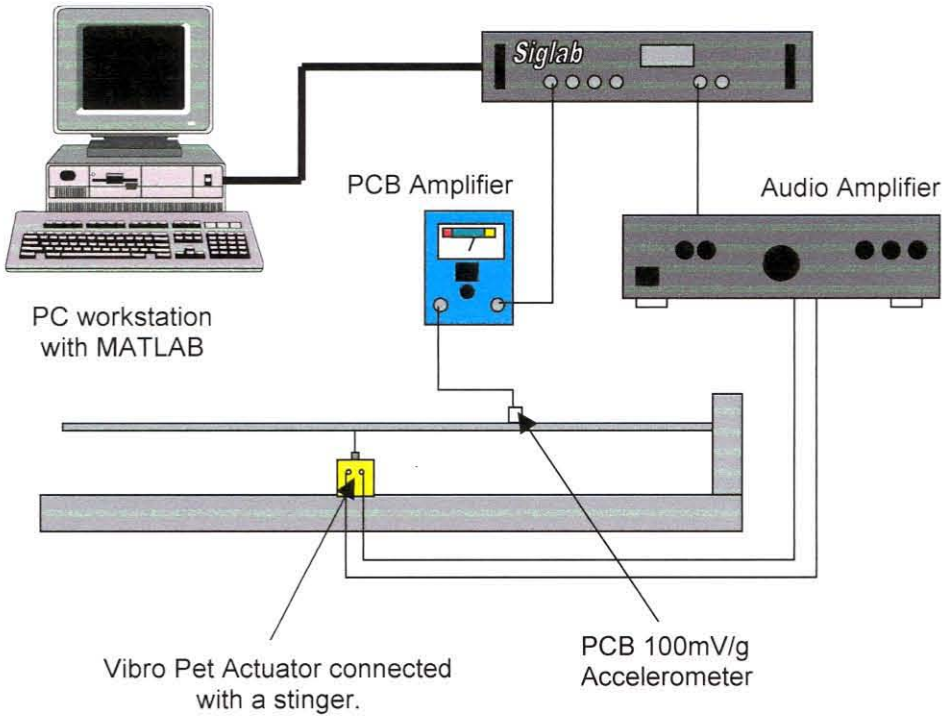

Figure C.1: Schematic of the experimental test structure used to verify the ARMAX technique

Since no input on the experimental fan blade damage simulator was going to be available, only the output from the accelerometer mounted on the aluminium cantilever beam was used to determine a suitable ARMAX model. A random stochastic signal with a 0-500Hz bandwidth was generated by the *Siglab* analyser to excite the beam. This signal was amplified using an audio amplifier. Due to the poor performance of the audio amplifier below 20Hz, the first natural frequency of the beam

(around 9Hz) was not excited properly and no attempt was made to correctly identify this frequency.

A typical time signal obtained from the validation model can be seen in figure C.2. The signal was filtered with a bandpass filter of 5Hz to 560 Hz and calibrated to give acceleration in m/s^2.

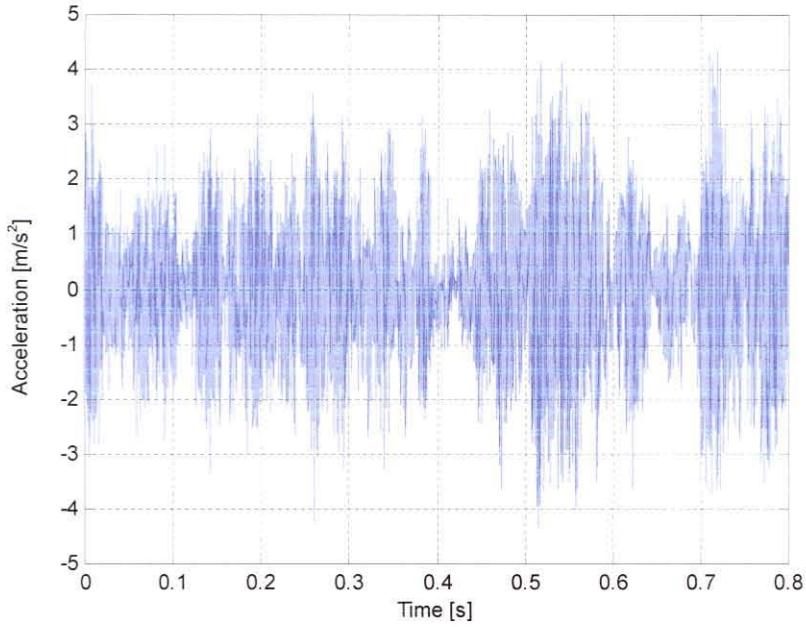

Figure C.2: Typical time signal (filtered and calibrated)

C.2 The effect of signal length

Since the ARMAX modelling technique made use of time signals to fit a curve, the length of the samples could be varied. Figure C.3 shows the typical power spectral densities and ARMAX curve fits for various sampling lengths, while tables C.1 through C.4 show the second, third and fourth natural frequencies found by means of a peak picking method on the ARMAX fit.

Table C.1: 0.8s sampling time results

Natural frequencies	f_3 (±63.7 Hz)	f_3 (±176.7 Hz)	f_4 (±332 Hz)
Measurement 1	59.41	173.61	320.78
Measurement 2	59.16	173.98	320.09
Measurement 3	59.54	173.98	320.09
Measurement 4	60.45	172.86	318.71

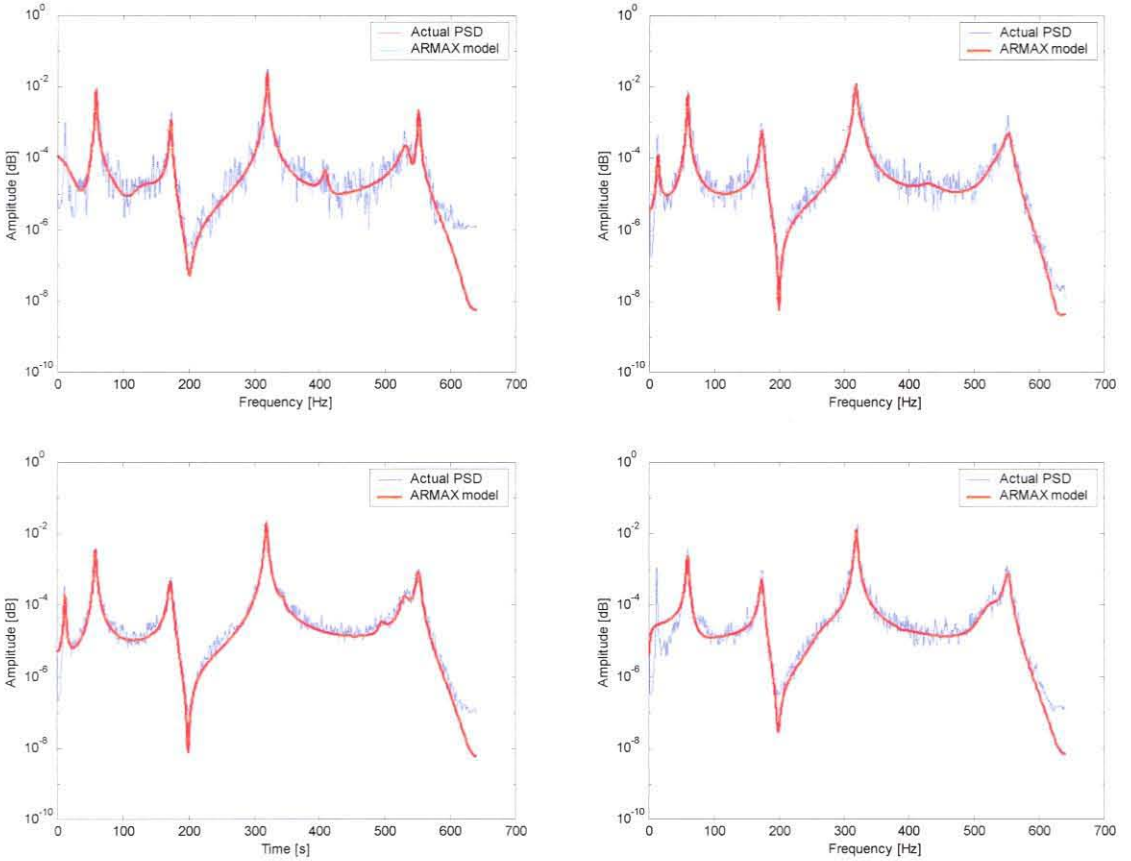

Figure C.3: Typical fits for, from top left clockwise, 0.8s, 1.6s, 3.2s and 6.4s samples.

It was readily apparent that a smoother PSD was obtained with longer sample lengths. This could be expected. Interestingly enough, the curve fits obtained provided accurate natural frequencies results even with shorter samples.

Table C.2: 1.6 s sampling time results

Natural frequencies	f_3 (≈63.7 Hz)	f_3 (≈176.7 Hz)	f_4 (≈332 Hz)
Measurement 1	59.93	174.36	318.71
Measurement 2	59.41	173.98	318.71
Measurement 3	59.54	173.61	320.09
Measurement 4	60.19	173.98	320.09

Table C.3: 3.2 s sampling time results

Natural frequencies	f_3 (≈63.7 Hz)	f_3 (≈176.7 Hz)	f_4 (≈332 Hz)
Measurement 1	60.06	174.36	319.40
Measurement 2	60.06	173.61	319.40
Measurement 3	59.80	173.48	318.71
Measurement 4	59.80	173.98	318.71

Table C.4: 6.4 s sampling time results

Natural frequencies	f_3 (≈63.7 Hz)	f_3 (≈176.7 Hz)	f_4 (≈332 Hz)
Measurement 1	59.28	173.61	318.71
Measurement 2	59.41	173.61	320.09
Measurement 3	59.33	173.98	319.40
Measurement 4	59.54	173.61	319.40

A comparison of the accuracy can be seen if figure C.4.

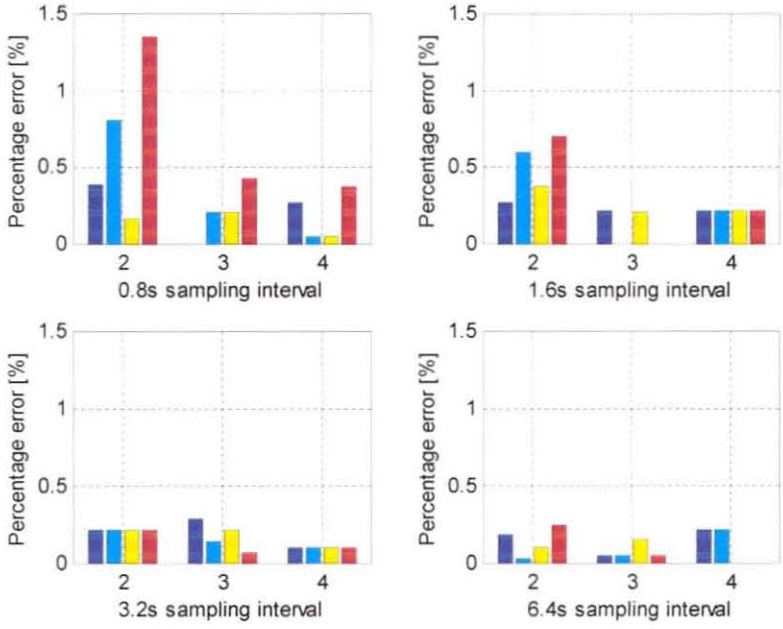

Figure C.4: Increasing accuracy with longer sampling times

While longer samples were the most accurate, the processing time did go up as the sample length increased. Table C.5 shows the processing time in seconds used for the four different sampling times (12^{th} order ARMAX models were used throughout).

Table C.5: Comparison of processing times for different sampling intervals.

Description	Central Processing Unit (CPU) time
0.8 second sampling interval	2.64 s
1.6 second sampling interval	3.79 s
3.2 second sampling interval	5.66 s
6.4 second sampling interval	13.96 s

These times included loading of data and the ARMAX subroutine and were the average of 4 runs on the same data file. The computer was a Pentium II ™ 350MHz with 128 MB of RAM.

C.3 Effect of model order

An order for the polynomial curve fit that the ARMAX subroutine fits through time domain data had to be specified. It is very difficult to compute an order for output only data. Curve fits of the 4^{th}, 8^{th}, 12^{th} and 16^{th} order can be seen in figure C.5. Clearly a certain minimum (12 in this case) was necessary to identify all the natural frequencies of the system.

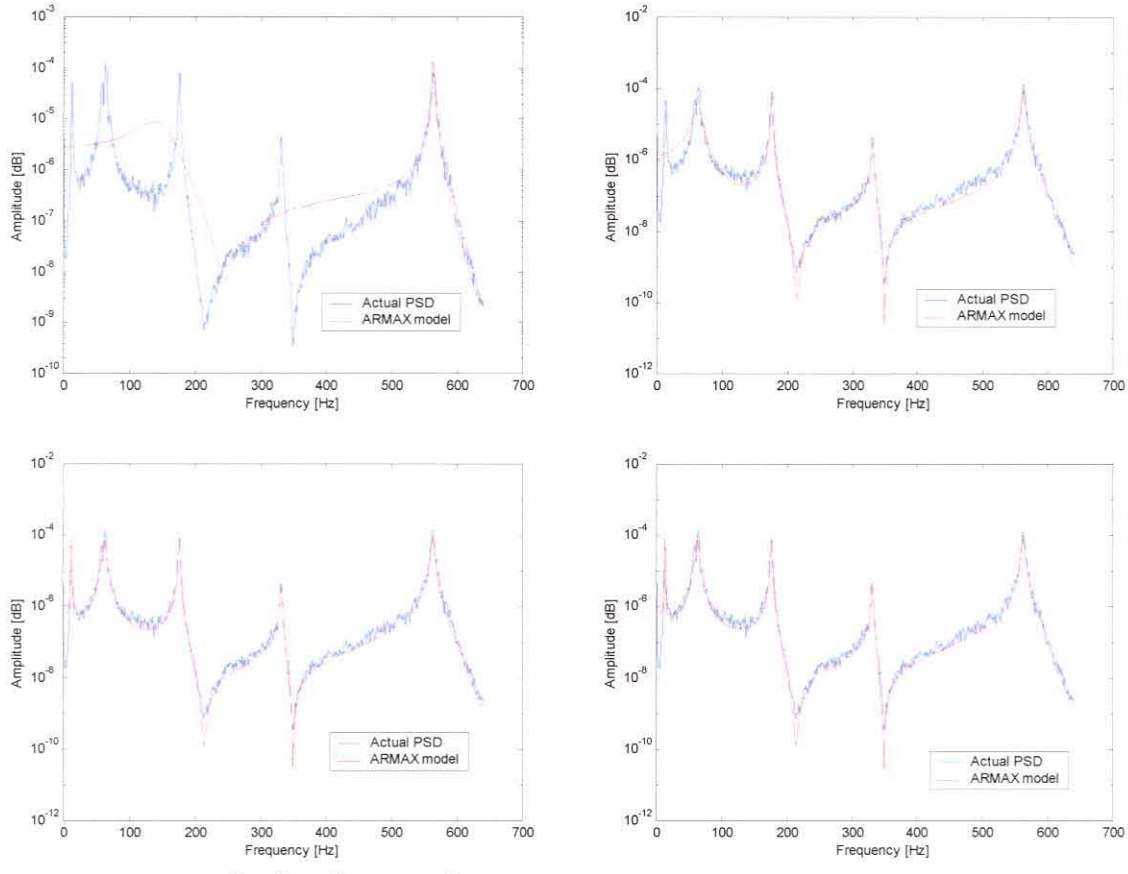

Figure C.5: 4^{th}, 8^{th}, 16^{th}, and 12^{th} order ARMAX models (from the top left clockwise)

Once all the natural frequencies had been found and fitted with a curve however, the remaining orders model noise. This resulted in unnecessary CPU time and inaccuracies in the model. CPU times can be seen in table C.6.

Table C.6: Comparison of processing times for different sampling intervals.

Description	Central Processing Unit (CPU) time
4^{th} order ARMAX model	4.78 s
8^{th} order ARMAX model	3.57 s
12^{th} order ARMAX model	5.66 s
16^{th} order ARMAX model	11.51 s

The best way to determine if too high an order was used, consisted of calculating the poles and zeros of the ARMAX model. A comparison between 4^{th}, 8^{th}, 12^{th} and 16^{th} order fits can be seen if figures C.6 and C.7.

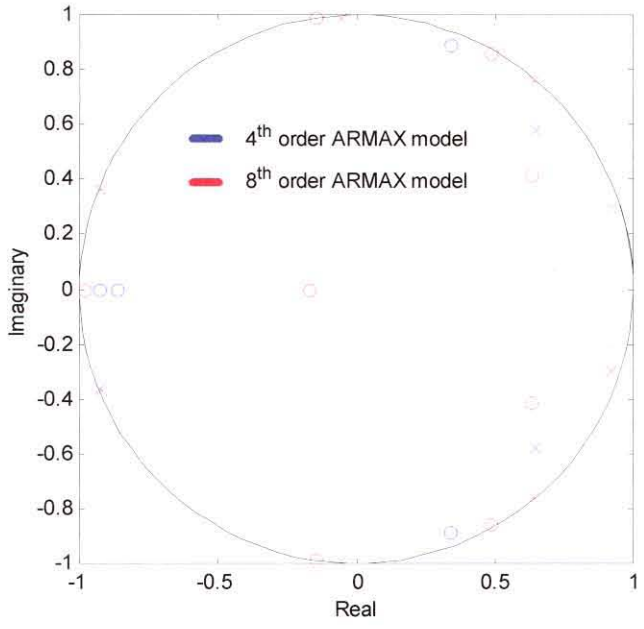

Figure C.6: The pole-zero plots for different order ARMAX models.

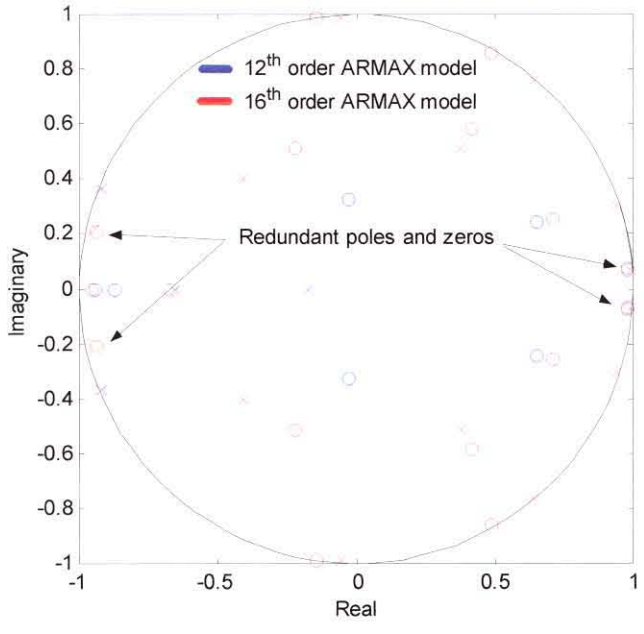

Figure C.7: Too high an order results in redundant poles and zeros

If poles and zeros coincide the system is over determined and redundant poles and zeros exist.

APPENDIX D

TYPICAL RESULTS FOUND

Table D.1: Frequency shifts for various channels and operating conditions

3rd natural frequency variation with increasing amounts of damage.					
Description	**0%**	**10%**	**20%**	**30%**	**40%**
Ch 1, 450 r.p.m, 500hz sampling frequency	284.72	279.96	275.64	271.38	266.5
Ch 2, 750 r.p.m, 1000hz sampling frequency	280.13	274.10	268.38	268.00	262.97
Ch 2, 750 r.p.m, 2000hz sampling frequency	278.87	277.93	268.42	267.81	262.89
Ch 3, 450 r.p.m, 500hz sampling frequency	284.72	279.96	274.57	270.68	266.5
Ch 3, 750 r.p.m, 500hz sampling frequency	279.96	279.6	274.92	270.68	266.5
Ch 4, 450 r.p.m, 1000hz sampling frequency	280.92	279.74	274.67	270.46	266.31

Table D.2: Frequency shifts for various channels and operating conditions

4th natural frequency variation withincreasing amounts of damage.					
Description	**0%**	**10%**	**20%**	**30%**	**40%**
Ch 1, 450 r.p.m, 500hz sampling frequency	435.68	435.68	435.68	436.25	436.25
Ch 2, 750 r.p.m, 1000hz sampling frequency	446.97	446.34	444.15	440.42	436.72
Ch 2, 750 r.p.m, 2000hz sampling frequency	446.67	446.16	444.14	440.46	436.48
Ch 3, 450 r.p.m, 500hz sampling frequency	446.55	446.55	444.24	440.8	436.81
Ch 3, 750 r.p.m, 500hz sampling frequency	446.55	446.55	444.24	440.8	436.81
Ch 4, 450 r.p.m, 1000hz sampling frequency	447.28	446.34	444.15	440.42	440.42

Table D.3: Frequency shifts for the finite element model.

Finite element model 3rd natural frequency variation with increasing amounts of damage.					
Description	**0%**	**10%**	**20%**	**30%**	**40%**
450 r.p.m. 1240 elements	284.85	283.097	268.863	245.229	213.756
750 r.p.m, 1240 elements	285.018	283.266	268.978	245.352	213.992
Finite element model 4th natural frequency variation with increasing amounts of damage.					
450 r.p.m. 1240 elements	434.932	434.023	431.429	427.463	421.905
750 r.p.m, 1240 elements	435.132	434.226	431.588	427.624	422.146